



UNIVERSITÀ
DEGLI STUDI
DI PADOVA

UNIVERSITÀ DI PADOVA

DIPARTIMENTO DI INGEGNERIA INDUSTRIALE

LAUREA MAGISTRALE IN INGEGNERIA CHIMICA E DEI PROCESSI INDUSTRIALI

**Tesi di Laurea Magistrale in
Ingegneria Chimica e dei Processi Industriali**

Adsorption and photocatalytic degradation of per- and polyfluoroalkyl substances (PFAS) in water by nanostructured membranes

Relatrice: Prof. Martina Roso
Correlatore: Ing. Abhishek Anand

Laureando: Gini Alessandro

ANNO ACCADEMICO 2023/2024

Abstract

The aim of this thesis is to develop a nanostructured membrane designed for removing fluorinated compounds from water, specifically targeting perfluorooctanoic acid (PFOA). PFOA falls under Persistent Organic Pollutants (POPs) due to its remarkable chemical and thermal stability, posing significant risks to both human health and the environment. Among various proposed techniques for degrading these substances, advanced oxidation processes stand out for their efficacy. These processes leverage the potent oxidative properties of hydroxyl groups (via Fenton reactions) and sulfate groups (via persulfate activation processes) to break down pollutant molecules. Heterogeneous photocatalysis, facilitated by the incorporation of an additional catalyst in the membranes, is particularly promising.

In this context, a nanostructured polymeric membrane serves as a support for the catalysts, including ferrous sulfate and hydrogen peroxide for Fenton reactions, potassium persulfate for persulfate activation processes, and titanium dioxide for heterogeneous catalysis. All of these methods are promoted by UV radiation.

The membranes are made of polyimide, a polymer renowned for its outstanding chemical and physical properties, ensuring superior performance even under high temperatures and exhibiting resistance to UV irradiation without any adverse effects. Different techniques were used to characterize the membranes, some of them are Fourier-transformed infrared spectroscopy (FT-IR, to understand if the imidation process is taking place), thermogravimetric analysis (TGA, to know the catalyst content of the membrane) and environmental scanning electron microscope (ESEM, to observe the nanostructure of the membrane).

In this experience, different polymer concentrations in solution were tested for the membrane production: a high viscosity of the polymeric solution is necessary to spin it to produce a membrane, moreover, low viscosities lead to the production of defects in the membrane texture. In addition, both ambient and inert atmospheres were tested to analyze PAA solution production: inert ambient ensures a proper viscosity for electrospinning and low temperature during solution storage maintains a high viscosity for long time.

Different tests were made to understand the distinct contribution related to the PFOA removal: adsorption of the pollutant in the membrane and degradation of it.

Experiments performed confirmed that a UV lamp is necessary to accelerate and increase the degradation process of the contaminant, however, its removal is not yet satisfactory.

Further future studies may be based on the degradation contribution of each individual reaction mechanism: Fenton, oxidation via persulphates and photocatalysis.

Table of contents

INTRODUCTION	1
CHAPTER 1 NAMING CONVENTIONS, USE AND RISKS OF PFAS	3
1.1 DEFINITION OF PERFLUOROALKYL SUBSTANCES	3
1.2 USES AND APPLICATIONS	5
1.3 CHEMICAL AND PHYSICAL PROPERTIES OF PFAS	6
1.3.1 Chemical properties	6
1.3.2 Physical properties	7
1.4 HUMAN AND ECOLOGICAL HEALTH EFFECTS OF PFAS	8
1.5 PREVENTION AND REGULATORY EVOLUTION	9
CHAPTER 2 ADVANCED OXIDATION PROCESSES	11
2.1 THEORETICAL BACKGROUNDS ON AOPs	11
2.2 PHOTO FENTON PROCESS	13
2.3 HETEROGENEOUS PHOTOCATALYSIS	15
2.3.1 TiO ₂ in heterogeneous photocatalysis	17
2.3.2 Mechanism of photocatalytic degradation	19
2.4 ACTIVATED PERSULFATE OXIDATION	20
2.4.1 Mechanism of persulfate oxidation	21
CHAPTER 3 ELECTROSPINNING	23
3.1 HISTORICAL NOTES ON ELECTROSPINNING	23
3.2 THEORETICAL BACKGROUNDS	24
3.3 PROCESS DESCRIPTION	25
3.3.1 Fiber formation mechanism	26
3.3.2 Process parameters	28
3.3.2.1 Process conditions	28
3.3.2.2 Environmental conditions	31
3.3.2.3 Solution conditions	32
CHAPTER 4 MATERIALS AND INSTRUMENTATIONS	35
4.1 MATERIALS	35
4.1.1 Membrane production materials	35

4.1.1.1 Structural part	35
4.1.1.2 Catalytic part	37
4.1.2 Chemicals used in advanced oxidation processes	39
4.2 INSTRUMENTATIONS	42
4.2.1 Viscometer	42
4.2.2 Electrospinning equipment	43
4.2.3 Fourier-Transformed infrared Spectroscopy	44
4.2.4 Environmental Scanning Electron Microscope	46
4.2.5 Thermo-Gravimetric Analysis	48
4.2.6 Photoreactor setup	49
4.2.7 High Performance Liquid Chromatography – Mass Spectroscopy	51
CHAPTER 5 IMIDATION PROCESS	55
5.1 THEORY OF POLYIMIDE SYNTHESIS	55
5.1.1 Polycondensation process description	56
5.1.2 Conversion of Polyamic acid in polyimide	59
5.2 POLYIMIDE CHARACTERIZATION	60
CHAPTER 6 MEMBRANE PRODUCTION AND CHARACTERIZATION	65
6.1 PAA MEMBRANE	65
6.1.1 PAA solution	66
6.1.2 Catalyst solution	69
6.1.3 Simultaneous electrospinning	69
6.2 PI MEMBRANE	71
6.2.1 TiO ₂ characterization	73
6.2.2 Membranes TiO ₂ content	74
6.3 FIBER DIMENSION ANALYSIS	76
6.3.1 PAA – PI fiber dimension	76
6.3.2 TiO ₂ nanorods dimension	80
CHAPTER 7 PFOA DEGRADATION TESTS AND RESULTS	83
7.1 TESTING SETUP	83
7.2 EXPERIMENTAL TESTS	84
7.2.1 No Membrane + reagents experiments	84
7.2.2 Membrane + reagents experiments	87
7.2.3 Membrane + UV experiments	90
7.3 RESULTS DISCUSSION	92

7.3.1 Result comparison	93
CONCLUSIONS	97
NOMENCLATURE	101
BIBLIOGRAPHY	103

Introduction

Circular economy, reclamation of land and waterways, recycling and disposal of dangerous materials are all topics with a common objective: the protection of human well-being and the environment. It is necessary to correct the mistakes occurred in the past to make the current world safe and guarantee a future for tomorrow's generations: it is essential to support scientific research relating to the disposal and elimination of dangerous substances increasingly present in the world around us.

One of the most recent cases of groundwater contamination occurred in 2013 in Italy, where a local company released catastrophic quantities of fluorinated compounds, better known as PFAS, into the environment. These extremely stable compounds are used for the production of hydrophobic and oleophobic materials, such as non-stick coatings for pans or technical fabrics (Goretex® is an example). Following numerous studies, it has been discovered that these species are extremely toxic for both humans and the environment: they tend to accumulate in living organisms to the point of resulting in neonatal pathologies and, in the case of chronic exposure, the formation of tumors. PFAS are also recognized on a medical level as endocrine disruptors, capable of altering all the body's processes involving hormones responsible for development of behavior, fertility and other essential cellular functions.

Due to their stability, traditional and natural degradation processes (photolysis, hydrolysis, aerobic and anaerobic decomposition) are not useful for their elimination; this has led the scientific community to develop new techniques for their degradation.

One of these innovative methods is based on the use of Advanced Oxidation Processes (AOPs), which exploit the high oxidative power of some radicals to degrade the fluorinated compounds: technologies employed are based on hydroxyl, persulfate radicals and photocatalysis. Each of these oxidative processes is promoted by the use of a UV lamp.

In this thesis work we attempted to exploit various AOPs to completely degrade the most used and produced perfluoroalkylated compound in the past, perfluorooctanoic acid (PFOA). To do this, we used a photoreactor and a polymer membrane produced by electrospinning.

The work carried out, focuses on the identification of various contributions that lead first to the removal and then to the abatement of PFOA, including AOP without the help of a source of UV radiation, adsorption of the contaminant on the membrane and effect of UV rays on the final degradation.

The study is subdivided into seven chapters:

- *Chapter 1*: generic overview of perfluorinated compounds, properties, applications and effects on humans and environment.
- *Chapter 2*: review on advanced oxidation processes used in this thesis work.
- *Chapter 3*: discussion on electrospinning technique, theoretical basis and parameters which affect the process.
- *Chapter 4*: materials and instrumentations used to produce, characterize the membranes and to analyze the water samples.
- *Chapter 5*: explanation of the imidation process which leads to the polyimide formation starting from a polyamic acid solution.
- *Chapter 6*: method adopted to produce nanostructured membranes and characterization techniques applied.
- *Chapter 7*: description of the removal and degradation tests and discussion of the results obtained.

All the experimental tests are carried out at the *Polymer Engineering Group* laboratories of *Industrial Engineering Department, University of Padua*.

Chapter 1

Naming conventions, use and risks of PFAS

Starting from a general overview of fluorinated compounds, this first chapter focus on uses and negative effect on the health of living beings of PFAS. The chapter ends with a brief discussion on the PFAS regulation over the years and how world health organizations worked to limit their spread.

1.1 Definition of perfluoroalkyl substances

“Fluorinated substances” is a general, nonspecific name that describes a large number of organic and inorganic substances that contain at least one fluorine atom; these compounds could have very different physical, chemical, and biological properties¹.

A subset of fluorinated substances are *per-* and *polyfluoroalkyl substances* (PFAS or PFASs), a category of synthetic organofluorine chemical compounds where more fluorine atoms are attached to an alkyl chain.

An early definition provided in 2011 defined PFAS as aliphatic substances containing the moiety $-C_nF_{2n+1}-$ within their structure, where n is at least one².

In 2021, the *Organization for Economic Co-operation and Development* (OECD) has revised definition of PFAS as fluorinated substances that contain ‘at least one fully fluorinated methyl or methylene carbon atom’ (without any H/Cl/Br/I atom attached to it), i.e. any chemical with at least a perfluorinated methyl group ($-CF_3$) or a perfluorinated methylene group ($-CF_2-$) is a PFAS³. Any new definition in the field of perfluoroalkyl substances should be easily implementable to distinguish between PFAS and not PFAS, both by experts and nonexperts. Figure 1.1 illustrates examples that are or not PFAS^{3,4}.

According to PubChem Classification, there are over 7 million species of PFAS chemicals found globally and the number of species is still growing⁵.

One of the most common in *per-* and *poly-*fluoroalkyl substances family is PFOA, which is shown in figure 1.2.

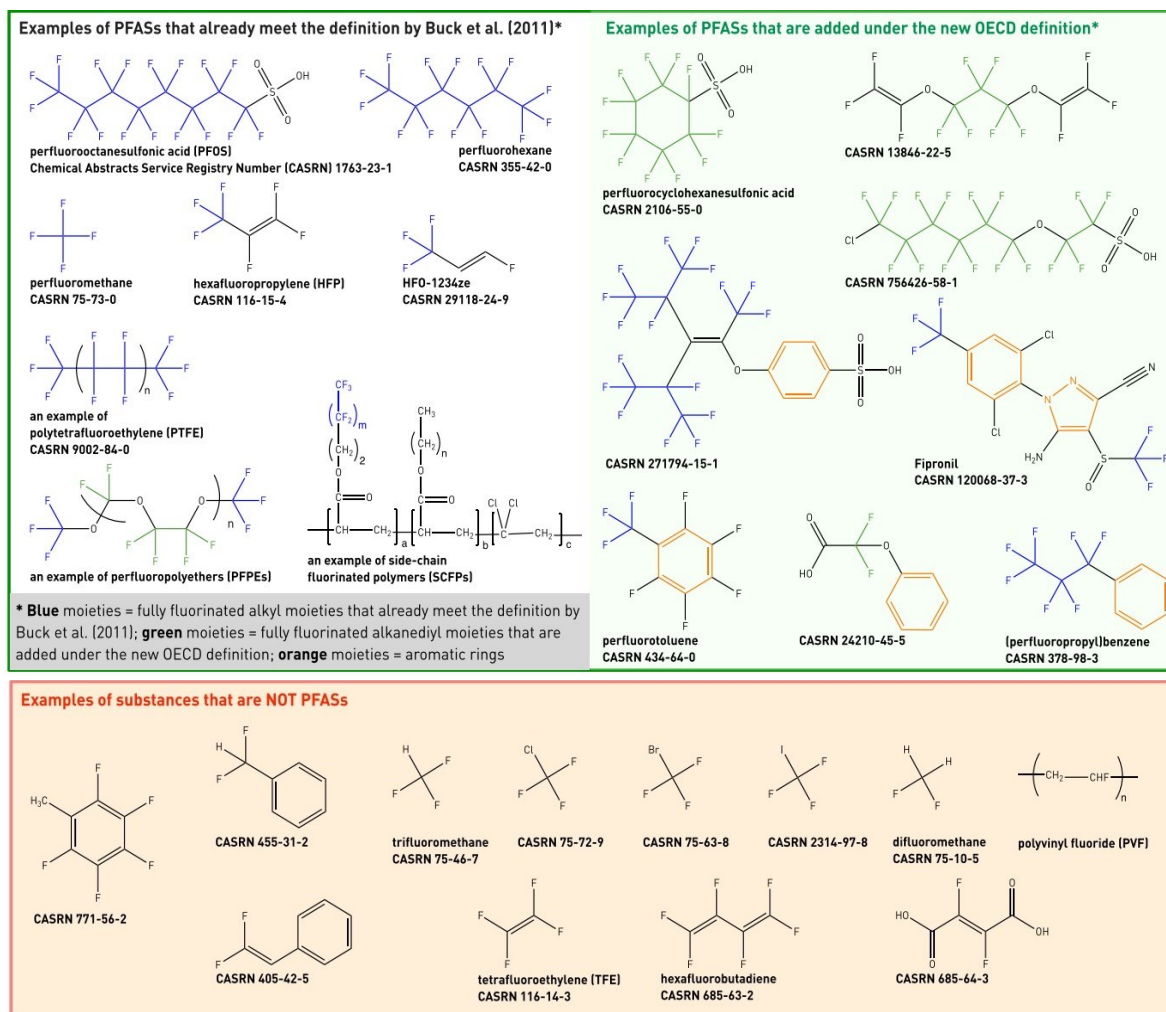


Figure 1.1. Compounds that are considered, or not, PFAS according to the OECD definition.

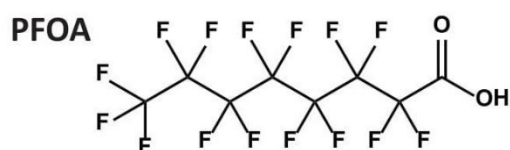


Figure 1.2. Molecular structure of PFOA.

Perfluorooctanoic acid was used as a waterproofing coating for fabrics, leather and sportswear (Nomex®, Gore-Tex®) as it gives the treated surfaces oil-repellent and hydrophobic properties. It was also used in glass etching and as foam in fire extinguishers. Its perfluorooctanoate salt was used industrially in emulsion polymerization for the production of perfluorinated polymers. Only after some years the scientific community discovered the negative effects of this compound to the human and environment.

1.2 Uses and applications

PFAS were first developed in the 1940s and have been used by numerous industrial and commercial sectors because of their unique properties: they are commonly described as persistent organic pollutants or "forever chemicals" because they do not break down via natural or traditional processes².

Thanks to the thermal and chemical stability, water and oil resistance, they can be found in:

- products for domestic use to give non-stick properties to the surfaces of pans;
- in oil processing and mining production;
- in the production of oil- and water-repellent textiles, leather, carpets, clothing, papers and packaging (Gore-Tex®);
- in the aeronautical, aerospace and defense sector to produce various mechanical components;
- in the automotive sector, to improve fuel delivery systems;
- in the production of cables and wiring, thanks to low flammability;
- in construction, to cover materials that become resistant to fire or atmospheric agents;
- in the electronic sector, thanks to its dielectric and water-repellent properties;
- in energy sector, to cover solar collectors and improve their resistance to atmospheric agents;
- in fire-fighting products, such as foams.

Figure 1.3 summarize the fields of use of per- and polyfluoroalkyl substances.

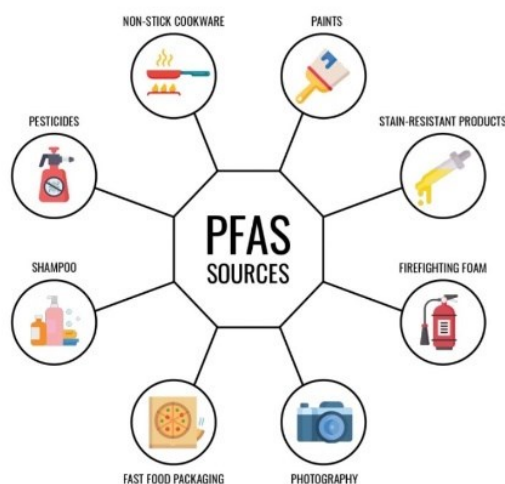


Figure 1.3. Products where PFAS is used.

As a consequence of the widespread use of PFASs (and their peculiar properties), a broad range of these substances have been detected in the environment, wildlife, and humans²: these residues have raised concerns for human and environmental health⁶.

Only at the beginning of the 21st century the environmental impact and toxicity of these products on human and mammalian life have been studied in depth.

1.3 Chemical and physical properties of PFAS

To examine the physicochemical interactions of PFAS, the first step is to understand their unique chemical structure.

All PFAS variants consist of two main components, namely a perfluorinated chain (tail) and a functional group (head) (Figure 1.4).

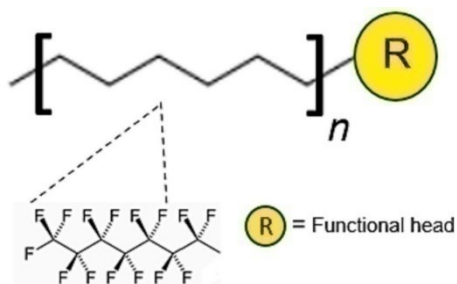


Figure 1.4. *Generic structure of a PFAS.*

A perfluorinated chain is essentially an alkyl chain with all the hydrogen atoms replaced by fluorine atoms, and the head can be a sulfonate, or carboxylate. The perfluorinated tail gives to PFAS their unique physical and chemical properties that are drastically different to their hydrogenated counterparts: fluorine is the most electronegative element in the periodic table, and when bonded to carbon, forms one of the strongest single bonds found in organic compounds with its bond dissociation energy up to 531.5 kJ/mol. This explains the much higher physical and chemical stability respect to the hydrocarbon family⁷.

As the term ‘perfluorinated’ suggests, the most abundant element in PFAS is fluorine; the atomic structure of fluorine is a key factor in shaping the chemical and physical characteristics of PFAS. In the following section, the physicochemical properties of PFAS will be introduced, describing the differences between fluorinated compounds and their hydrocarbon counterparts.

1.3.1 Chemical properties

The properties of PFAS are principally due to the unique properties of the carbon-fluorine bond. Properties such as the high electronegativity and small size of fluorine lead to a strong C-F bond, the strongest covalent bond in organic chemistry^{8,9}. The low polarizability of fluorine further leads to weak intermolecular interactions, such as Van der Waals interactions and hydrogen bonding⁸. These singular characteristics of fluorine grant numerous PFAS their dual hydrophobic and lipophobic (stain-resistant) properties, as well as surfactant properties, while also rendering them thermally and chemically stable.

Thermal stability, which measures how well a chemical withstands heat, is crucial for predicting environmental persistence of a substance. PFAAs, like PFOA and PFOS are highly stable both

chemically and thermally, resisting breakdown and oxidation. This stability is mainly due to the strong C-F bond in their fluoroalkyl tail. The exact temperatures needed to break down PFASs are actively researched; reports vary, but it appears temperatures over 1,000°C may be necessary to destroy PFASs in soil^{10,11}.

Understanding a molecule's chemical stability, much like its thermal stability, aids in forecasting how long it will persist in the environment. In the perfluorinated tail of alkyl acids, factors such as the strength of the C-F bond, the protective effect of fluorine surrounding carbon (shielding effect), and fluorine's electronegativity contribute to chemical stability. Typically, chemical species rich in electrons, known as nucleophiles, would naturally be drawn to the partial positive charge of carbon. If they could reach the carbon to form a bond, they might replace a fluorine atom with the nucleophile, potentially making the molecule susceptible to degradation. However, the relatively large size of the fluorine atoms around the carbon, compared to hydrogen, prevents this interaction from occurring¹².

This phenomenon elucidates the inefficacy of classical abatement processes like hydrolysis, wherein one or more fluorine atoms are removed from the perfluorinated tails of PFAS. Furthermore, numerous PFASs exhibit resistance to oxidative degradation processes reliant on electron loss. Additionally, PFAS demonstrate resistance to reductive processes involving electron gain. Despite fluorine's high electron affinity, it does not have vacant orbitals ready for additional electrons¹³.

1.3.2 Physical properties

PFAS exhibit weak intramolecular and intermolecular interactions primarily due to the low polarizability of fluorine atoms. This property contributes to their higher volatility and lower boiling points compared to hydrocarbon compounds of similar molecular mass¹⁴. Furthermore, the low intermolecular force also led to very low surface tension.

The absence of significant Van Der Waals forces (London dispersion forces) respect to the hydrocarbons, imparts an oleophobic characteristic to PFAS¹⁵, a consequence of fluorine's large electronegativity and small bond length. Despite the highly polarized nature of the carbon-fluorine bond, the cancellation of local dipole moments within the PFAS molecule makes it overall nonpolar and hydrophobic¹⁴. The amphiphilic nature of PFAS allows them to segregate from both polar and non-polar solvents, forming their own distinct partition¹⁶: in fact, when combined with water and an organic solvent, PFAS create a distinct fluoruous phase that resides separately from the aqueous or organic layers. A representation is provided by figure 1.5.

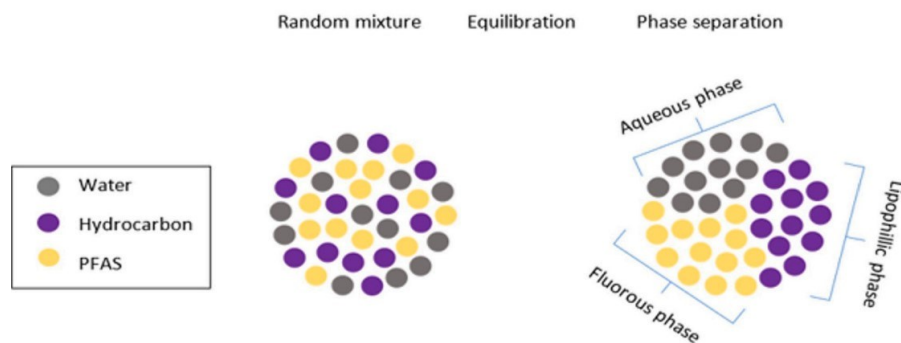


Figure 1.5 Formation of a fluorinated phase with an aqueous phase and a lipophilic phase⁴.

1.4 Human and ecological health effects of PFAS

At the time of their introduction in the 1940s, PFAS were initially perceived as inert substances^{17,18}. However, early occupational investigations observed heightened concentrations of fluorochemicals, such as perfluorooctanesulfonic acid (PFOS) and perfluorooctanoic acid (PFOA), in the bloodstream of industrial workers exposed to these compounds. Notably, these studies did not report any discernible health impacts. Nevertheless, owing to the persistent nature of PFAS, coupled with widespread environmental dissemination, there is evidence of human accumulation of these molecules, consequently posing health hazards¹⁷.

Perfluorooctanesulfonic acid (PFOS) and perfluorooctanoic acid (PFOA) are among the most extensively produced PFAS compounds and have been subject to comprehensive toxicity assessments. Consequently, PFOA, its salts, PFOS, and their salts have been designated as new Persistent Organic Pollutants (POPs) under the Stockholm Convention¹⁹ due to their well-documented histories of production and toxicity²⁰. Animal studies have demonstrated that chronic exposure to PFAS poses significant health risks, particularly in terms of immunotoxicity and carcinogenicity^{21,22}.

Furthermore, exposure to PFAS inhibits fetal growth and development and is correlated with hormonal dysfunction and various diseases such as ulcerative colitis, hypertension, and high cholesterol^{23–25}. PFAS exhibits high mobility in the natural environment and can permeate various environmental matrices, including surface water, groundwater, and soil²⁶. Additionally, PFAS is prone to bioaccumulation and is resistant to removal by conventional municipal water and wastewater treatment processes^{26,27}. Although regulations and limitations concerning PFAS have been updated in more developed regions, they remain lax in many developing countries²⁸. However, as PFAS contamination emerges as a global concern, regulations in less developed regions are expected to become more stringent.

1.5 Prevention and regulatory evolution

These fluorinated compounds reached industrial production in the early 1940s thanks to the US company *3M* and, in 1951, *3M* began selling these compounds to *DuPont* which used them for its own productions (an example is Teflon®).

Since the 1960s, companies have known about the harmful effects of perfluoroalkyl substances. For instance, *3M* was aware that PFAS caused liver enlargement in mice, rabbits, and dogs, yet they didn't disclose this information publicly. In 2001, following numerous years and a protracted legal dispute, the United States Environmental Protection Agency (EPA) acknowledged the toxicity of PFOA. Until then, no perfluoroalkylated substance had been regulated or limited.

After the scandal in the USA, the European Union established the initial concentration thresholds for PFOS and PFOA in continental waters, which are detailed in Table 1.1. Subsequently, following additional pollution incidents and extensive research, PFOS was designated as a Persistent Organic Pollutant (POP) under Appendix B of the Stockholm Convention and REACH recommended classifying these compounds as PBT (Persistent, Bio-accumulative, Toxic).

Table 1.1. PFAS concentration limit in Europe for continental water in 2006.

POLLUTANT	CONCENTRATION LIMIT [ng/l]
PFOA	300
PFOS	3000

Currently, the European Union sets the limit for PFAS in drinking water at 0.5 µg/l for all PFAS compounds combined²⁹, following the guidelines suggested by the World Health Organization. However, several countries, have established or suggested much lower limits for PFAS in drinking water compared to WHO guidelines. In Canada, for instance, the government has proposed a limit concentration of 30 ppt of combined PFAS in drinking water^{30,31}.

Chapter 2

Advanced Oxidation Processes

In this thesis project, Advanced Oxidation Processes (AOPs) are proposed for the abatement of pollutant present in water, specifically fluorinated compounds as PFOA. Every method used for the degradation of PFOA is reported below: since PFOA is a very resistant compound, in this work we tried to exploit different degradation techniques such as photo-Fenton, photocatalysis and oxidation via persulfate radicals.

2.1 Theoretical backgrounds on AOPs

Elimination of PFOA is tedious, undesirable, or practically impossible by most conventional water remediation processes owing to its stability and chemical structure, more especially related to the strong C–F bonds. Therefore, there is an urgent need to find effective technologies for the defluorination and complete mineralization of the pollutant.

One of the most common water treatment technologies is adsorption on powder or granular activated carbon, which is then followed by incineration of spent sorbent: a limited efficiency of physical purification methods and biodegradation imposed significant interest in typical chemical methods of decomposition of pollutants.

Various wastewater treatment technologies (adsorption^{32,33}, coagulation³⁴, nanofiltration³⁵, membrane elimination processes³⁶, photochemical decompositions³⁷) have been widely investigated for the PFOA remediation, however, there are some drawbacks for most of the processes indicated^{38,39}: some of the techniques are multi-step with a large consumption of reactants^{40,41} and in some cases they could lead to a considerable production of secondary pollution^{42,43}. The development of an efficient abatement technique for PFAS is still a goal of various research groups.

The recent decades have brought an increasing interest in methods based on the use of free radicals as unusual reagents: the most exploited in this sense is the hydroxyl radical OH \cdot .

In 1987⁴⁴ was introduced the term Advanced Oxidation Processes (AOP) for water treatment processes performed at room temperature and based on the in-situ generation of a powerful oxidizing agent, such as hydroxyl radicals, at a sufficient concentration to effectively decontaminate waters from different pollution agents.

Radical species are very reactive and unstable due to the unpaired number of electrons in the external orbital: to achieve stability, they try to interact with electron-donor compounds and in this specific case these compounds are organic contaminants. Among radical species, hydroxyl and sulfate radicals are the most considered for this type of processes as they possess a very high redox potential. Despite having an extremely short average lifetime, they are able to oxidize functional group in an efficient way, causing the chain fragmentation of contaminants. Even though hydroxyl group is the most widely used and known radical, several studies⁴⁵ stated that it has a weak ability to attack and decompose fluorinated compound, consequently, in this work it is coupled with other radicals to maximize the oxidation of pollutants.

In the advanced oxidation process, radicals are produced through a chemical reaction while in the case of photocatalytic processes, photoexcited species are generated: both species can potentially attack the C–C and C–F bonds of the PFOA thus lead to its complete degradation and mineralization to F^- and CO_2 . These reactive oxidant species are electrophilic (i.e. they are attracted to high electrostatic potentials) and the highest potential in the PFOA molecule is situated near the carboxylic head, decreasing in direction of the tail: for this reason, decarboxylation is suggested to be the first step in PFOA photodegradation⁴⁶.

Figure 2.1 present the electrostatic potential of a PFOA molecule.

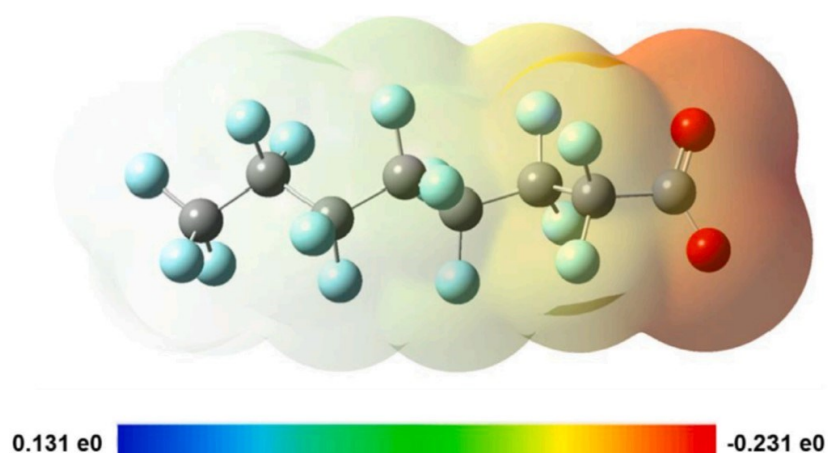


Figure 2.1 Electrostatic potential map of a PFOA molecule⁴⁶.

The different type of radical activation is the basis of advanced oxidation processes; consequently, we could refer to photolysis, sonolysis as systems that use chemical reagents, or to processes that seek a sharing of multiple modalities such as photocatalysis and Photo-Fenton processes.

The presented research work deals with the photo-degradation of PFOA caused by the combination of UV radiation, hydroxyl, sulfate, persulfate radicals and catalyst presence (TiO_2).

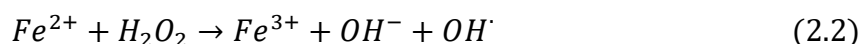
2.2 Photo Fenton process

John H. H. Fenton, in 1876, almost accidentally discovered that some salts of transition metals (in particular Fe(II), Cu(I) and Co(II) salts) could catalyze the production of hydroxyl radicals through the hydrogen peroxide breakdown. Fenton process is defined as the production of hydroxyl radicals catalyzed by transition metals.

Initially this technique was used for organic compound synthesis and analytical chemistry, but only in 1930' scientists understood the various fields of application of Fenton's discovery. From then, its use for degradation of polluting compounds, mainly organic ones, increased so much that it is still in the present one of the most exploited water treatment methods. The degradation process takes place thanks to the action of OH^\cdot and H^\cdot radicals, which reacts in an aggressive and non-selective way towards the contaminating species present in the solution. Hydroxyl radicals have one of the highest redox potential values (2.7 V) and is one of the highest if compared with other species. The generation of OH^\cdot follows reaction (2.1) that combines UV-rays (visible rays in less contribution) and H_2O_2 contribution.



If ferrous ions are added to the reaction environment, they can lead to the formation of hydroxyl radicals by the reaction of Fe^{2+} with hydrogen peroxide (2.2).

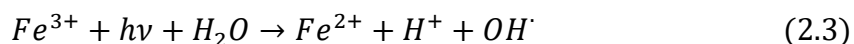


Unfortunately, the Fenton process alone is considered ineffective for PFOA degradation, due to the insufficient quantity of hydroxyl radicals (OH^\cdot) produced upon reaction with H_2O_2 ^{47,48}. To address this shortcoming, researchers have introduced the application of energy from sunlight or artificial source to assist the process for the generation of OH^\cdot species. The photo-Fenton process is described as a reaction between Fe(II) and H_2O_2 initiated by the UV light which generates OH^\cdot radicals. Subsequently the hydroxyl radical is ready to react with the organic pollutant causing its abatement^{49,50}.

The introduction of light is not only accompanied by an acceleration of the process but also by a recycling of ferrous ions (2.3): the light stimulates the reaction of Fe^{3+} with water, new Fe^{2+} ions are introduced into the system (positive aspect for reaction 2.2), more OH^\cdot are generated and the oxidation of pollutant is accelerated.

Therefore, the Photo-Fenton process consists of three main steps:

- Photo-reduction of Fe^{3+} to Fe^{2+} .
- Fenton reaction, production of hydroxyl radicals.
- Foul up component oxidation.



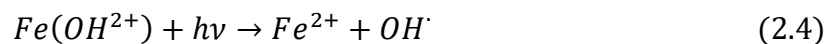
The most often occurring reactions of OH^\cdot with organic pollutants involve an addition to unsaturated carbon-carbon bonds, a substitution to aromatic rings, abstraction of hydrogen atom from target molecule or mono-electronic oxidation.

Production of OH^\cdot radicals and Fe^{2+} ions are determined both by definite radiation with an adequate wavelength (between 180 and 400 nm) and from the concentration of H_2O_2 in solution; the concentration of hydrogen peroxide is a crucial parameter because, if it is in excess, recombination of free OH^\cdot radicals occurs and they are no more available for the contaminant degradation.

The photo-Fenton process is greatly influenced also by pH conditions and operating temperature.

A pH value between 2 and 4 is optimal because recombination of radicals are limited and these species remain active for more time⁵¹. At higher pH values, Fe^{2+} ions are reduced to Fe^{3+} , resulting in their deactivation associated with iron oxide precipitation and the reduction of hydroxyl radical concentration. Too low pH values, instead, promote excessive production of H^+ ions inhibiting the generation of OH^\cdot radicals in reaction (2.3); at pH lower than 2, the species most present are Fe^{3+} ions which absorb UV radiation in a restricted region, which translates in less chance of reacting according to reaction 2.3.

At optimal pH, hydrolysis reaction of Fe^{3+} ions happens and $\text{Fe}(\text{OH})^{2+}$ ions are formed: these ions are characterized by a broad region of UV-rays absorption and, once irradiated, they generate Fe^{2+} and OH^\cdot according to the reaction (2.4):



This reaction represents in the best way the difference between the traditional Fenton process and the Photo-Fenton one: following reaction (2.4), it can be noted that hydroxyl radical production occurs in the absence of hydrogen peroxide, and Fe^{2+} is formed by Fe^{3+} reduction under UV radiations. The real advantages concern the achievement of a faster pollutant degradation, less consumption of hydrogen peroxide and Fe (II) precursor since Fe (II) species are not trapped like Fe (III).

The optimal operating temperature for these tests is between 20°C and 30°C: ambient temperature is sufficient. However, the temperature must never cross the threshold of 57°C because, H_2O_2 volatilizes easily, with the consequent decline in process performance.

Iron ions availability in Fenton reaction occurs mainly in two ways: homogeneous process (salts dissolution in water that must be treated) or heterogeneous process (with the adsorption of ions on a solid matrix). The first guarantees a greater interaction between contaminated water and reactive particles but an additional water treatment process step is required. In the second one there is not the necessity of further treatments but there is not a total interaction between the entire water volume and the ions.

In literature, there is no specific technique for abatement of fluorinated compounds in water that exclusively exploit Fenton reactions since they were born for the degradation of organic compounds such as phenol or formaldehyde. The objective here is to combine the action of different methods and increase the oxidation reactions efficiency by supplying the system with a greater quantity of oxidizing agents, including the OH^\cdot radicals coming from the Photo-Fenton processes.

Hence, iron ions and hydrogen peroxide quantity are weighted following experiments on formaldehyde in water (Qingfeng Zhou, 2017). Under the most favorable conditions of their study, they used a Fe^{2+} concentration of 25 mg/L, with a relative amount of H_2O_2 equal to 100 mg/L.

These values are taken as a starting point for the treatment of PFAS under analysis, and they can be modified to optimize the oxidation effects.

2.3 Heterogeneous Photocatalysis

In recent years, interest in photocatalysis has focused on the use of semiconductor materials as photocatalysts for the removal of organic and inorganic species from aqueous or gas phase systems: it can be defined as the acceleration of photoreaction in the presence of a catalyst⁵².

Generally, two or more phases take part in a photocatalytic reaction, a light source and a semiconductor material are used to promote the photoreaction: a photocatalyst exploits the energy of UV radiation from sunlight or artificial light to decompose different substances including organic materials, organic acids, pesticides, dyes and inorganic molecules^{53–55}. When a semiconductor photocatalyst absorbs light photon of energy greater than or equal to its band gap, the unpaired electron in the outermost orbital is excited and from the valence band it can shift to the conduction band.

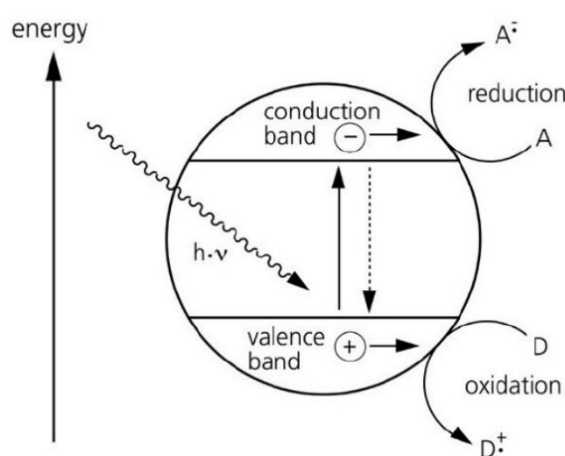


Figure 2.2 Representation of a photocatalytic process on a general catalyst particle.

In this way, a positive hole is generated in the valence band and a negative charge in the conduction one. The holes attend to the production of hydroxyl radical useful for breaking down organic compounds and the electrons participate to reduction and oxidation reactions forming radicals superoxide species⁵².

Figure 2.2 represents a redox system that occurs on the semiconductor's surface where the electronic excitation, makes the semiconductor both an electron donor (path of compound A) and a negative charges acceptor (path of compound D).

However, the involved charges can also follow other paths by recombination on the catalyst matrix releasing thermal energy: these phenomena decrease the efficiency of the process. To understand which reaction a compound can undergo (path A or D), flat band potential (V_{fb}) and redox potential of species absorbed (V_r) are defined: the former describes the characteristic energy of holes and electrons while the latter is the tendency of a species adsorbed to either be reduced by accepting electrons or oxidized by donating electrons⁵⁶.

Hence, situations are two:

- $V_r > V_{fb}$ (conduction band): absorbed species reduction by electrons present in the band;
- $V_r < V_{fb}$ (valence band): absorbed species oxidation by the gaps.

In photocatalytic oxidation of pollutants, gaps (h^+) react with water and hydroxide ions forming hydroxyl radicals by oxidation reactions, as follows:



instead, reaction between electrons (e^-) of conduction band and oxygen generates superoxide radical.



Species generated in this way participate in other reactions that lead to other radical species formation, promoting the organic compound's degradation.

The band gap threshold of a particular catalyst must be known to determine the precise wavelength that photon must have to activate the process: it is the minimum energy to be overcome to initiate redox reactions. Reaction (2.8) is employed to compute the wavelength to make the catalyst active:

$$\lambda = hc/E \quad (2.8)$$

where λ is the wavelength, h the Planck constant, c the vacuum speed light and E the photon's energy.

The main semiconductor catalysts used in photocatalytic processes are shown in Figure 2.3, in which purple and light blue indicators stand for the highest value of the valence band and the lowest value of the conduction band, respectively.

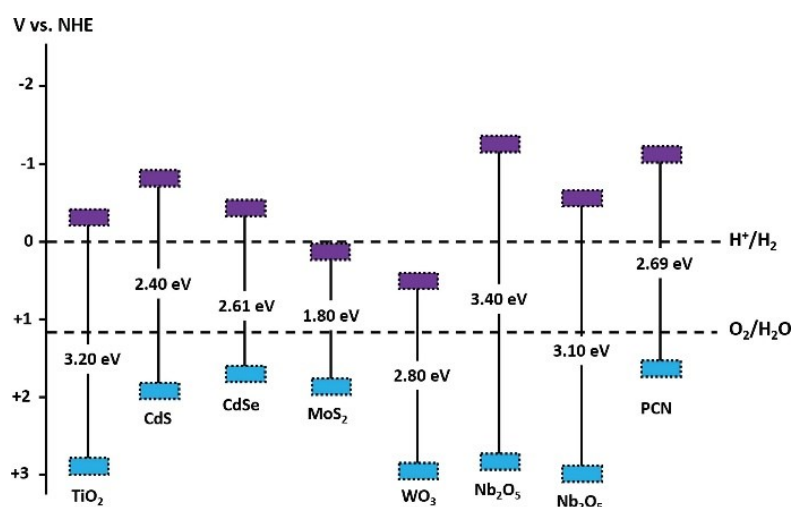


Figure 2.3 Main photocatalysts band gap values⁸⁶.

Ideally, a photocatalyst should possess the following properties: photoactivity, biological and chemical inertness, stability toward photo-corrosion, suitability for visible or near UV light energy harnessing, low cost and lack of toxicity⁵⁷. TiO₂ is characterized by thermal and chemical stability, high ultraviolet absorption and high stability which allow it to be used in different applications.

Finally, low cost, high availability and non-toxicity are added to a discrete band gap value equal to 3.2 eV (shows in figure 2.), which corresponds to an ultraviolet wavelength of 388 nm.

Only drawback concerns the almost no activity under the sunlight action: to overcome this issue, doping with transition metals (for example, vanadium, chromium and iron) or non-metals (carbon, nitrogen and sulfur above all) has been proposed for shifting the absorption band toward the visible region⁵⁶.

2.3.1 TiO₂ in heterogeneous photocatalysis

Here is reported the mechanism of activation and promotion of abatement processes of an organic compound containing TiO₂ following the past research of Madras and Vinu (2008). As mentioned above, the photocatalytic process involves the formation of holes in the valence band (h^+_{VB}) and electrons in the conduction one (e^-_{CB}), after photon irradiation on the semiconductor (reaction 2.9).



Photon energy must be greater than or equal to the band gap (in this case, 3.2 eV) to be effective. Thus, because of irradiation, the TiO_2 particle can behave either as an electron donor or acceptor for molecules in contact with the semiconductor. An event that can limit the photocatalysis efficiency is the electron-hole recombination, which releases the absorbed light energy as heat, with no chemical reaction taking place. If recombination does not happen, electrons and holes can participate in redox reactions with adsorbed species, remembering that the valence band hole is strongly oxidizing and the conduction band electron is strongly reducing⁵².

Figure 2.4 shows the photocatalysis mechanism on a Titanium dioxide particle once irradiated by light.

Gaps in the valence band can be filled by hydroxyl groups present on the catalyst surface (2.10). Also, electrons of the conduction band can be affected by these charges (2.11) or be trapped by the depth of this band (2.12).

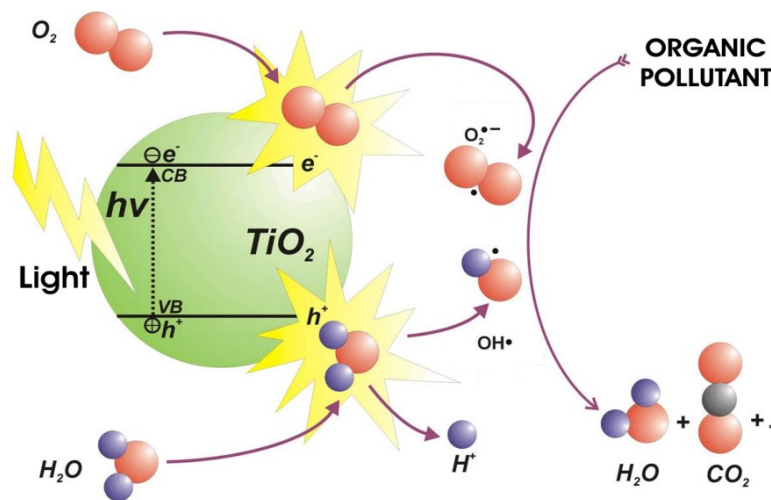
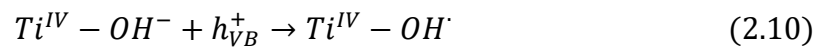
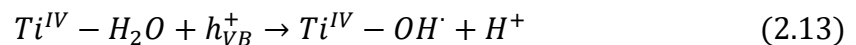


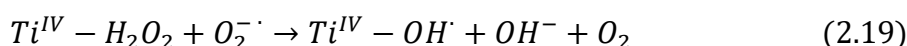
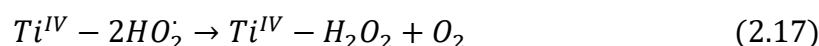
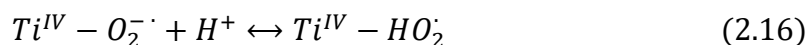
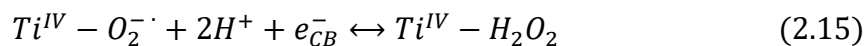
Figure 2.4 Semiconductor excitation by band gap illumination⁵².

The reaction of electronic lacunae with water leads to hydroxyl radical generation (2.13):



On the other hand, the reaction between electrons and oxygen forms a superoxide radical (2.14): this prevents the electron from recombining with the hole and results in an accumulation of oxygen radicals that can also participate in degrading contaminants in solution^{58,59}.

Radical species thus originated, are involved in other reactions that generate other radical species, i.e. hydroperoxide radical (HO_2^\cdot), hydrogen peroxide and molecular oxygen (2.15-2.19):



Since active radical species are present in the reactive system, reagents are absorbed on the catalyst surface. If the contaminant is an organic compound S, it can follow one of these reactions.

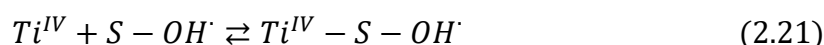
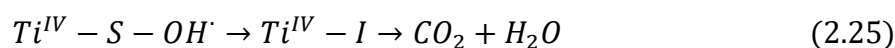
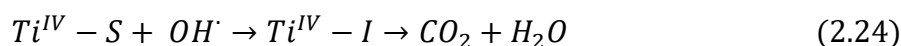
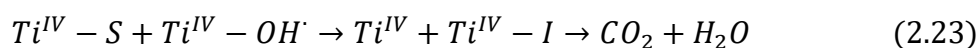
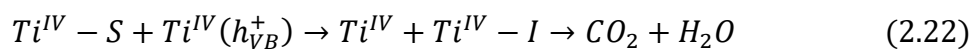


Photo-oxidation of reducing agent can occur through two ways: direct attack of $h^+_{(\text{VB})}$ (reaction 2.22), otherwise through OH^\cdot attack (reaction 2.23).



Published work indicate that heterogeneous photocatalytic process involves at least five separate reaction steps⁶⁰ and include (1) diffusion of reactants to the surface of semiconductor, (2) adsorption of reactants onto the surface of semiconductor, (3) reaction on the surface of semiconductor, (4) desorption of products from the surface of the semiconductor and (5) diffusion of products from the surface of the semiconductor.

In this way, organic contaminant will be degraded in CO_2 and H_2O through intermediate stage I and then catalyst active sites are set free by desorption of component I (reaction 2.26).

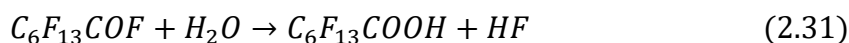
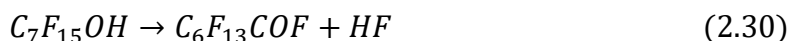
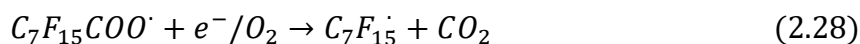


2.3.2 Mechanism of photocatalytic degradation

The mechanism for PFOA photocatalytic degradation has been proposed in various works of literature. In most cases, shorter-chains PFCA's are generated as intermediates before arriving to the complete mineralization⁶¹.

During the photocatalytic process, photogenerated holes destabilize PFCAs into perfluorocarboxylic radicals by direct electron transfer⁶² (2.27). This reaction is followed by the cleavage of the carboxylic head by a photo-Kolbe-like decarboxylation (2.28), creating a C_7F_{15} radical⁶³.

This radical is easily attacked by the OH^\cdot of the photocatalyst and transformed into thermally unstable alcohol, $C_7F_{15}OH$ (2.29). This unstable species undergoes HF elimination to form $C_6F_{13}COF$ (2.30) which further lost the CF_2 molecule upon hydrolysis to form PFHpA (2.31). The process proceeds further with decarboxylation and elimination of F^- , resulting in the formation of shorter-chain PFCAs until complete mineralization (Li et al., 2020a). The final degradation product is CO_2 and F^- ions⁶¹.



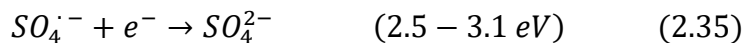
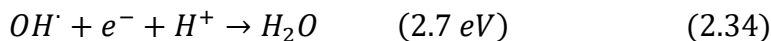
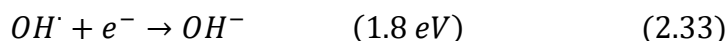
2.4 Activated Persulfate oxidation

The last technique used for PFOA abatement is the activated persulfate oxidation. It is a modality analogous to Fenton, the only difference is that reactive radicals are not hydroxyl radicals but persulfate and sulfate groups. Persulfate has attracted great attention as an alternative to H_2O_2 for AOPs due to its high redox potential (2.5V~3.1 V) and longer lifetime than OH^\cdot ⁶⁴⁻⁶⁸.

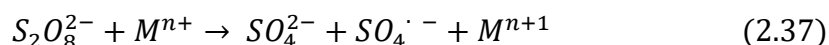
Persulfate anion ($S_2O_8^{2-}$) is a strong oxidant (redox potential of 2.0 V) which can easily break down into sulfate anions (2.32).



This step is crucial because, despite being a good oxidant, its potential redox value does not exceed the one of hydroxyl ions that are not the most powerful oxidants against fluorinated components. However, two sulfate ions are formed for each persulfate ion and, when activated, they both possess extremely high redox potential, according to reactions (2.33-2.35) in neutral conditions.



$S_2O_8^{2-}$ can be activated with various activation approaches, employing heat, microwave, ultraviolet, iron, or ultrasound as activation technique: generally, these methods are based on homolysis of peroxide bond using (2.36) or through redox processes with electron-donor species such as e^- coming from hydrolysis or metals as Fe^{2+} , similar to Fenton reaction (2.37).



Thanks to their oxidizing properties, stability and independence from pH conditions, sulfate and persulfate radicals are required to decompose organic compounds. Several studies asserted their efficiency in the degradation of perfluorooctanoic acid, PFOA, and similar shorter chain compounds. In this thesis work, the main objective is to activate the persulfate through UV radiation and analyze the fluorinated pollutant decomposition, also making use of the the degradation techniques proposed above (Fenton and Photocatalysis).

The molecule that allows the availability of reactive sulfate radicals is potassium persulfate, $K_2S_2O_8$, briefly explained in Chapter 4. In aqueous solution it forms two potassium ions ($2K^+$) and one persulfate ion ($S_2O_8^{2-}$) fulcrum of subsequent activation reactions.

2.4.1 Mechanism of persulfate oxidation

The oxidative decomposition process of PFOA by persulfate radicals is proposed in figure 2.5⁶⁹⁻⁷¹.

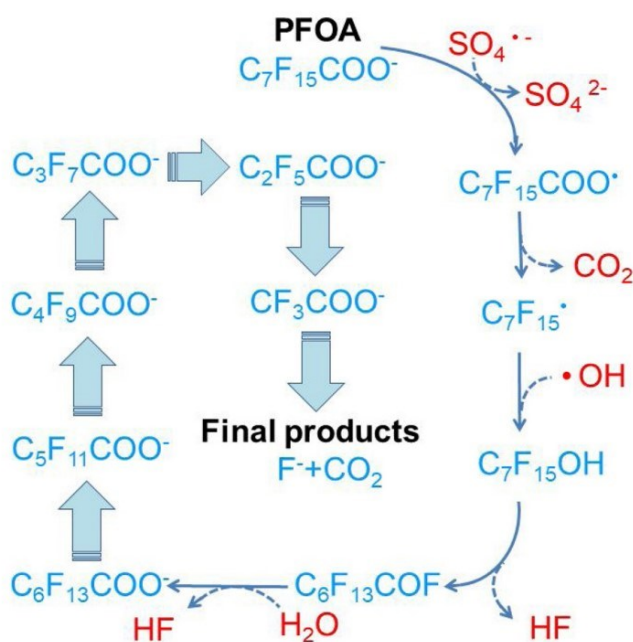
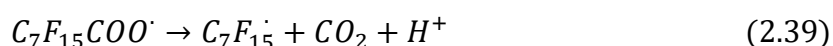
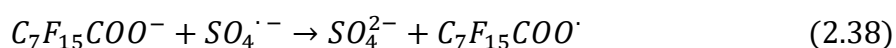
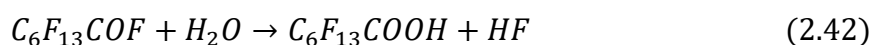


Figure 2.5 Proposed decomposition pathway of PFOA with persulfate oxidation⁶⁹⁻⁷¹.

The fluorinated molecule in water releases H^+ ions, leaving the carboxylic functional group with a pendent negative charge, $C_7F_{15}COO^-$. UV-rays meet the persulfate radicals at a suitable wavelength, (254 nm is usually used as the radiation wavelength for persulfate⁷²), to homolytically split the central peroxide bond. PFOA molecule body is very stable and C-F bond has an extremely high bond strength (3.6 eV), which is difficult to dissociate with SO_4^- . One of the two newly generated sulfate ions oxidized PFOA into alkyl radicals followed by decarboxylation (2.38-2.39): the same decarboxylation mechanism was reported for different heterogeneous persulfate activation systems^{73,74}.



The alkyl radicals formed can react with hydroxyl radical producing unstable perfluorinated alcohol such as $C_7F_{15}OH$ (2.40). The instability of this product brings it to lose a hydrogen and a fluorine ions (2.41). Subsequently, a hydrolysis reaction takes place releasing another fluorine ion to produce a shorter perfluorocarboxylic acid chain formed by seven carbon atoms⁷⁴ (2.42).



The PFOA decomposition path pass through the formation of small perfluoroalkyl chains such as perfluoroheptanoic acid (PFHpA, $C_6F_{13}COOH$), perfluorohexanoic acid (PFHxA, $C_5F_{11}COOH$), perfluoropentanoic acid (PFPA, C_4F_9COOH) and perfluorobutanoic acid (PFBA, C_3F_7COOH)⁷⁵ till the complete mineralization.

Chapter 3

Electrospinning

This section delves the fundamental aspects associated with the production of nanofibers through electrospinning. Nanofibers are situated within the realm of nanotechnology, which explores materials with dimensions equal to or less than hundreds of nanometers. To attain these highly distinctive morphological characteristics, state-of-the-art methodologies are employed, which have garnered prominence across numerous scientific disciplines in recent decades. Electrospinning process is one of these methodologies, which plays a significant role in this thesis. This chapter delineates the key elements of this technique, encompassing process variables that can be modified to optimize the structure and performance of the final product.

3.1 Historical notes on electrospinning

The term "electrospinning" refers to the process of using an electric field to spin a polymer solution, with varying degrees of density. This method was initially observed by Rayleigh in 1897 and further studied by Zeleny in 1914. The early solutions examined included cellulose acetates in acetone and monomethyl ether of ethylene glycol. The first patent related to this, dating back to 1934 and belonging to Anton Formhals, described the initial experimental setup for producing polymeric filaments using electrostatic force⁷⁶.

Subsequent efforts aimed to enhance the process: in 1952, Vonnegut and Neubauer developed an electrical atomization device capable of producing highly electrified uniform flows of droplets with a diameter of 0.1 mm; in 1955 Drozin investigated dispersion in aerosols of various liquids due to high potentials and in 1966, Simons patented a machine for producing lightweight non-woven fabric through electrospinning. Geoffrey Taylor's contributions were pivotal for establishing the theoretical foundations of electrospinning. Between 1964 and 1969, Taylor modeled the shape of the cone formed by the flow of fluid droplets under the effect of a magnetic field, a condition known as *Taylor's cone* which will be further explored in the following paragraph. In 1971, Baumgarten constructed a machine for electrospinning acrylic fibers with a diameter of 0.05 micrometers.

In the early 1990s, research groups demonstrated that many organic polymers could be electrospun into nanofibers, leading to a continuous increase in publications on electrospinning since then.

Initially, the procedure described above experienced limited success due to various gaps, including limited yield, inadequate mechanical properties of the product and non-homogeneous distribution of the spun fiber diameters. However, in recent years, technological advancements have mitigated these issues and facilitated the development of electrospinning on an industrial scale, making it one of the most widely used techniques.

3.2 Theoretical backgrounds

Electrospinning is one of several methods used for producing nanofibers, alongside melt spinning, wet spinning, dry spinning, and gel spinning. It involves applying a high electric field potential to generate a solution flow from a tubular needle. The resulting fibers have nanometer-scale diameters and exhibit properties such as high surface area, porosity, strength, and weight, which vary depending on the polymer used. The range of polymers suitable for electrospinning is extensive, encompassing traditional spinning polymers like polyamides, polyolefins, and polyesters, as well as conductive and photonic polymers. Additionally, this technique enables the modification of polymer properties by incorporating insoluble particles into the polymer nanostructure during the drying process.

After the electric field is applied to the surface of the polymeric solution, charges are generated, which are held at the tip of the needle due to the action of surface tension. The mutual repulsion between these charges creates a force counteracting the surface tension. Therefore, increasing the intensity of the electric field leads to the elongation of the hemispherical surface and the formation of the "Taylor's cone," as depicted in Figure 3.1.

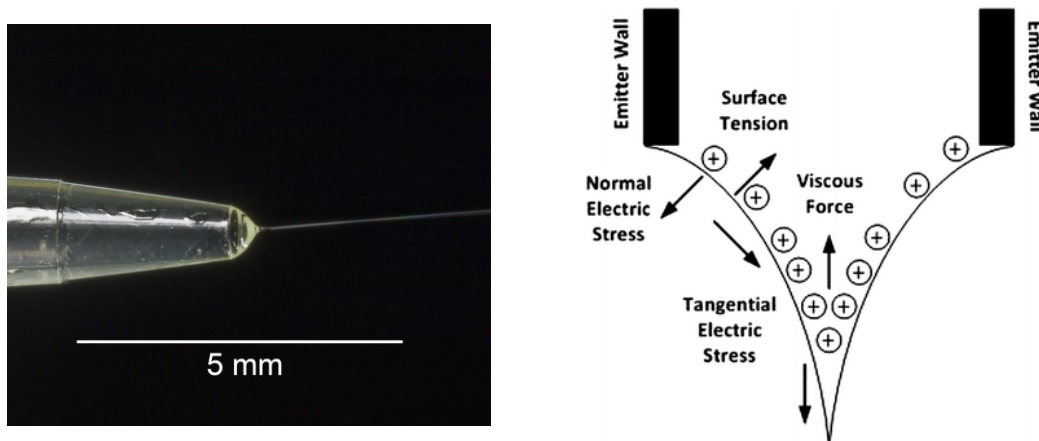


Figure 3.1 Taylor's cone photo and forces acting on it^{87,88}.

When the repulsive force overcomes the surface tension (in absolute value), a solution jet emerges from the Taylor cone tip and its path is determined by the electric field to which it is subjected. As the fluid jet travels from the needle orifice to the manifold, it undergoes thinning due to solvent evaporation before depositing randomly onto the metal collector.

Several factors influence the ultimate outcome, they can be categorized as follows:

- Properties of the polymer solution (conductivity, viscosity, and surface tension);
- Process parameters (such as solution flow rate, electric voltage at the tip, needle-manifold distance, and needle hydrostatic pressure);
- Environmental conditions (including temperature and relative humidity).

By adjusting these variables, it is feasible to optimize the process, resulting in fibers with a high surface area-to-volume ratio. Under optimal conditions, the best performance is achieved in terms of mechanical strength, flexibility, and functionality.

3.3 Process description

The system which describes the electrospinning process is quite simple and is composed by⁷⁷:

- A syringe containing a polymer solution and equipped with a tubular needle
- A volumetric pump
- A high potential current generator (kV)
- A metal collector.

Once the syringe is filled with a known amount of solution and the needle is inserted, the pump mechanically pushes the solution out through the needle's terminal orifice. This pump facilitates the regulation of the fluid flow. Subsequently, a droplet exits from the needle, acting as the first electrode, waiting for the voltage to be increased so as to overcome the surface tension and viscous forces. This process forms a fluid jet directed towards the second electrode, the metal collector. The grounding of the collector ensures that any residual charges in the fibers are discharged upon contact between them.

As the electrically charged flow progresses, it accelerates and gradually diminishes, leading to solvent evaporation. The resulting fibers are deposited on the collector and solidify, forming an interconnected network. To effectively deposit dehydrated fibers on the collector, several parameters must be assessed, including the appropriate solvent for polymer solubilization, the distance between the needle and manifold, and the environmental temperature and relative humidity. Each of these parameters will be examined individually in the subsequent paragraph.

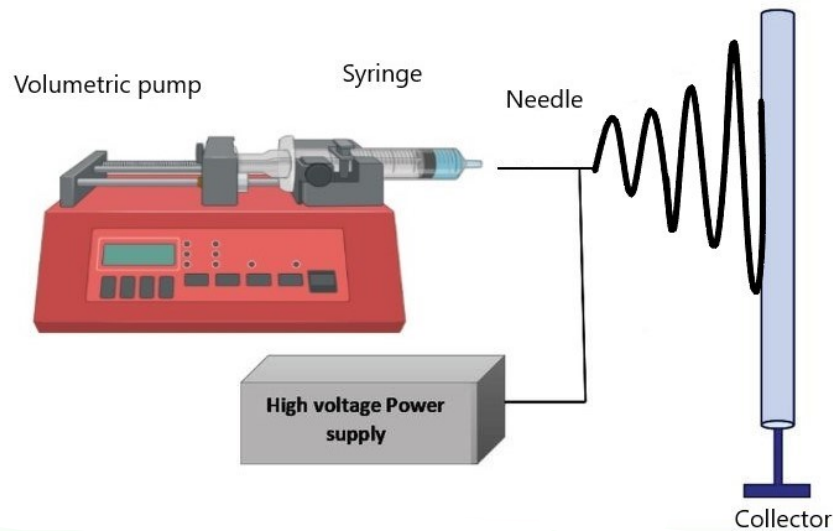


Figure 3.2 *Generic electrospinning setup.*

Figure 3.2 illustrates a typical electrospinning setup.

3.3.1 Fiber formation mechanism

To comprehend the mechanism of the process, it is essential to evaluate forces. As previously noted, the process initiates when the force induced by the electric field overcomes the solution's surface tension, leading to the formation of a jet that extends from the needle to the collector. In past research work, four distinct stages have been outlined to elucidate this mechanism: jet formation, segment elongation, instability zone, solvent evaporation, and filament solidification^{78,79}. Each stage will now be discussed in greater detail.

I. Jet formation

The initial step involves determining the desired solution flow rate by adjusting the pump setting. This allows for the formation of drops, with gravity and surface tension being the only active forces at this stage.

When a potential difference is applied between the two electrodes, both gravity and the electric force counteract surface tension, leading to a reduction in drop diameter. This reduction is balanced at the tip of the needle without the drop falling.

As the voltage is further increased, the drop diameter continues to decrease until it becomes unstable (Figure 3.3). Consequently, a charge separation occurs within the drop.

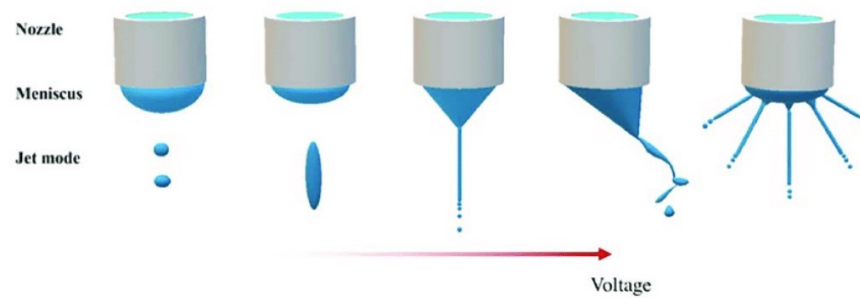


Figure 3.3 Jet mode in the electrospinning process. Increasing the voltage the jet becomes more and more unstable.

Since the needle works as the positive electrode, it attracts negative charges within the inner part of the droplet, while positive charges accumulate on the surface. The droplet remains stable as long as the inward force of surface tension, which tends to keep the negative charges together, surpasses the repulsive force generated by the accumulation of positive charges on the surface, which acts in the opposite direction. This configuration facilitates the movement of charges along the electric field.

The Rayleigh condition establishes a critical charge threshold, beyond which the droplet begins to assume a conical shape, giving rise to the so-called "Taylor cone." The angle formed by the cone with the vertical line is 49.2° and remains stable due to the balance between solution surface tension and electrostatic force. When the repulsive force exceeds the surface tension, a solution filament forms, directed towards the metal collector.

II. Segment elongation

After surpassing the critical voltage threshold, a jet is formed, driven along the electric field lines towards the second electrode. The speed of this jet rises in tandem with the distance of the Taylor cone, resulting in a reduction of fiber diameter due to both stretching and solvent evaporation⁸⁰. During this phase, the jet remains stable due to entanglements among polymer chains.

III. Instability zone

Following the stability phase, the jet initiates oscillations and adopts an undulating pattern. This behavior is also called *whipping instability* and leads to an expansion in surface area, resulting in a reduction of surface charge density. Assorted studies have investigated the flow of casting within the electric field. Findings indicate that filament movement takes place within a conically shaped region, where fibers are symmetrically distributed around the linear casting axis.

In Figure 3.4, various filament modes are depicted, including the instability zone. In this phase occurs the significant reduction in diameter due to the combined effects of multiple forces: gravity, surface tension, viscoelasticity, electrostatic forces, environmental interactions, and Coulomb forces.

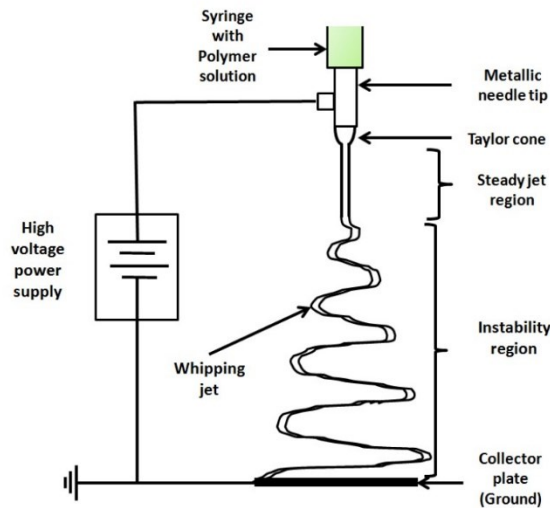


Figure 3.4 Different jet phases during electrospinning process.

IV. Solvent evaporation and filament solidification

Solvent evaporation takes place along the path between the needle and the collector, resulting in the deposition of dry fibers on the collector without any solvent residue. In cases where process conditions are suboptimal, complete evaporation may not occur, leading to the presence of solvent on the collector, which can dissolve the fibers. To prevent this, various factors need consideration, such as the distance between the needle and the collector and the vapor pressure of the solvent, as these factors greatly influence the rate of evaporation and the diameter of the fibers. Additionally, environmental factors like temperature and relative humidity can contribute to efficient separation of the solvent from the fibrous matrix.

3.3.2 Process parameters

Below are detailed all the conditions that require attention during the electrospinning process. They are categorized into three groups: process conditions, environmental conditions, and solution conditions.

3.3.2.1 Process conditions

In this category are presented potential difference, flowrate, needle diameter, collector type and needle-collector distance.

▪ Potential difference

The potential difference induced by the generator results in the movement of charges on the liquid's surface, generating a specific electrostatic force. When the voltage exceeds a critical threshold, the induced electrostatic force overcomes the surface tension of the solution, leading to the formation of the Taylor cone. As a result of electrostatic repulsion and the electric field, the liquid jet is elongated and thinned, demonstrating that voltage directly affects the diameter of the fibers. Specifically, higher voltage values create a stronger electric field, resulting in increased stretching and finer fibers. Conversely, when the potential difference is exceedingly high, the jet experiences greater acceleration, significantly reducing the travel time between the needle and collector. Consequently, the elongation time of fibers decreases as the solvent evaporates, resulting in a product with larger diameters.

▪ Flowrate

Flowrate denotes the quantity of solution processed in the electrospinning procedure within a specific timeframe. Increasing the flowrate enhances the available solution volume, consequently affecting the diameter of the fibers produced. To maintain a stable fiber flow, the flowrate dispensed by the needle must match that consumed by the electric field, accounting for the initial Taylor cone formation: thus, voltage and flowrate are closely interconnected (see Figure 3.5). When operating at high flowrates, the volume of solution deposited is greater, necessitating more time for solvent evaporation. Insufficient drying time (i.e. needle too close to the manifold) may result in fibers touching the collector containing solvent, which can potentially dissolve the previously formed structure, leading to significant repercussions in the final result.

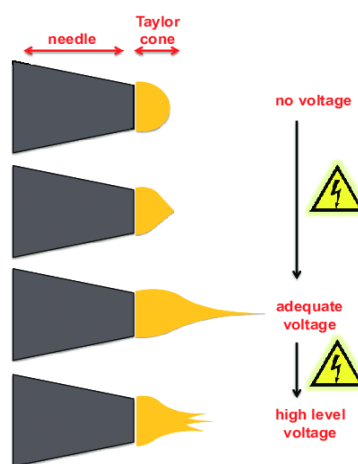


Figure 3.5 Effect of voltage to a set flowrate. Increasing the voltage, repulsive forces overcome the surface tension⁸⁹. The application of an excessive voltage causes a multi-jet situation.

▪ Needle diameter

The size of the needle diameter influences the resulting fiber size; using a relatively small internal diameter needle leads to a reduction in the produced fiber section. This phenomenon occurs because the increase in surface tension within the solution at the needle's end is more pronounced with smaller needle diameters. Consequently, with the same voltage, the Coulomb force required to break the drop becomes greater, resulting in decreased jet acceleration and increased deposition path time. Additionally, the choice of needle size should consider the characteristics of the polymer solution; very viscous solutions may not flow properly through needles with small diameters. Furthermore, it's possible to work with different diameter sizes simultaneously in a single deposition, a technique known as coaxial deposition.

▪ Collector type

The collector is constructed from metallic material and grounded to prevent the accumulation of charges, which could otherwise lead to a decrease in potential difference and adversely affect deposition. Collectors can be categorized as static or dynamic. Static collectors include simple plates, rings, and parallel electrode structures, while dynamic collectors can be a rotating plate or a cylinder with axial rotation. Figure 3.6 illustrates various collector types.

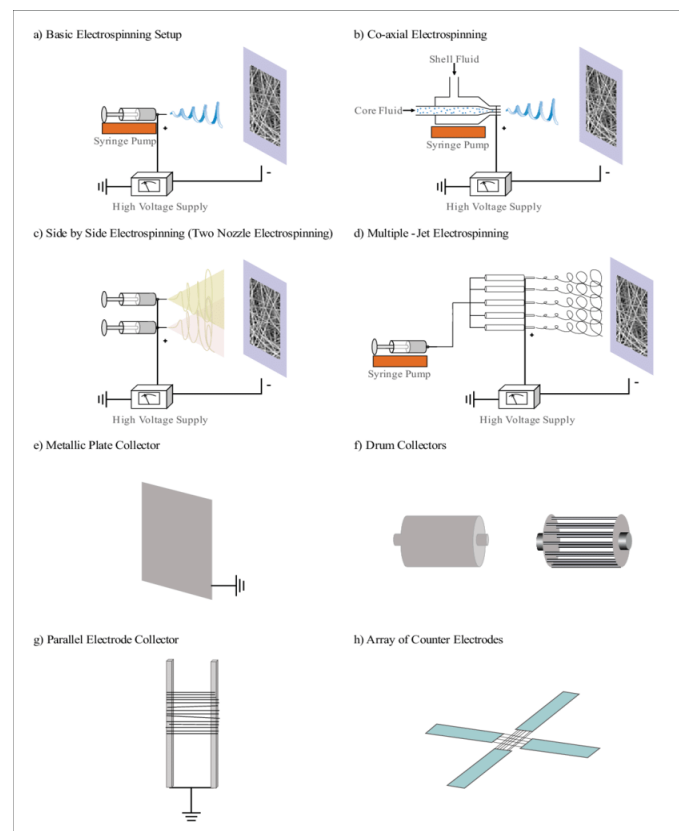


Figure 4.6 Different collector that can be use during the depositions⁹⁰.

In this thesis work, only one type of collector was employed to produce membrane: the rotating cylindrical collector, which enables perpendicular deposition to the rotation axis for better fiber alignment.

- **Needle collector distance**

The needle and collector serve as the two electrodes in the system. Therefore, adjusting their distance alters the electric field and the available settling time for the fibers. Generally, when two electrodes are closer, both the electric field and flow acceleration increase. Consequently, the deposition time becomes insufficient for complete solvent evaporation, leading to defects on the membrane. Conversely, increasing the distance between the two electrodes allows fibers more time to become thinner, resulting in a smaller diameter. However, reaching a critical distance renders the electric field insufficient, causing no deposition to occur.

3.3.2.2 Environmental conditions

The surrounding environment can influence alterations in the morphological structure of fibers. Regarding this, the primary factors to consider are temperature, pressure, and relative humidity.

- **Temperature**

An increase in temperature not only promotes solvent evaporation along the needle-collector path but also lowers the solution viscosity, enhancing polymer solubility. Consequently, the fiber diameter decreases as the stretching force exerted by the Coulomb force intensifies.

- **Pressure**

Operating below atmospheric pressure does not support the electrospinning process as it leads to flow instability and variations in pump flow rate. Additionally, excessive reduction of pressure can result in the polymer solution at the needle tip reaching its boiling point and the dissipation of electrical charge, halting the process.

- **Relative humidity**

Depending on the level of humidity in the environment, pores may develop along the fibers. As the solvent evaporates and the jet cools, water from the surrounding environment can condense on the surface. Once the water evaporates, pores form. The rate of evaporation is affected by relative humidity; lower humidity speeds up evaporation. However, if this rate surpasses the speed at which the solution exits the needle, the process halts due to needle blockage.

3.3.2.3 Solution conditions

Another crucial aspect is defined by solution properties. Factors such as molecular weight, viscosity, surface tension, conductivity, and solvent type necessitate thorough examination.

- **Polymer molecular weight and solution viscosity**

The relationship between solution viscosity and polymer molecular weight is direct. As the molecular weight increases, the solution becomes more viscous. Polymer chains are characterized by entanglements, which are responsible for the cohesion in casting. The number of bonds is directly related to the length of polymer chains, which, in turn, is determined by the polymer molecular weight.

Achieving a high viscosity solution is crucial for producing nanofibers, as it prevents the solution from breaking up into multiple droplets, resembling a spray process. As the viscosity increases, fibers with globular defects (commonly called beads) are formed and, in optimal conditions, fibers without defects are present. Figure 3.7 shows a texture with defects and another free of it.

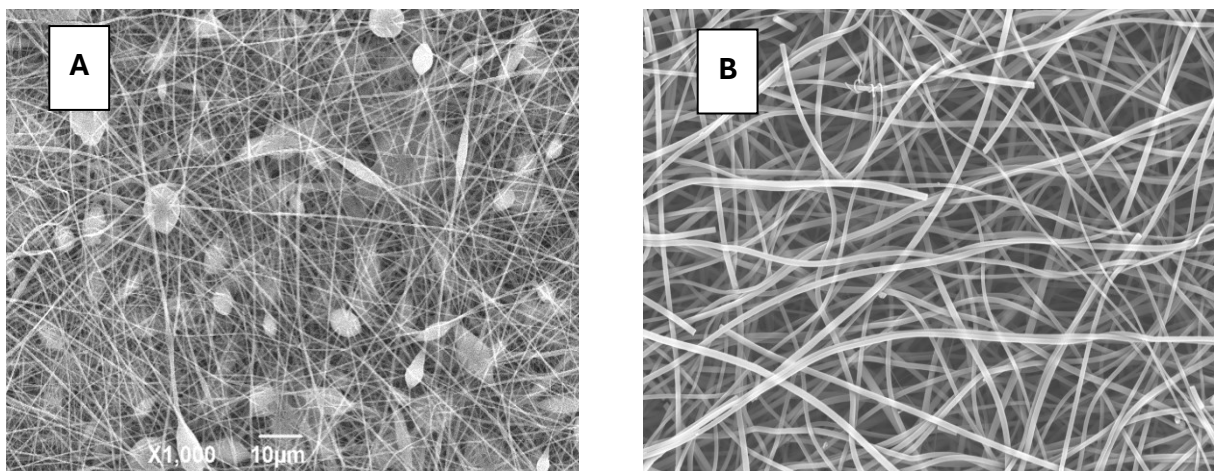


Figure 3.7 Polyimide membrane which present beads (A) and the same polymer without defects (B).

- **Surface tension**

Electrospinning initiates when the force generated by the electric field surpasses the surface tension modulus. This leads molecules to aggregate due to surface tension, forming minimal surface area aggregates. In solutions with low viscosity, solvent molecules remain free as their interactions with polymer chains are weak.

Conversely, in solutions with high viscosity and stronger solvent-polymer interactions, solvent molecules align with polymer chains as the jet stretches during the electrospinning process, resulting in a decrease in the aggregation of solvent molecules. Smooth nanofibers are formed using polymer solutions with low surface tension.

- **Conductivity**

Solution conductivity correlates directly with the quantity of charges present, making it a crucial parameter that significantly influences the process. It's important to note that the system functions due to repulsion among charges on the solution's surface, meaning higher conductivity corresponds to a greater number of charges within the solution. Increased charge density in the flux intensifies the stretching phenomenon, resulting in finer diameter fibers. If the polymer solution's conductivity is insufficient, adding a suitable amount of salt can rectify it and work without change the operative conditions. However, there's a critical conductivity threshold, surpassing which leads to jet instability. Achieving thin and smooth fibers necessitates an operational conductivity range tailored to the specific polymer-solvent system employed.

- **Solvent nature**

The solvent selected for the polymer solution should establish robust interactions with the polymer to effectively solubilize it. Another consideration influencing solvent selection is its dielectric constant. As this property's value rises, the instability zone of casting expands, leading to a larger deposition area. Consequently, thinner and smoother fibers are produced.

Chapter 4

Materials and instrumentations

This chapter provides an overview of the materials utilized in the fabrication of nanostructured membranes and the chemical compounds employed in PFOA degradation tests. Additionally, it describes the instruments essential for characterization purposes.

4.1 Materials

The materials described below are used for the synthesis of polyimide membranes, a polymeric material exploit in this thesis work to capture and degrade PFOA.

4.1.1 Membrane production materials

The membranes used in this work must necessarily possess both good mechanical properties (resist the pressure of the water that continues to flow above them) and high catalytic capacity (to make the most of the photocatalysis phenomenon presented in Chapter 2).

The quest for a membrane possessing both photocatalytic activity and self-sustaining properties has prompted exploration through an approach involving a simultaneous deposition on a cylindrical collector.

Membranes obtained via simultaneous electrospinning arise from the deposition of two separate solutions: one serving a purely structural purpose, and the other endowed with catalytic capabilities. For both solutions, the preparation method closely resembles each other: solid compounds are dissolved in a specific solvent through stirring at room temperature to be, then, electrospun.

4.1.1.1 Structural part

The membrane's structural component produced in this preparation consists of a polyimide (PI) matrix, chosen over other matrices for its high elasticity and thermal resistance properties.

To achieve the final polyimide structure, the formation of an intermediate compound is necessary: its name is polyamic acid (PAA) and it is the general term for intermediate polymeric compounds in polyimide synthesis.

PAA is produced by the reaction that take place between two solid granular compounds, an aniline and a dianhydride, in a suitable solvent. In this work, 4,4'-oxydianiline (ODA, aniline) and Pyromellitic dianhydride (PMDA, dianhydride) are employed as reactants.

ODA is an ethereal derivative of aniline, a colorless organic compound commonly employed as a crosslinking agent for polymers such as polyimide. Table 4.1 provides some parameters regarding ODA.

Table 4.1 Properties of 4,4'-oxydianiline.

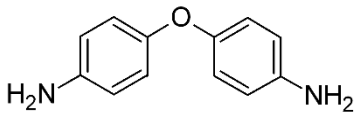

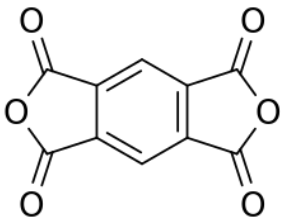

	Chemical formula	$C_{12}H_{12}N_2O$
	Molecular weight [g/mol]	200.24
	Density [kg/m ³]	-
	Melting point [°C]	188-192
	CAS	101-80-4
	Pictograms	

Table 4.2 provides information on Pyromellitic dianhydride (PMDA). PMDA is the dianhydride form of a carboxylic acid, appearing as a white organic solid primarily utilized in polyimide manufacturing. Both compounds, PMDA and the one previously discussed, exhibit toxicity and are established carcinogens.

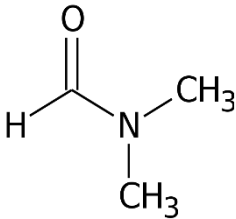

Table 4.2 Properties of Pyromellitic dianhydride.

	Chemical formula	$C_{10}H_2O_6$
	Molecular weight [g/mol]	218.12
	Density [kg/m ³]	-
	Melting point [°C]	286 - 288
	CAS	89-37-2
	Pictograms	

The final crucial component for the successful formation of the membrane is the solvent in which these two solids need to be dissolved. Dimethylformamide (DMF) is a common solvent in chemical reactions and derived from dimethylamine and formic acid. It presents as a colorless liquid with a slight amine odor at room temperature. Despite its toxic and irritating nature, as well as its harmful effects on reproduction, DMF serves as a commonly used aprotic solvent in

nucleophilic substitution reactions across various organic substrates in laboratory settings. Due to its high water solubility, DMF can be easily removed from products insoluble in aqueous solutions through simple washing. Further details about DMF are presented in Table 4.3.

Table 4.3 Properties of *N,N*-Dimethylformamide.

	Chemical formula	C ₃ H ₇ NO
	Molecular weight [g/mol]	73.1
	Density [kg/m ³]	944
	Boiling point [°C]	153
	CAS	68-12-2
	Pictograms	

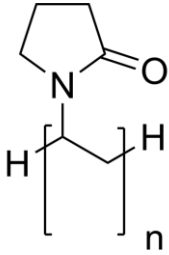
4.1.1.2 Catalytic part

The catalytic solution is slightly more difficult to produce, and it is made up of two different components: the catalyst precursor and a polymer that acts as a support for the catalyst itself. For this purpose, two different solutions are initially prepared (one containing the catalyst precursor and the other having a support phase) which will then be combined after having been appropriately mixed.

The first solution presented is the support one: the sustain is provided by Polyvinylpyrrolidone (PVP), a polymer that readily dissolves in water, alcohol, or other solvents, possessing favorable mechanical properties and ease of electrospinning. In this context, PVP serves to uphold the catalyst and, commonly, it manifests as an electrostatic white powder.

Its key data are detailed in Table 4.4.

Table 4.4 Properties of Polyvinylpyrrolidone.

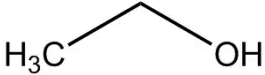


	Chemical formula	- [C ₆ H ₉ NO]-
	Molecular weight [g/mol]	1300000
	Density [kg/m ³]	-
	Melting point [°C]	150 - 180
	CAS	9003-39-8
	Pictograms	-

A suitable solvent capable to dissolve this polymer and making it available for the electrospinning is ethanol.

Ethanol, also known as ethyl alcohol, is selected due to its compatibility and rapid evaporation. It is a volatile, colorless liquid that is flammable at room temperature, widely utilized across various industries including medicine, pharmaceuticals, fuel, and food. Ethanol serves as a ubiquitous solvent in chemical processes owing to its ready accessibility and low cost.

Table 4.5 summarizes its characteristics.

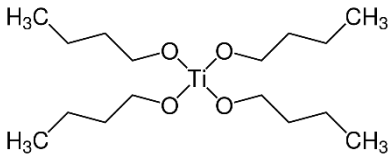



Table 4.5 Properties of Ethanol.

	Chemical formula	C ₂ H ₆ O
	Molecular weight [g/mol]	46.07
	Density [kg/m ³]	789
	Boiling point [°C]	78.4
	CAS	64-17-5
	Pictograms	 

The second solution which complete the catalytic part contains the catalyst precursor dissolved in a solvent.

Tetrabutyl titanate (TBT), also known as titanium butoxide, is a metal-organic liquid compound that lacks odor at room temperature and exhibits a pale yellowish hue. It dissolves in numerous organic solvents, excluding ketones, and undergoes hydrolysis to produce titanium dioxide, the catalyst required for degrading pollutants under specific conditions. For this reason, TBT acts as TiO₂ precursor. Its fundamental properties are presented in table 4.6.

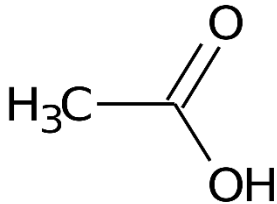

Table 2.6 Properties of Tetrabutyl Titanate.

	Chemical formula	C ₁₆ H ₃₆ O ₄ Ti
	Molecular weight [g/mol]	340.32
	Density [kg/m ³]	998
	Boiling point [°C]	312
	CAS	5593-70-4
	Pictograms	  

Here acetic acid acts as a solvent for TBT, thanks to its properties as a hydrophilic and polar protic liquid, similar to ethanol and water.

Colorless liquid with an unpleasant smell, it denotes many applications in the chemical and biochemical field, such as PET (Polyethylene Terephthalate) production, which is used for about 10% of world production. Table 4.7 describes its characteristics.

Table 3.7 Properties of Acetic acid.

	Chemical formula	C ₂ H ₄ O ₂
	Molecular weight [g/mol]	60.05
	Density [kg/m ³]	1005
	Boiling point [°C]	117.9
	CAS	64-19-7
	Pictograms	

These two distinct solutions (PVP/ethanol and TBT/acetic acid) are initially prepared separately and then, after a proper mixing, are coupled together.

Sigma – Aldrich provides all these materials.

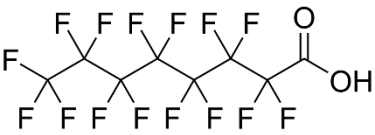

4.1.2 Chemicals used in advanced oxidation processes

Here are described the substances which are dissolved in water before to take part in the experiments.

- *Perfluorooctanoic acid*

It is the contaminant present in the water that we are trying to degrade. It appears as a semitransparent white powder and, as described extensively in chapter 1, it is a compound that has been extremely exploited in the past due to its excellent properties, briefly shown in table 4.8.

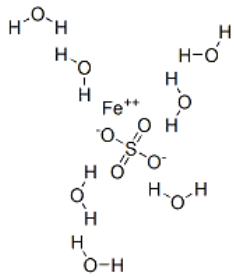

Table 4.8 Properties of PFOA.

	Chemical formula	C ₁₇ F ₁₅ COOH
	Molecular weight [g/mol]	414.07
	Density [kg/m ³]	900
	Melting point [°C]	55-56
	CAS	335-67-1
	Pictograms	

- *Ferrous sulfate*

As highlighted in Chapter 2, for advanced oxidation reactions to occur, it is essential that free radical groups are present in the solution. These oxidizing groups derive specifically from two compounds activated by UV irradiation. The first one is Ferrous sulfate heptahydrate and it is the salt of Fe(II) and sulfuric acid. At room temperature, it exists as a harmful blue-green solid. Typically, it is produced by reacting metallic iron with diluted sulfuric acid or synthesized from metallic iron and copper sulfate through simple substitution. Its applications include precursors for other ferrous compounds and use in the field of photography.

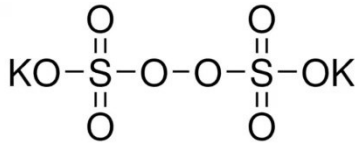

Table 4.9 Properties of Ferrous sulfate.

	Chemical formula	FeSO ₄ ·7H ₂ O
	Molecular weight [g/mol]	278.02
	Density [kg/m ³]	1890
	Melting point [°C]	64 (release of crystal water)
	CAS	7782-63-0
	Pictograms	

- *Potassium persulfate*

It is the compound used to ensure the presence of SO₄^{•-} radicals in the reactive system. It is the salt of potassium and peroxidisulfuric acid. It is an odorless, noxious, and irritating white solid. Preparation methods include electrolysis of potassium bisulfate in a sulfuric acid solution or by adding potassium disulfate to a solution of ammonium peroxidisulfate. This salt serves as an initiator for the polymerization of various alkenes, leading to the production of commercially important polymers like PTFE or SBR rubbers. It is widely utilized in chemistry as an oxidant since the dianion in solution dissociates, releasing radicals.

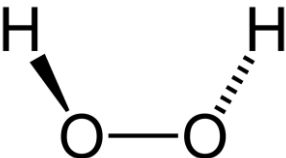

Table 4.10 Properties of Potassium persulfate.

	Chemical formula	K ₂ S ₂ O ₈
	Molecular weight [g/mol]	270.32
	Density [kg/m ³]	2477
	Melting point [°C]	100
	CAS	7727 - 21 - 1
	Pictograms	

- *Hydrogen peroxide*

Hydrogen peroxide stands as the simplest among peroxides and was initially synthesized in 1818 by French chemist L.J. Thénard. It manifests as an aqueous, colorless, corrosive liquid at room temperature, featuring a distinct pungent odor. Due to its pronounced sensitivity to temperature changes and high instability, it is never utilized in its pure form but rather in aqueous solutions. Its pivotal role emerges in Fenton reactions where, upon reacting with iron ions from previously introduced salts, it generates hydroxyl radicals capable of further degrading the targeted compound.

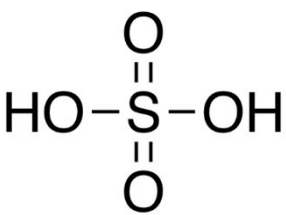

Table 4.11 *Properties of hydrogen peroxide.*

	Chemical formula	H ₂ O ₂
	Molecular weight [g/mol]	34
	Density [kg/m ³]	1130
	Boiling point [°C]	107
	CAS	7722 - 84 - 1
	Pictograms	

- *Sulfuric acid*

Sulfuric acid, a potent mineral acid, is a strong, viscous liquid that is colorless and odorless at room temperature. It readily dissolves in water and ethanol, capable of causing severe burns upon skin contact. It is added in a small quantity to the water because Fenton reaction is favored in an acidic environment, (while it is not wet certain that persulfate oxidation is favored). Table 4.12 presents its properties.

Table 4.12 *Properties of Sulfuric acid.*

	Chemical formula	H ₂ SO ₄
	Molecular weight [g/mol]	98.08
	Density [kg/m ³]	1840
	Boiling point [°C]	310
	CAS	7664 - 93 - 9
	Pictograms	

Also these materials are provided by Sigma – Aldrich.

4.2 Instrumentations

This paragraph is focused on the instruments employed for the production and characterization of the nanostructured membranes.

4.2.1 Viscometer

The viscosity is an analysis performed to characterize the structural solution: it is of extreme importance to have high viscosity to spin the PAA. The viscosimeter used is an *ATAC NuLine Cone and Plate* viscometer, shown in figure 4.1.



Figure 4.1 *ATAC NuLine cone and Plate viscometer used to measure the viscosity of the PAA solution.*

The sample is placed on the flat metal plate and the cone is brought down into contact with the test material, causing a spreading action. Sample material flows out to the circumference of the cone; excess material is removed, and the instrument is ready to run tests.

The cone seems to have a flat bottom, but there is a slight angle between 0.5 and 2 degrees relative to horizontal. Figure 4.2 offers a simple representation of the geometry of the system⁸¹.

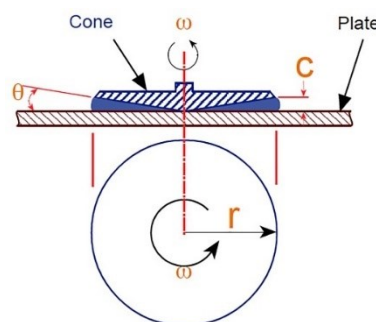


Figure 4.2 *Simple description of cone and plate viscometer⁸¹.*

Because the geometry is precisely defined and there is a known “gap” between the sample plate and rotating surface of spindle, shear rate and shear stress values are calculated using equations (4.1) and (4.2), respectively. The viscosity of a fluid is defined as the proportionality factor which link shear rate with shear stress and is simply computed as ratio between them (eq. 4.3)⁸¹.

$$\tau = \frac{3T}{2\pi R^3} \quad [N/m^2] \quad (4.1)$$

$$\dot{\gamma} = \frac{\omega}{\sin \theta} \quad [1/s] \quad (4.2)$$

$$\mu = \frac{\text{shear stress}}{\text{shear rate}} = \frac{\tau}{\dot{\gamma}} \cdot 10 \quad [Poise] \quad (4.3)$$

In these equations, T represents the torque [$N \cdot m$], R [m or cm] the cone radius, ω [rad/sec] the cone speed and θ the angle between the cone and the plate.

4.2.2 Electrospinning equipment

Electrospinning of polymeric solutions is performed to produce nanostructured membranes. The setup proposed and depicted in figure 4.3 was used for the production of all the membranes present in this work.



Figure 4.3 Electrospinning setup used for the production of all the membranes.

This experimental setup is composed of:

- A chamber made of polycarbonate: used to enclose the system properly while maintaining suitable temperature and humidity levels.

- Delta Ohm HD 2301 thermo-hygrometer: utilized to monitor the temperature and humidity within the chamber.
- High voltage generators: employed to subject the solutions to a high tension in order to overcome the surface tension and start spinning.
- Volumetric pumps: they regulate the solution flowrate.
- Plastic syringes: act as solution reservoirs.
- Needles: placed at the end of the syringes, they act as a positive electrode during electrospinning.
- Cylindrical collector: it is wrapped by an aluminum foil and act as the negative electrode of the system, where the fibers are deposited. All these equipment is grounded.
- Pressurized air pipe: used to blown air inside the chamber to regulate the humidity inside it (if there is the necessity).

The syringes are filled with the solution (structural and catalytic solutions, as explained before) and placed in the cavity of the volumetric pumps while the manifold is covered with an aluminum foil. Clamps are used to connect needles and voltage generators: once the flowrate is set, the generators are started, and the solutions begin to flow out depositing on the collector. The flowrates and the voltages can be adjusted until stable jets come out from the needles (at optimum operative conditions the Taylor cone is followed by a stable and linear jet which then turns into an unstable jet). It is fundamental to verify the presence of fibers before every deposition.

4.2.3 Fourier-Transformed infrared Spectroscopy

Fourier-transform infrared spectroscopy (FTIR) is a method utilized to analyze the molecular structure of solid, liquid, or gas samples by examining their absorption or emission of infrared radiation. This approach relies on molecules' ability to alter the lengths and angles of their bonds, resulting in stretching and bending motions. Infrared light is absorbed at specific frequencies corresponding directly to the vibrational energy levels of the atomic bonds within the molecule. When the vibrational energy of a bond matches the energy of the infrared radiation, absorption occurs. Each type of bond within a molecule vibrates at distinct energy levels, leading to absorption of different wavelengths of infrared radiation. The position (frequency) and intensity of these absorption bands collectively form the molecule's unique spectral fingerprint.

The relationship between energy and frequency is fundamental and expressed as follows:

$$E = h \cdot \nu \quad (4.4)$$

where E is the radiation energy, h is the Planck's constant, and ν is the radiation's frequency. The Michelson interferometer plays a crucial role in FTIR spectroscopy, distinguishing it from traditional infrared spectroscopy. While dispersive IR spectroscopy employs monochromatic light to sequentially irradiate a sample across an infrared wavelength range, FTIR spectroscopy utilizes an interferometer and subsequent processing of transmitted light to expose a sample to multiple frequencies of IR light simultaneously, spanning from 4000 cm^{-1} to 500 cm^{-1} .

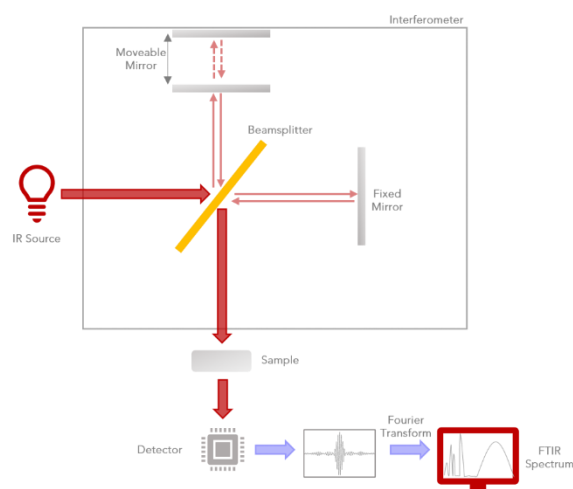


Figure 4.4 Interferometer scheme in a FTIR instrument.

Figure 4.4 illustrates a schematic of the interferometer: a beam splitter divides a beam into two paths, one reflected by a stationary mirror and the other by a movable mirror. Upon recombination at the beam splitter, interference arises between the beams due to their path disparities. Consequently, the resulting IR light exhibits a shifting frequency distribution attributable to variations in the travel distance of the second beam induced by the rotating mirror.

The detector signal is captured as a time-domain interferogram, which is subsequently transformed into the frequency domain via a Fourier Transform to acquire the IR spectrum.

The spectrophotometer used in this thesis is a *Nicolet IS50 Thermo Scientific*, shown in figure 4.5.



Figure 4.5 Nicolet IS50 ThermoScientific spectrophotometer used for infrared analysis.

Two distinct types of FTIR analysis can be identified:

- *Transmittance analysis*: it involves directing infrared (IR) light directly into a solid, liquid, or gaseous sample, where it absorbs specific wavelengths or frequencies of light. The frequencies not absorbed by the sample are transmitted to a detector, generating a spectrum. While versatile, this method requires sample preparation such as forming pellets, mulls, or films before measurements can be conducted.
- *Reflectance analysis*: this method involves determining the absorbing properties of the sample by analyzing its reflection. It's a faster and more versatile approach because there are no restrictions on measuring reflected light, eliminating the need for sample preparation beforehand.

Reflectance analyses utilize attenuated total reflectance (ATR) technology, where infrared (IR) light traverses through an internal reflection element (IRE) crystal material, in contact with either a solid or liquid sample. The interface between the sample and the crystal interacts with the light at a 45° incident angle as it traverses the crystal, as depicted in Figure 4.6.

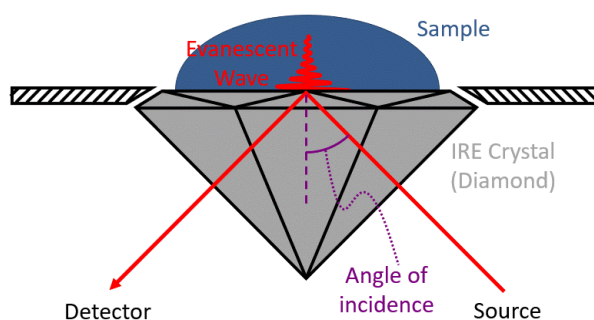


Figure 4.6 Schematic representation of an ATR technology.

Subsequently, the detector assesses the attenuation caused by the sample's bond absorbance. The accessory employed is the Smart iTR with a single-bounce diamond configuration (as the beam reflects only once within the material), capable of capturing 64 scans from 4000 to 650 cm^{-1} with a resolution of 4 cm^{-1} .

4.2.4 Environmental Scanning Electron Microscope

The Environmental Scanning Electron Microscope (ESEM) allows for morphological characterization of membranes by utilizing an electron beam as its radiation source, achieving a resolution several orders of magnitude greater than optical microscopes, which rely on light as radiation source. Another advantage of the SEM is its substantial depth of field, ensuring

high magnification and excellent three-dimensional imaging. Figure 4.7 provides a schematic representation of the instrument.

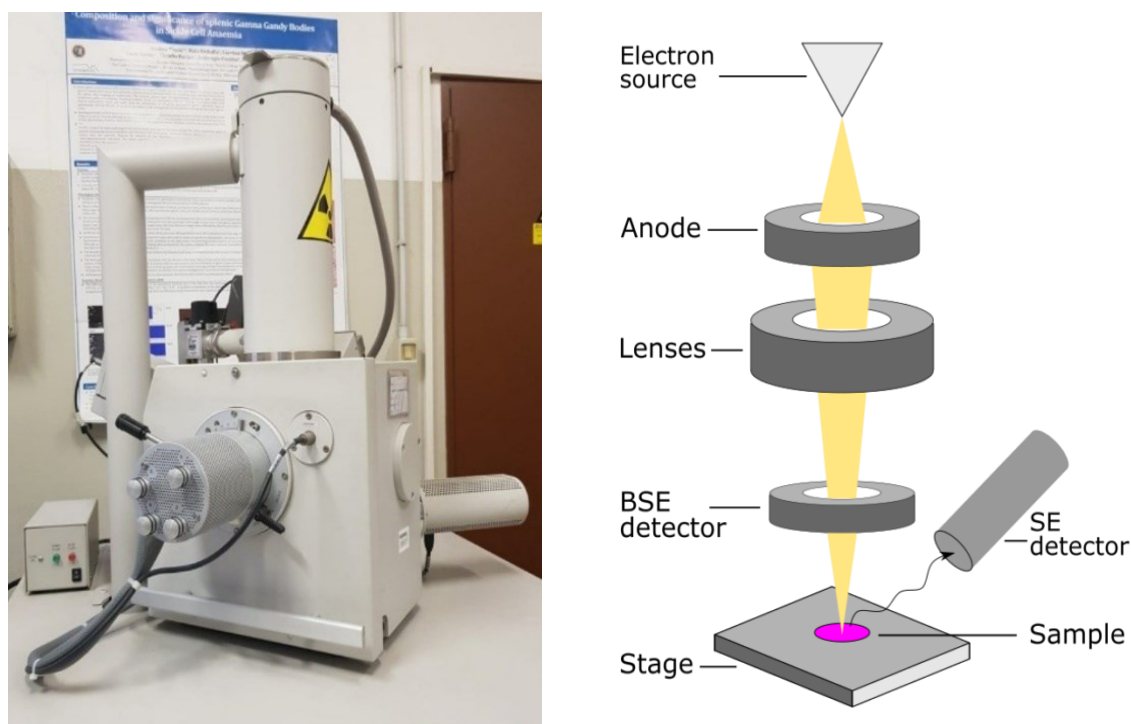


Figure 4.7 Microscope Philip XL30 used for the analysis and its schematic representation.⁹¹

The electron beam, generated by an electron source, undergoes acceleration via magnetic lenses and is directed onto the sample through a sequence of consecutive scans. Interactions between the electrons and the material's atoms yield various signals, which are utilized to reconstruct the image on the screen of a cathode ray tube. Among these signals, those derived from secondary electrons, originating from an average depth of approximately 10 nm, are commonly employed for analyzing the sample's external surface.

A high level of vacuum is necessary in the area encompassing the electron source and the magnetic lens, while a lower vacuum is employed in the region where the detectors and samples are situated. Samples are typically affixed firmly onto a specimen holder or stub using conductive adhesive. Non-conductive materials, like polyamic acid or polyimide, undergo an ultrathin coating of electrically conductive material, applied to the sample via methods such as low-vacuum sputter coating, electroless deposition, or high-vacuum evaporation.

From the analysis of the SEM images, it is possible to determine the average size of the fibers which compose the membranes.

The ESEM can also be combined with Energy-dispersive Spectroscopy (EDS) to perform SEM-EDS microanalysis, which offers qualitative information into the elements present in a sample. An example is given in figure 4.8⁸².

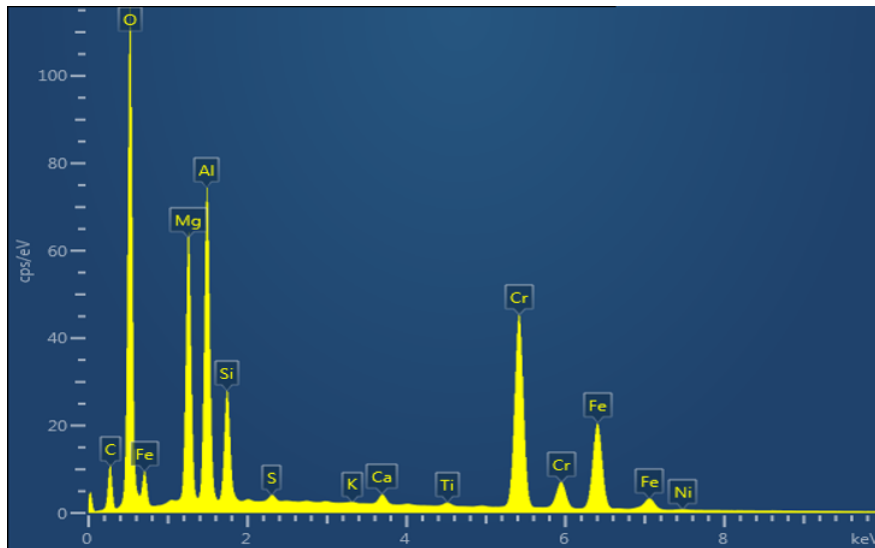


Figure 4.8 Example of EDS spectra⁸².

When irradiated with electrons, the sample emits x-rays specific to its constituent elements. These energy emissions are then converted into spectral peaks of varying intensity, generating a spectrum profile that identifies the elements present (e.g., lead, iron, copper, zinc, etc.). The intensity of the X-rays (size of the spectrum peaks) is correlated with the concentration of elements in the sample. This analysis can be focused on specific areas of interest, such as individual layers of a cross-section, allowing characterization of layers or particles within the sample.

4.2.5 Thermo-Gravimetric Analysis

Thermogravimetric analysis (TGA) is a method of thermal analysis that tracks the change in mass of a sample over time as temperature is varied. A typical thermogravimetric analyzer comprises a precision balance with a sample pan housed within a furnace equipped with programmable temperature control. A schematic representation of the instrument is depicted in figure 4.9.

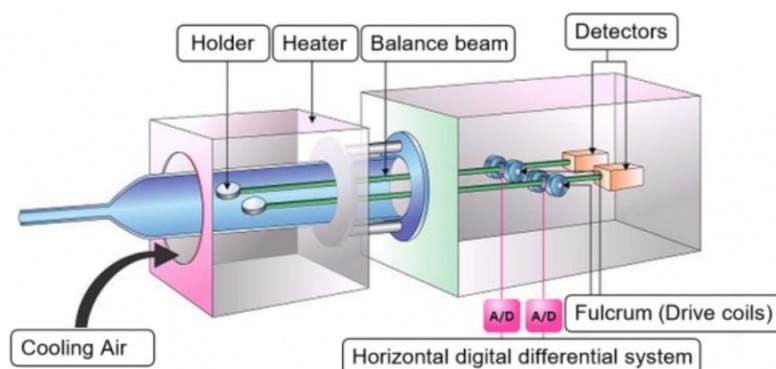


Figure 4.9 Thermo-Gravimetric analyzer representation.

Temperature is typically increased at a constant rate. Analysis can be conducted under various atmospheric conditions, including ambient air, vacuum or inert atmosphere (nitrogen) and different pressure ranges.

TGA consists of a precision balance situated within a controlled environment furnace. An empty capsule (reference) and the sample are positioned on the balance and heated at a predetermined rate. While the weight of the sample fluctuates as the program progresses, that of the reference remains constant. The thermogravimetric data collected during a thermal reaction is plotted as mass or percentage of initial mass on the y-axis against temperature or time on the x-axis. This resulting plot, often smoothed, is referred to as a TGA curve.

This analysis yields information about the polymer, including the presence of volatile substances, the onset temperature of decomposition, the concentration of inorganic materials, decomposition mechanisms, and kinetics.



Figure 4.10 TGA SDT-650 produced by TA Instruments.

For all TGA analyses performed in this thesis work the SDT-650 shown in figure 4.10 was used: the objective was to evaluate the catalytic content of the spun membranes (at high temperature, polymeric material starts to degrade while TiO_2 remains stable).

4.2.6 Photoreactor setup

The photoreactor is the most interesting instrument of the experimental apparatus: it is a stainless-steel container where the membrane is placed inside. Three holes are drilled in its perimeter to allow water to flow continuously into it. The water, drawn by a centrifugal pump, arrives inside the reactor, subsequently it can flow over the membrane without crossing it (retentate) or cross the membrane (permeate). The retentate is sent directly to the water reservoir (a polypropylene container) while the permeate flows through a peristaltic pump and

then also sent to the reserve. The use of a second pump is necessary to try to force the water through the membrane. The system also involves the use of a UV-C lamp to exploit the photocatalytic reactions presented in chapter 2.

The experimental apparatus including the photoreactor present in the laboratory and a scheme of it are represented in figures 4.11 and 4.12.

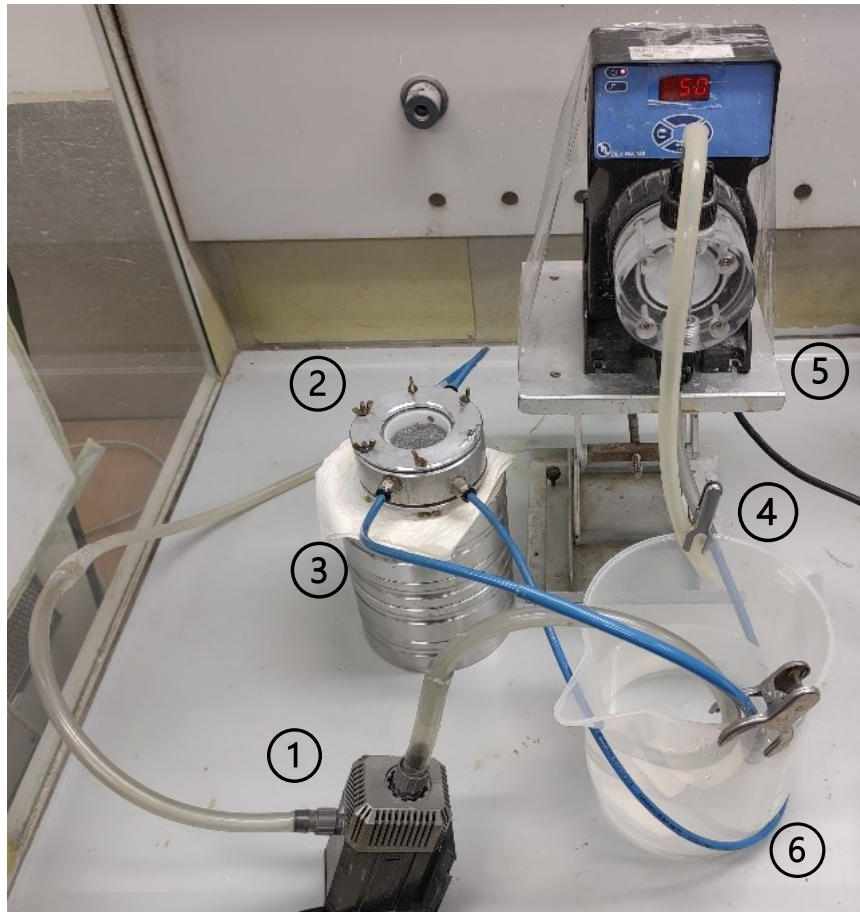


Figure 4.11 *Experimental apparatus for the degradation of PFOA in water.*

From figure 4.11 it is possible to notice the centrifugal pump (1), the photoreactor (2), the retentate (3), the permeate (4), the peristaltic pump (5) and the water reservoir (6).

The UV lamp is missing but it is placed over the photoreactor thanks to a support that covered all the reactor area to avoid light dispersion.

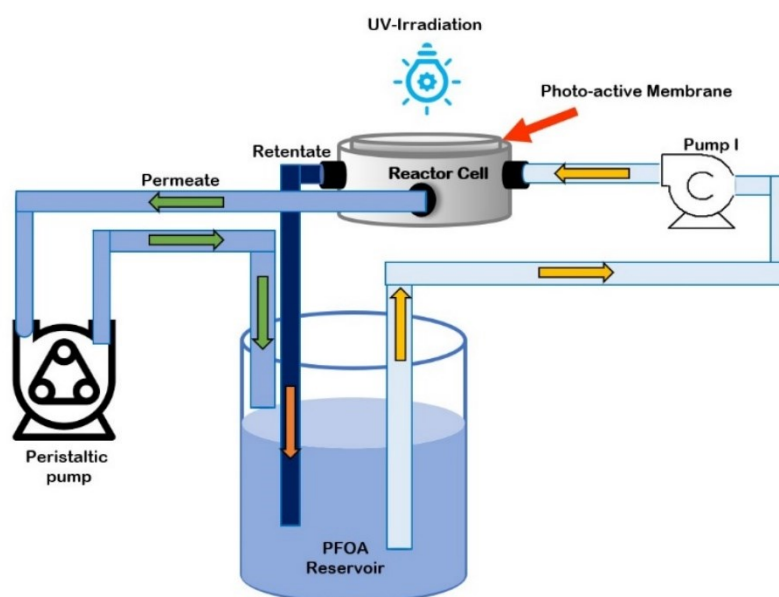


Figure 4.12 Schematic representation of the photoreactor apparatus.

In this thesis work, the contaminant to be removed (PFOA) and all the chemicals necessary for the photo-Fenton and persulfate oxidation reactions (FeSO_4 , $\text{K}_2\text{S}_2\text{O}_8$, H_2O_2 , H_2SO_4) are added to the water and sonicated for 45 minutes (to encourage the solubilization of the compounds). After 45 minutes the polypropylene container can be filled with it and, once the pumps have been started, the water continues to flow through the system for 5 or 7 hours. Every hour a sample is taken which will then be analyzed using HPLC-MS.

4.2.7 High Performance Liquid Chromatography – Mass Spectroscopy

High-performance liquid chromatography (HPLC) is an analytical method utilized for the separation, identification, and quantification of specific components within a mixture.

The process involves the use of pumps to drive a pressurized liquid eluent (such as water, acetonitrile, methanol, or a combination of them) containing the sample mixture through a column densely packed with solid adsorbent granules.

The extent of interaction between different components and the adsorbent material alters their flow rate and consequently their retention time within the column, facilitating their separation. At the end of the separation system lies a detector, which may be either UV/Vis-based or reliant on mass spectrometry. This detector produces a signal proportional to the concentration of the components as they exit the column, enabling quantitative analysis. The results are shown graphically in a signal (V) versus time (min) plot.

The method utilized to analyze perfluoroalkyl compounds in drinking water is founded on the EPA 537: 2009 protocol.

This method entails an initial sample separation using liquid chromatography with a mobile phase (HPLC), followed by identification and quantification using a triple quadrupole mass spectrometer.

Contaminated water samples are analyzed by an HPLC *Agilent 1200 series chromatograph* coupled with a *Thermo Scientific LTQ XL mass spectrometer* equipped with an electrospray source and a linear ion trap analyser. The chromatographic separation was performed using an *InfinityLab Poroshell 120 EC-C18 2.1x100 mm 2.7 μ m column (Agilent Technologies)* with the following eluents: ammonium acetate 5 mM in Milli-Q water and methanol. The flowrate was set at 0.3 mL/min and the injection volume was 10 μ L. Samples ionization was performed in negative mode (ESI-), with a spray of 2.5 kv and a source temperature of 300°C.

In all cases perfluorononanoic acid (PFNA, C₈F₁₇COOH) was used as the internal standard and calibration curves were built considering the ratio of the signals of the analyte and PFNA⁸³.

Figure 4.13 shows the HPLC-MS models used to perform the analyses.



Figure 4.13. HPLC Agilent 1200 coupled with MS Thermo Scientific LTQ XL used for the analyses.

The samples, collected in polypropylene containers, can be stored at a temperature below 6°C (fridge) from the time of collection⁸³.

The substance's determination, upon release from the column, is carried out by the triple quadrupole. Prior to entering the latter, molecules are charged positively or negatively (depending on instrument settings) and directed to the first quadrupole. Here, by adjusting the mass/charge ratio, precursor molecular ions are selected. Subsequently, they traverse the collision cell, where induced dissociation occurs through collision and potential variable

differences of the precursor ions. Finally, they reach the second quadrupole, which determines the structure and thus identifies the molecule.

In this study, this technique is useful to determine the concentration of PFOA and correlated by-products over time, to understand if an effective degradation is taking place.

Chapter 5

Imidation process

In this chapter there will be discuss the polymerization reactions that occurs to arrive to the final product which are made the membranes, polyimide. Then, a brief characterization of polyimide is presented.

The chapter therefore opens with a description of the imidation process which will be followed by some characterization techniques that have been carried out to analyze the membranes and the intermediate compounds that lead to them.

5.1 Theory of polyimide synthesis

Marston Taylor Bogert, an American chemist, was the first one able to produce aromatic polyimides in 1908 through the polycondensation of ethers and anhydrides of aminophthalic acid. Following this milestone, numerous efforts were made to enhance the product, leading to the emergence of high molecular weight polyimides in 1955 (Buhler ku. spezialplaste. berlin: academie-verlag, 1978). This development involved a two-stage polycondensation process between pyromellitic anhydride and a diamine, marking the beginning of modern polyimide research.

In general, the term "polyimide" denotes a polymer containing a benzamide group, or more precisely, an imide group composed of a benzene ring and two carbonyl groups bonded to a nitrogen atom.

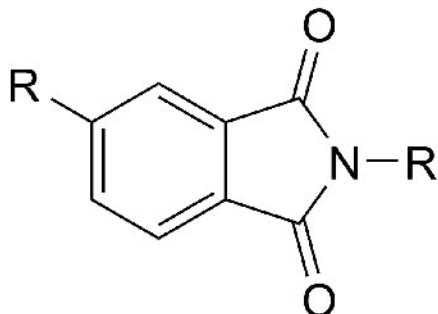


Figure 5.1 A generic imide group.

There are various methods to incorporate an imide group into a polymer chain, contingent upon the precursors and solvent utilized. However, the formation of polyimide follows a distinct and straightforward concept: the polyacylation of a heterocyclic aromatic diamine with a tetracarboxylic acid derivative. This process can occur in a single step or a double step, depending on the desired product. A single step is adequate for producing a polyimide soluble in organic solvents. Conversely, if an insoluble and infusible polyimide is desired, an additional intermediate step is necessary, leading to the formation of polyamic acid (PAA, also called poly-orthocarboxamide).

In this research, the need for a structure that can withstand solvents and water led us to opt for an insoluble polyimide. This polyimide is the outcome of two distinct reactions: the initial polycondensation reaction and the subsequent imidization reaction. These steps can be summarized as follows with figure 5.2 and 5.3, considering a general radical residue (Q) from the tetracarboxylic acid and any radical residue (R) from the aromatic diamine. Figure 5.2 describe the first step which lead to the production of polyamic acid (PAA) while figure 5.3 represent the second step, where polyimide is finally formed.

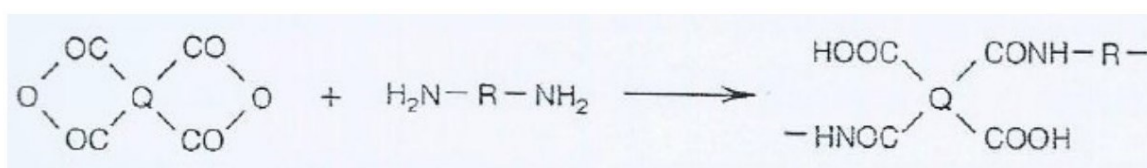


Figure 5.2 Polycondensation of a generic dianhydride and a generic diamide to give PAA.



Figure 5.3 Imidation by PAA cyclization to form Polyimide (PI).

In the next section these reactions are explained in a more detailed way.

5.1.1 Polycondensation process description

The initial phase of polyimide production might seem simple, but it requires meticulousness and attention because even the slightest negligence can cause significant variations in the final result. The process involves gradually introducing powdered dianhydride into a pre-prepared diamine solution within a mixing-equipped container. It becomes apparent that viscosity doesn't immediately increase but steadily over time as the dianhydride interacts with the solution. Maintaining a temperature range of 15°C to 35°C is crucial; for vessels holding less than one liter, a temperature control system is advisable.

PAA solutions are highly sensitive to temperature, necessitating storage below 0°C, if it is expected to use it a few days after preparation. The initial concentration of reactants is based on the intended use of polyamic acid, serving as a mechanism for controlling its molecular weight. In this work, the concentration of reagents (ODA and PMDA) in the solution ranges between 15% and 21.7%.

Various dianhydrides and diamines have been utilized for polyimide membrane production, but in our work pyromellitic dianhydride and 4,4'-oxydianiline have been adopted; the details are summarized in Chapter 4.

To comprehend the polycondensation mechanism, delving into the examination of the fundamental chemical reactions involved in the process (whether direct, inverse, or parallel) is essential. The investigation of these fundamental reactions is reason of debates within the scientific community. A considerable number of studies is paying attention on the production of polyamic acid, its degradation during storage, and ultimately, its cyclization to polyimide. The central reaction in this context is the formation of PAA, depicted in Figure 5.4.

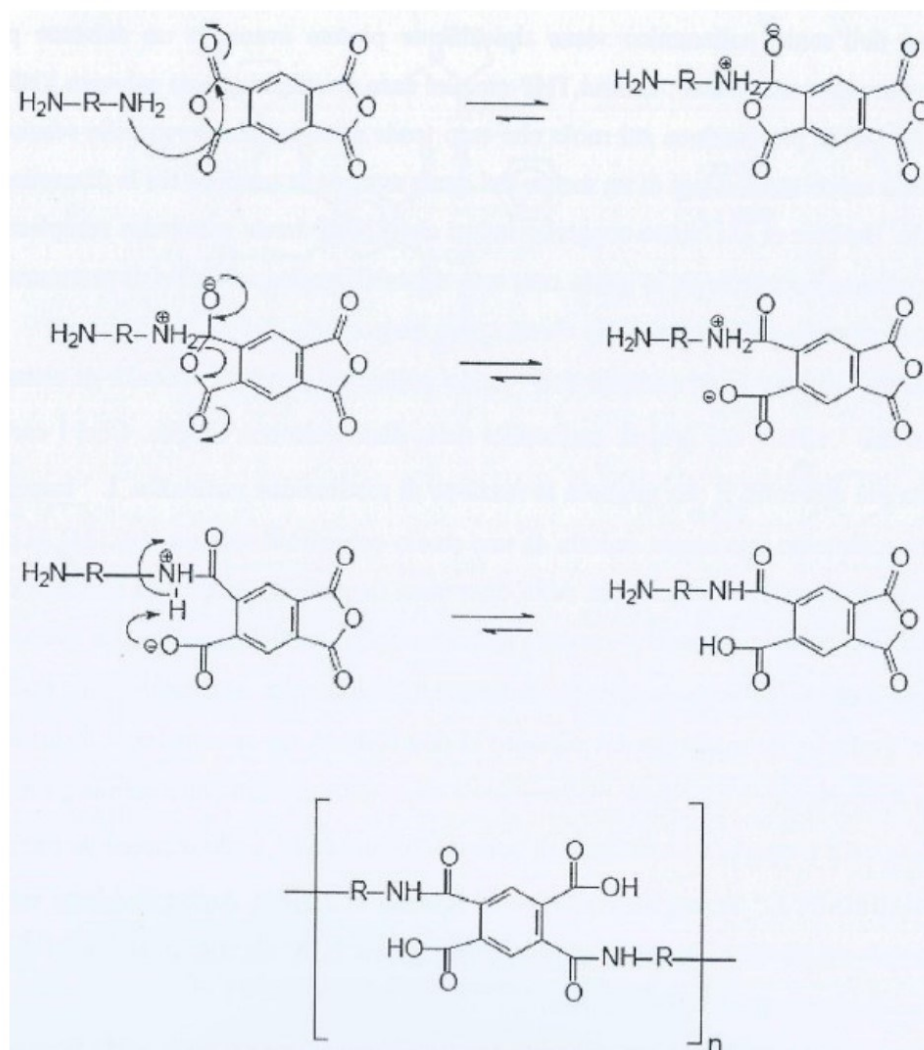


Figure 5.4 PAA formation mechanism by polycondensation reaction.

A chain reaction occurs, leading to the synthesis of macromolecules via a nucleophilic substitution mechanism. In the initial step of the proposed mechanism (Figure 5.4), the amino group attacks the carboxylic group, resulting in a positive charge on the amino nitrogen and a negative charge on the carboxylic radical. This instability prompts the opening of the anhydride ring and the formation of the characteristic bond of polyamic acid (second step). Subsequent nucleophilic substitution reactions, facilitated by aprotic polar solvents, contribute to the formation of PAA. In this context, dimethylformamide (DMF) serves as an optimal compromise between an ideal working environment and limited involvement in the reaction progress. Other suitable examples include 1-methyl-2-pyrrolidone (NMP) and tetrahydrofuran (THF), although they may actively participate in polyamic acid formation, particularly NMP, not always with favorable outcomes.

Secondary reactions may occur which may disturb the production and storage of PAA. The degradation of polyamic acid during the storage period initiates a cascade of reactions that target the ortho-carboxamide units of PAA, resulting in their cyclization and subsequent elimination of amines (Frost L.W., 1964). This instability reflects the reversible nature of polyamic acid synthesis: essentially, it represents the inverse reaction of PAA formation. Furthermore, solvent interaction with reactants, particularly with the anhydride, can diminish efficiency, forming complexes of electron donor and acceptor groups that alter the molecular weight and properties of the polyimide. Additionally, a reaction that hinders the creation of the final product is the interaction of PMDA with water: hydrolysis of the anhydride group leads to the opening of the ether ring, creating two carboxyl groups (Figure 5.5).

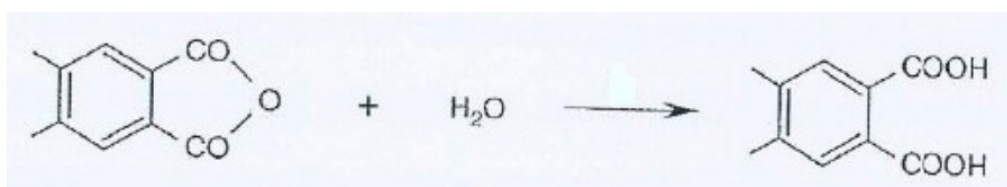


Figure 5.5 Hydrolysis reaction that can occur between a dianhydride and water molecule.

This tendency of the anhydrides to react with ambient humidity, resulting in the formation of the corresponding acid, reduce the availability of dianhydride molecules for polycondensation and, consequently, a decrease in reaction yield. Working in an environment with minimal moisture content is essential to achieve a product with favorable chemical and physical properties. To this end, even powders are dried prior to use.

In addition, it is fundamental to dissolve first ODA in the solvent and then the PMDA. If the PMDA is dissolved before ODA, much lower molecular weights are attained. These facts can be explained in this way: when PMDA is added after ODA there is a competition between the water-PMDA reaction and ODA-PMDA reaction while, inserting first PMDA, it has enough

time to interact with water (hydrolysis, figure 5.5), leading to its consumption (and it will no longer be available to form PAA).

Another factor which can bring to the PAA degradation is its hydrolysis: if water is present after the PAA formation, it can form amine salt structures and, thanks to the capacity of DMF to dissolve these groups, the chain cleavage leads to a decrease in viscosity⁸⁴. This process is shown in Figure 5.6.

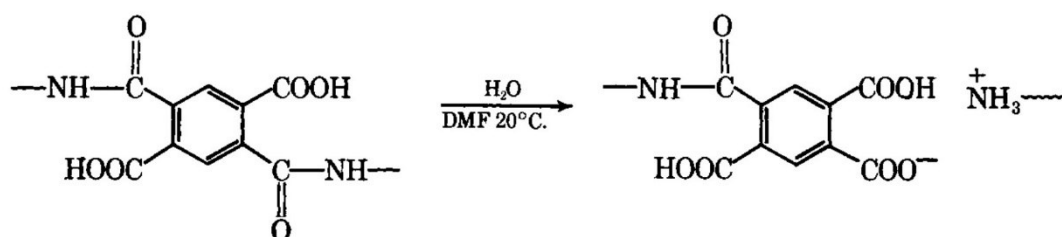


Figure 5.6 PAA hydrolysis reaction which lead to a decrease in viscosity⁸⁴.

This reaction is favored at high temperature: if it is expected to use PAA after a few days after preparation, it is important to store it in fridge or freezer.

It is useful to remember that water may be present within the reaction environment following the spontaneous imidation process, however, existing literature suggests that the small amount of water produced should not be considered a significant source of accumulation capable of damaging polyamic acid.

The subsequent paragraph explains the process that leads from polyamic acid to polyimide.

5.1.2 Conversion of Polyamic acid in polyimide

To complete the process of obtaining a polyimide, it is essential to undergo cyclodehydration of polyamic acid. The most common methods for continuing the synthesis are outlined below (Chiarello, 2009):

- Low-temperature polycondensation of the dianhydride with the aromatic diamine in an amide solvent, followed by thermal imidization of the polyamic acid.
- Low-temperature polycondensation of the dianhydride with the aromatic diamine in an amide solvent, followed by chemical (catalytic) imidization of the polyamic acid using a catalytic system based on acetic anhydride, pyridine, or triethylamine.
- High-temperature polycondensation of the dianhydride with the aromatic diamine in a solvent based on phenol or m-cresol, followed by catalytic imidization under the action of isoquinone or benzoic acid.

The initial two methods yield an insoluble polyimide, commonly utilized for manufacturing films, coatings, or fibers, while the latter approach results in amide-soluble polyimides. Most aromatic-based polyimides are insoluble in typical solvents due to the strong electrostatic

interactions within the imide rings, facilitated by the presence of electro-donor and electron-acceptor groups, along with Van der Waals forces.

Our research exploits low-temperature polycondensation followed by thermal imidization of polyamic acid to produce the polyimide. This process ensures the resulting product is insoluble, enabling it to effectively support catalysts in aqueous environments without requiring additional substances to achieve the desired polyimide state.

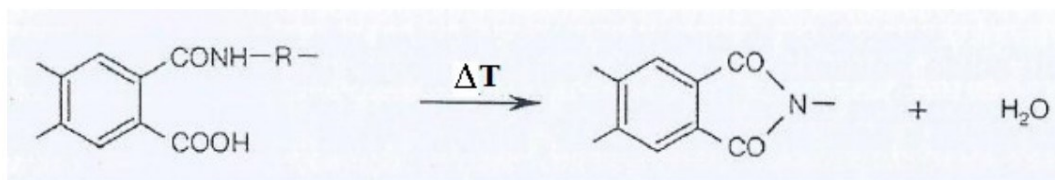


Figure 5.6 PAA cyclodehydration under heat treatment.

Figure 5.6 schematizes the reaction that take place in our work to pass from PAA to polyimide (PI).

5.2 Polyimide characterization

The characterization of a synthetic polyimide involves assessing all its basic properties, including thermal stability, various transition temperatures, mechanical properties, and density. In this chapter, only FT-IR spectra and thermal stability of polyimide are analyzed.

FT-IR is the most used method for tracking structural changes in the formation process of polyimides, starting from polyamic acid. FT-IR enables sufficiently well-founded conclusions about the structure of a given material compared to another. It's worth noting that not all functional groups exhibit the same absorption characteristics. For instance, typical bonds of polyamic acid, which absorb near 1600 cm^{-1} , are not as effective as the carbonyl groups linked to the imide cycle, despite their similarity. Consequently, the peak related to polyamic acid decreases as the reaction progresses until it overlaps with the absorption range of the imide groups and disappears. Tables 5.1 and 5.2 present the values of characteristic peaks for the two compounds.

Table 5.1 Generic PAA absorption bands.

PAA bonds	Absorption band (cm^{-1})
C=O (CONH)	1640
C=O (COOH)	1710
O-H (COOH)	2400 – 3200
N-H (CONH)	3200 - 3400

Table 65.2 Generic PI absorption bands.

Polyimide bonds	Absorption band (cm ⁻¹)
C=O (linked to the imide group)	722-880
C - N	1370
C=O (imide asymmetric stretch)	1715
C=O (imide symmetric stretch)	1775

All the characteristic peaks of PAA and PI, respectively, are indicated in the spectra below. Values in the tables above were compared with school libraries and with Soohyun Kim (2013) studies, reporting positive matches.

Figure 5.7 compares the IR spectra of polyamic acid and polyimide.

In figure 5.7 can be noticed the IR spectra of the membrane before and after the heat treatment, which corresponds to polyamic acid and polyimide, respectively.

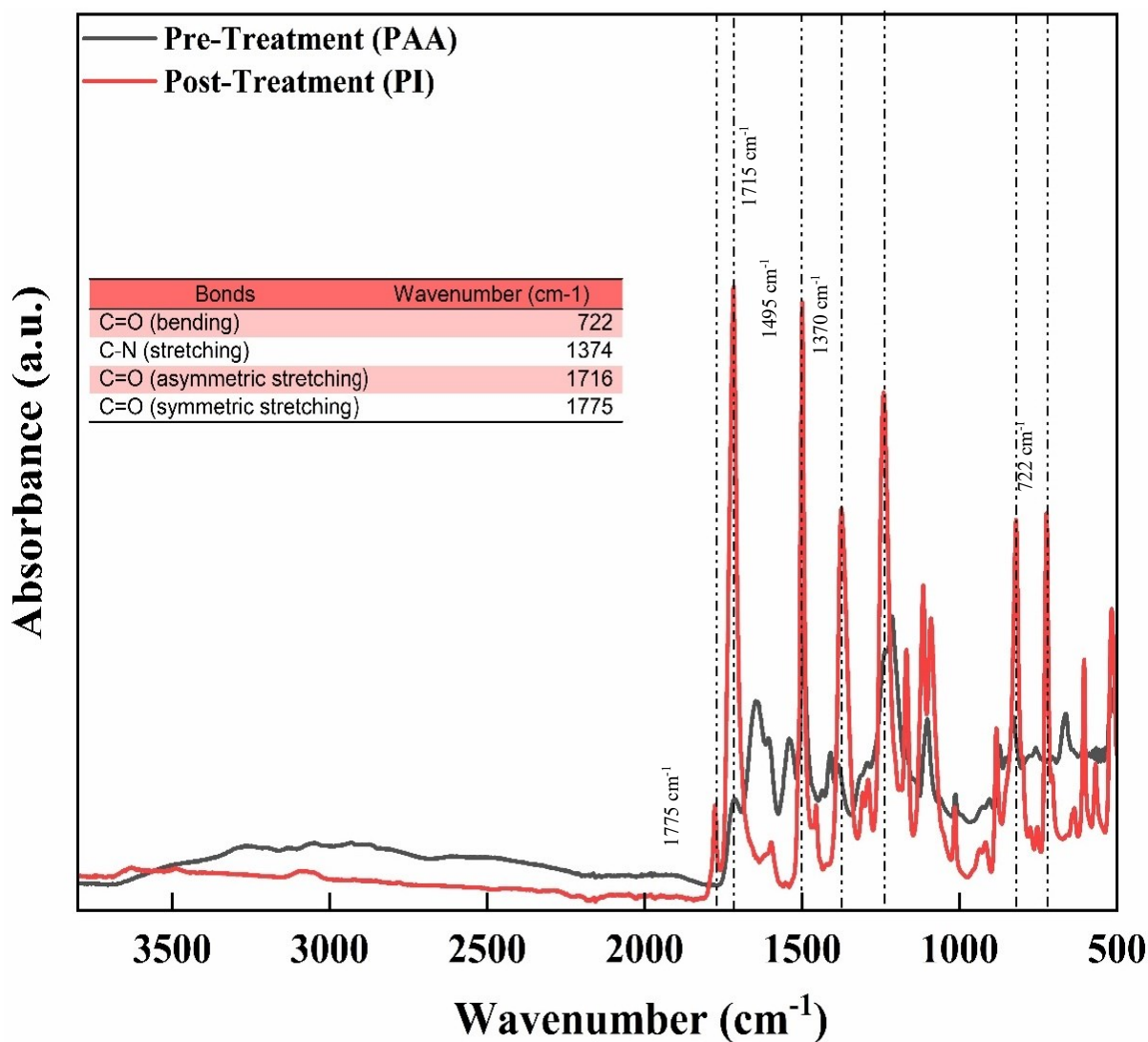


Figure 5.7 Comparison between PAA and PI infrared spectra.

The peak at 722 cm^{-1} corresponds to the bending of the C=O double bond associated with the imide ring, while the peak at 1370 cm^{-1} indicates the stretching of the carbon-nitrogen bond within the imide ring. Peaks at 1715 cm^{-1} and 1775 cm^{-1} signify the asymmetric and symmetric stretching of the carbon-oxygen double bond, respectively. The peak at 1495 cm^{-1} is attributed to the aromatic ring, serving as an internal standard as it remains unaffected during the reaction and is not involved in it (in Figure 5.7, PAA peak at 1495 cm^{-1} is covered by the same PI peak). Peaks crucial for understanding the imidization process are those at 1370 cm^{-1} and 722 cm^{-1} , as they accurately represent the molecule without being obscured by solvent-related or other group-related peaks.

A part of the thermal characterization involves thermogravimetric analysis (TGA). The examination employs a ramp method with an increase of $10\text{ }^{\circ}\text{C}/\text{min}$ on a polyimide sample. It is interesting to observe how these specific polymers can endure exceedingly high temperatures, which are nearly inconceivable for other polymers.

Figure 5.8 represents a thermo-gravimetric analysis for a sample made of pure polyimide.

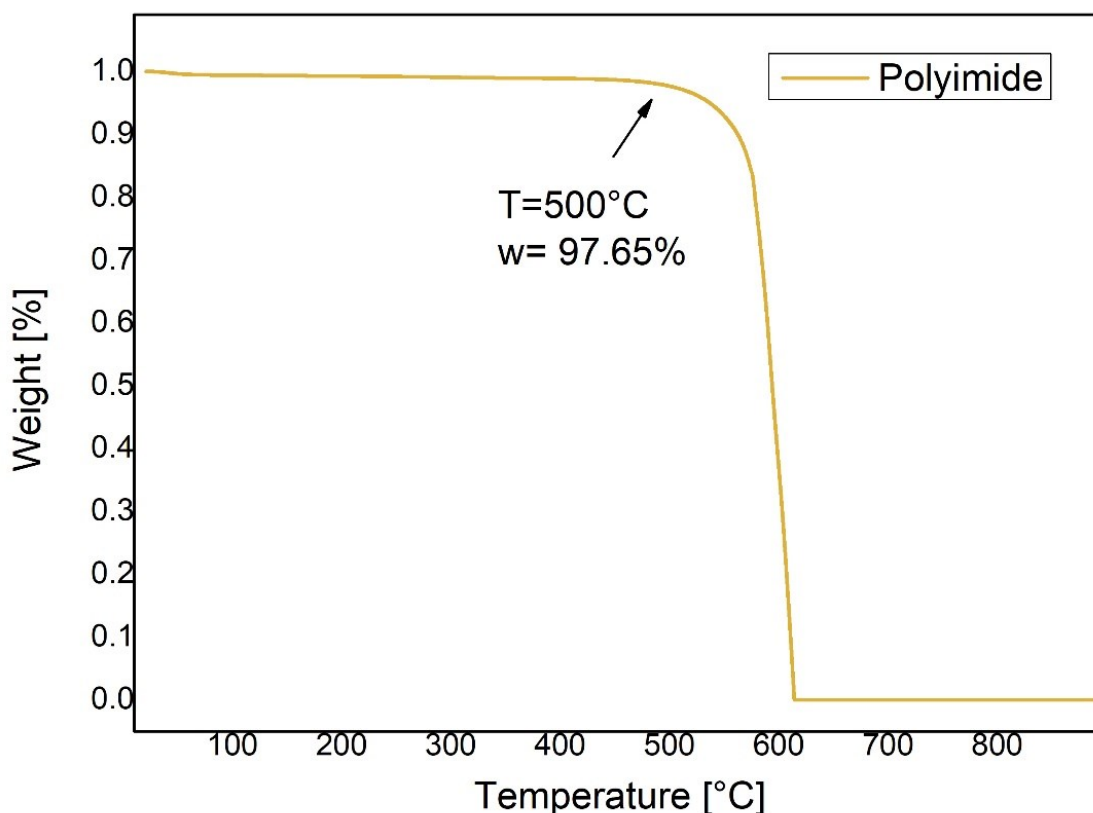


Figure 5.8 Thermo-gravimetric analysis of pure polyimide.

No significant weight loss or sample transition is observed until a temperature of approximately $500\text{ }^{\circ}\text{C}$ is reached, beyond this threshold, degradation initiates.

Conversely, in the analogous analysis conducted on a PAA sample, distinct inflections are evident in the initial part of the curve. Initially, the evaporation of residual solvent leads to the

first reduction in sample weight (153°C, boiling temperature of DMF). Subsequently, the imidization process induces a transformation in the sample structure (around 180 °C), resulting in a reduction in weight to attain the desired product.

In the next chapter, TGA technique will be adopted to measure the catalytic content of the membrane: at 800°C there are no traces of polyimide as it is completely degraded. The remaining weight will be addressed to the inorganic part of the membrane (i.e. TiO₂) that is the quantity of catalyst that has deposited on the membrane, and which can be useful for the photocatalysis in the abatement tests.

Chapter 6

Membrane production and characterization

The primary aim of this study is to create a fibrous structure capable of serving multiple functions, including:

- Supporting the catalyst utilized in advanced oxidation reactions.
- Resisting UV radiation.
- Remaining insoluble in water, the medium in which the subsequent reactions will occur.
- Maintaining satisfactory mechanical properties.
- contain a high catalyst content to promote photo-oxidative reactions to break down PFOA.

The proposed approach involves a polymeric membrane primarily comprising a structural element and a catalytic element, in line with the aforementioned specifications.

The membrane production involves a straightforward simultaneous deposition of the two components onto a rotating cylindrical collector, resulting in their random aggregation.

This chapter deals with the preparation of PAA solution, the electrospinning of the membranes and their characterization after the heat treatment. In particular, it is focused on the membranes' morphological properties based on viscosity measurements of the initial PAA solution.

In the next paragraph, the preparations of the structural and catalytic solutions are presented, subsequently the conversion to polyimide is described.

6.1 PAA membrane

Before arriving at the final product (polyimide membrane), an intermediate product (polyamic acid) must be passed through: this paragraph will therefore deal with the procedure for preparing the catalytic solution and the PAA solution which will then be electrospun to give a membrane in polyamic acid.

PAA membrane conversion to polyimide conversion is not covered here but in section 6.2.

6.1.1 PAA solution

The structural part of the membrane is prepared by solubilizing the two reagents inside DMF (solvent): 4-4' oxydianiline (ODA) and pyromellitic dianhydride (PMDA).

The order in which these two reactants are added is of fundamental importance: if ODA is the first to be added, PAA with a high molecular weight and high viscosity is obtained, otherwise, if PMDA is added as first, the solution does not reach high molecular weight and high viscosity, due to the hydrolysis of the dianhydride explained in Chapter 5.

Another factor that should not be underestimated is the reaction environment: the humidity present in the air can interact with the reagents and not make them available for the polymerization reaction. For this reason, the formation of the polyamic acid solution is carried out in an inert environment by continuously flowing nitrogen for the entire duration of the reaction.

Different concentrations of PAA in solution were tested but, in the end, a 21.6% PAA solution was the mostly used because it ensures high viscosity for several days. To obtain fibers during PAA electrospinning, high viscosities are necessary: knowing that the viscosity of the solution tends to decrease over time due to reactions that degrade PAA, starting with a high viscosity solution ensures that the solution itself can be used even days after its preparation compared to solutions that initially appear to have low viscosity.

To prepare a 21.6% PAA solution, 16.4 grams of DMF are weighted and put in a flask containing a magnetic stirrer. The flask is put over a magnetic plate for mixing.

Nitrogen is immediately blown into the flask to eliminate the humidity present in the air. After some minutes it is possible to insert 2.144 grams of ODA while maintaining the nitrogen flow. When ODA has completely dissolved, it is possible to insert 2.372 grams of PMDA very carefully: if it is added too quickly, the solvent is not able to solvate it completely and it will remain in solid state without reacting. It is advisable to insert the PMDA carefully and to increase the speed of the magnetic stirrer (at least 800 rpm) to increase the turbulence in the system so as to favor solubilization. The procedure can be summarized as follows:

1. Insert DMF into the flask and start the magnetic plate. Blow N₂ for half an hour.
2. After 30 minutes, add ODA.
3. When ODA is completely dissolved (~15 minutes), add PMDA increasing the speed of the magnetic stirrer.
4. Wait for the reaction to complete (~15 minutes). Turn off the nitrogen flow and close the flask.
5. Leave to mix for 24 hours.

Figure 6.1 shows the experimental setup.

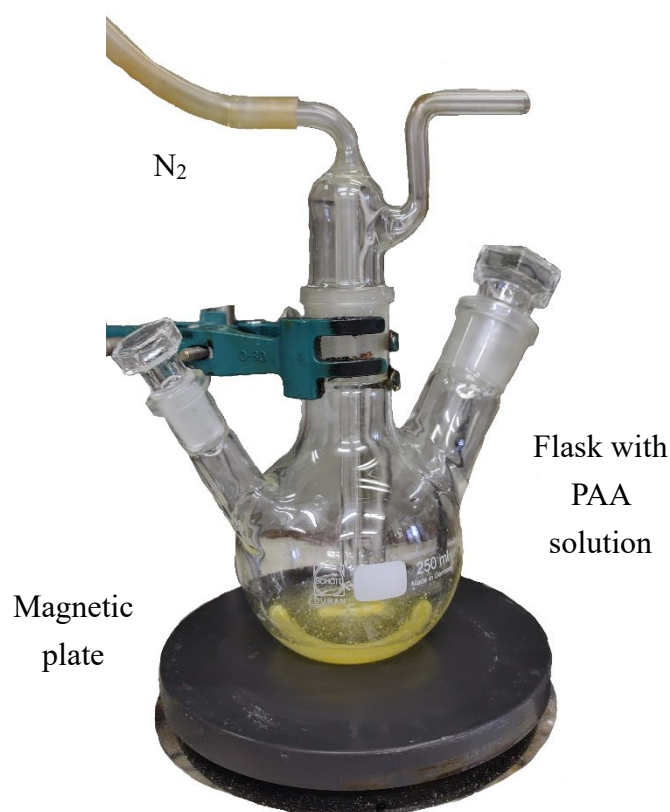


Figure 6.1 Experimental apparatus used for the preparation of PAA solution. It is composed by a glass flask which contains the solution, a magnetic plate and a tube from which the nitrogen comes out.

As soon as the PMDA is added, the solution acquires a yellowish color and reaches completion in a few minutes: at a certain moment the stirrer is no longer able to rotate due to the high viscosity. The newly produced solution is not homogeneous and is therefore left to mix for 24 hours before being used.

It is important to monitor the viscosity of the solution during time and how the preparation and storage conditions affect it (inert atmosphere/ambient atmosphere and storage in fridge vs storage at ambient temperature, respectively).

To understand how these conditions influence the viscosity of the mixture, two solutions at 21.6% in PAA were prepared: in one an inert environment was maintained (via nitrogen) for the entire duration of the reaction while in the other any inert atmosphere was created, and it remained in contact with the ambient atmosphere.

After leaving them to mix for 24 hours, they were separated to store one part at room temperature and another part in the fridge. Viscosity was monitored for 10 days. Results are shown in figure 6.2 and 6.3.

Figure 6.2 compares the viscosities of PAA solutions produced in different environment (maintaining the same temperature condition during the storage), figure 6.3 shows how viscosity changes if the solution is stored in fridge or at ambient temperature (comparison between solutions made with the same reaction environment, i.e. inert or uncontrolled ambient).

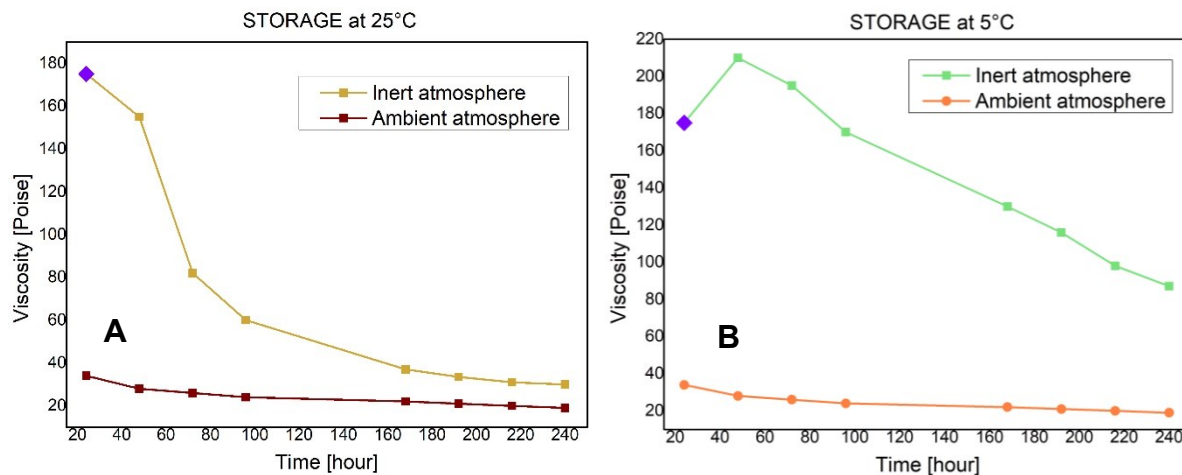


Figure 6.2 Effect of reaction ambient on PAA solution viscosity between solution stored at the same temperature (25°C in case A and 5°C in the case B).

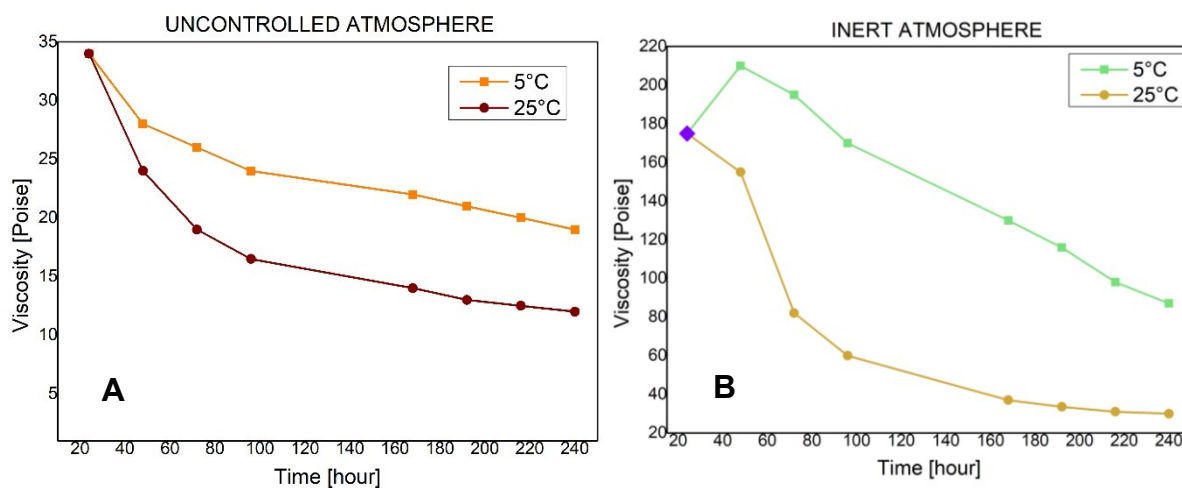


Figure 6.3 Effect of storage condition on PAA solution viscosity between solution produced in the same reaction environment (uncontrolled atmosphere case A and inert atmosphere case B).

The first viscosity measurement was carried out 24 hours after the preparation of the solutions: PAA solutions were separated only after the first viscosity measurement to be stored at different temperatures. The measurements were all carried out at 25°C except for the purple point present in some curves: the viscosity at that point was calculated at 50°C because it appeared outside the measurement range of the instrument (> 220 Poise).

Figure 6.2 shows how it is essential to maintain an inert atmosphere during the preparation of the solution: it is possible to see how the viscosity of those that have been in contact with air is immediately very low (close to the limit of 20 Poise, explained later). Using such solutions for the preparation of membranes can lead to the formation of defects in the membrane texture due to low viscosity. On the contrary, the inert atmosphere (in this case guaranteed by a N₂ blowing) prevents unwanted reactions from taking place, guaranteeing a high viscosity in the first measurements.

In Figure 6.3 *B* it is highlighted that an inert atmosphere alone is not sufficient to ensure a high viscosity of the solution in the days following the preparation of it: at low temperatures the solution maintains high viscosity for several days (probably because the hydrolysis reaction of the PAA results inhibited) and it can be electrospun even 10 days after its preparation; the same solution stored at 25°C must be spun as soon as possible due to its rapid decline. The storage temperature also influences the viscosity of the solution prepared in an uncontrolled environment: in figure 6.3 *A* the decrease in viscosity is slighter at 5°C but still takes on an exponential trend and in no way makes this solution suitable for spinning.

Concluding, an inert atmosphere and a storage at 5°C are the best conditions to obtain a solution with a high viscosity prolonged in time. In all the membranes prepared during this work, these conditions were adopted.

6.1.2 Catalyst solution

The catalytic solution is composed of the catalyst precursor and a support phase (PVP, polyvinylpyrrolidone).

To prepare the support part, 1.65 grams of polyvinylpyrrolidone are weighed, poured into 11.15 grams of ethanol and left to mix for at least two hours.

The catalyst precursor, TBT, is also weighed (4.5 grams), poured into 8.65 grams of acetic acid and left to mix for two hours. When both solutions are homogeneous, they are mixed together: the result is a yellowish liquid that smells of acetic acid. The mixture is left to mix for 24 hours. The solution is stored in the fridge to be used a few days after preparation. When the mixture ages, phase separation occurs and a white powder settles at the bottom of the container: in this case it is no longer considered usable.

To increase the deposition of catalyst on the membrane, some tests were done with a double content of TBT in the catalyst solution (9 grams instead of 4.5). The results will be presented in the paragraph relating to polyimide membranes.

6.1.3 Simultaneous electrospinning

When both the structural and the catalytic part of the membrane are ready, it is possible to proceed with spinning.

Two different syringes are filled with the solutions and placed in the cavity of the volumetric pumps. Once the process parameters are set, the deposition onto the collector can start. Experimental setup of a simultaneous deposition is depicted in Figure 6.4.

Every PAA solution has its own process parameters (mainly dependent on the PAA concentration): in table 6.1 are reported the process parameters for the catalytic solution and the 21.6 % PAA solution.

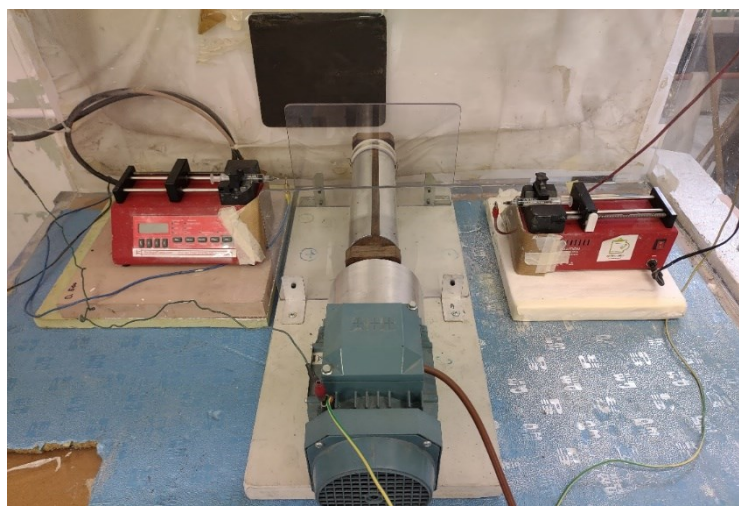


Figure 6.4 Electrospinning setup used for simultaneous deposition.

Table 6.1 Operative conditions during electrospinning for structural and catalytic solution.

Material	Flowrate [mL/hr]	Voltage [kV]	Needle	Distance [cm]	Collector speed [rpm]	Humidity [%]
PAA	1	18	21G	15	900	55
TBT/PVP	1.5	11	22G	10	900	55

The whole operation is carried out at room temperature. The deposition time varies between 240 and 360 minutes (4-6 hours). After this time the result is a yellowish-white color membrane placed over the aluminum foil. An example is given in figure 6.5.

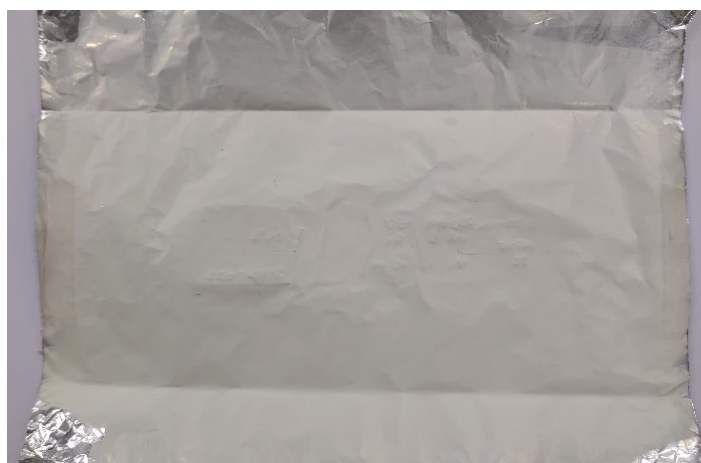


Figure 6.5 PAA/PVP/TBT membrane obtained via electrospinning.

Figure 6.6 provides a SEM image of a 21.6% PAA membrane. Fibers are almost straight, homogeneous and there is no difference between PAA and PVP/TBT fibers.

After 4-6 hours of deposition, what forms, therefore, is a yellowish-white membrane that can be easily removed from the aluminum foil and handled with great ease.

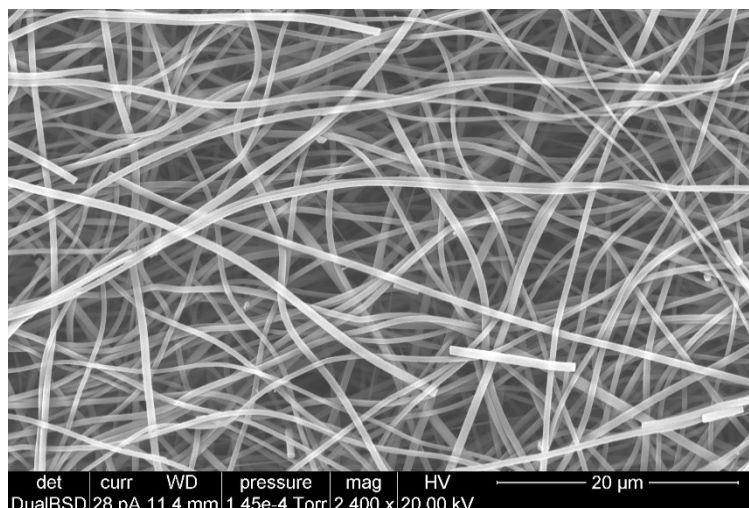


Figure 6.6 SEM image of a PAA/PVP/TBT membrane sample.

Initially, these favorable characteristics are credited to the presence of PVP. The polymer structure supporting the catalyst exhibits satisfactory mechanical properties within a certain temperature range, beyond which it starts to degrade. However, to activate the catalyst, a heat treatment reaching temperatures up to 400°C is required.

6.2 PI membrane

To obtain a polyimide membrane, a heat treatment is required which leads to the cyclodehydration of the PAA.

It is important to note that the catalytic material deposited serves as a precursor to titanium dioxide, which needs to undergo transformation into its reactive phase. Previous research⁸⁵ indicates that the most reactive phase of TiO₂ is anatase, achievable through thermal processes. The grafting of imide support serves the specific purpose of maintaining membrane integrity even after exposure to high temperatures. The ability to withstand high temperatures and maintain excellent mechanical properties, even exceeding 200°C, makes PI a perfect candidate for such applications. Therefore, the subsequent stage involves treatment in the oven, during which two main processes occur:

- Activation of the catalyst and degradation of the support polymer, resulting in the retention of only catalytic elements on the polyimide structure.
- Imidization of polyamic acid, cyclodehydration of the molecules to form the ultimate polyimides.

A controlled thermal ramp is necessary to promote each individual process without inducing cracks in the membrane.

Incrementally increasing the temperature will aid in smooth transitions and ensure effective treatment. The suggested thermal ramp is as follows⁸⁵:

1. 80 °C, for 1 hour
2. 160 °C, for 30 minutes
3. 200 °C, for 30 minutes
4. 250 °C, for 30 minutes
5. 300 °C, for 2 hours
6. 350 °C, for 2 hours
7. 400 °C, for 3 hours

The rate of temperature increase for each phase is 2 °C/min, with a total duration of 770 minutes (almost 13 hours).

In Figure 6.7, two membranes are depicted. On top is shown before heat treatment: it remains clear, elastic, and wrinkle-free but catalytically deactivated. On the other hand, the membrane depicted on the bottom has undergone the treatment. Its smaller size and yellowish color are immediately noticeable, indicating the desired transformations have occurred. Additionally, it is less flexible while still maintaining good malleability.

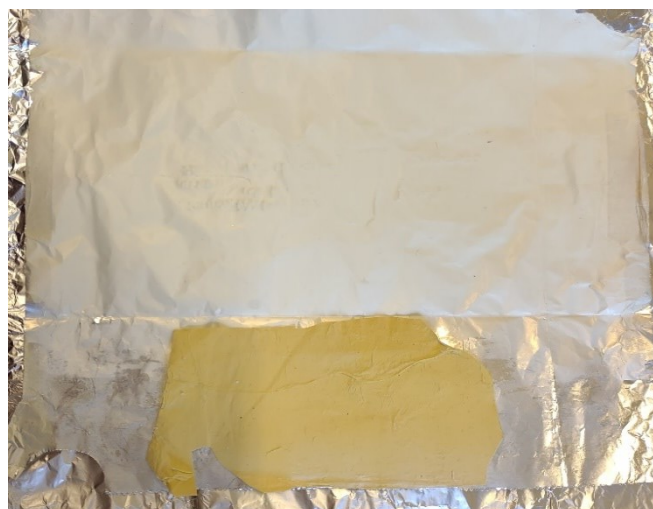


Figure 6.7 Effect of heat treatment on the membrane. Conversion to PI gives a yellowish color to the membrane.

Figure 6.8 shows a SEM image of a PI membrane obtained from a 21.6% PAA solution spun with the catalytic solution.

From figure 6.8 can be seen that the main texture of the membrane is based on polyimide fibers dispersed in a random way. In addition, there are some rods scattered randomly (highlighted with red circles): this is the final form of the catalyst after the heat treatment.

The next paragraph gives some elucidation about TiO₂ structure once activated.

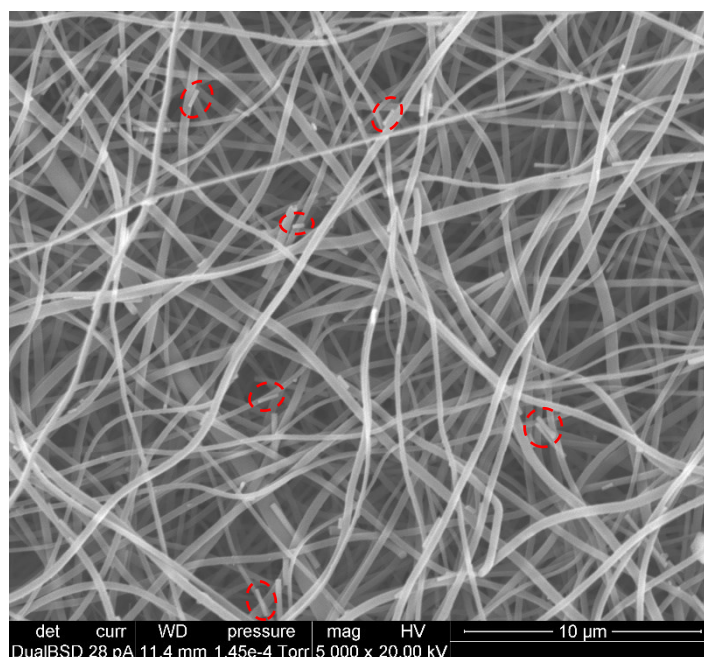


Figure 6.8 *PI/TiO₂ membrane structure.*

6.2.1 TiO₂ characterization

The heat treatment presented in the previous section causes the evaporation of the PVP and the conversion of the TBT into TiO₂. Following the heat treatment, the polyimide membranes have an intense yellow color, and, in some places, they can be covered by a white layer: this is nothing other than the form that the TiO₂ takes after calcination. Figure 6.9 compares a homogeneous membrane (with an even catalyst dispersion) and a membrane partially covered by a white layer (uneven dispersion of TiO₂): the color of that part of the membrane indicates a high TiO₂ content in that area.



Figure 6.9 *Homogeneous and uneven TiO₂ dispersion in a PI membrane.*

To confirm this, a SEM image of the white structure with the relative EDS spectra is presented in figure 6.10.

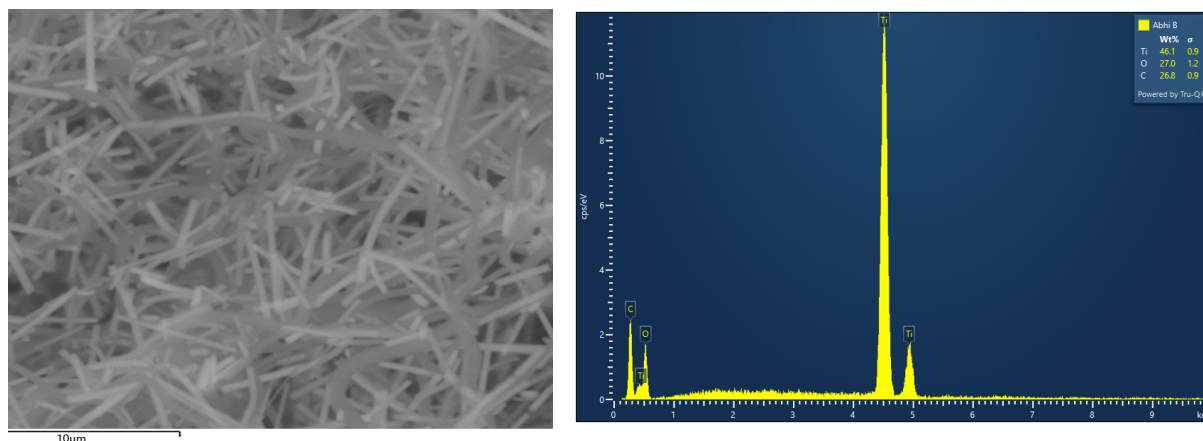


Figure 6.10 SEM image of a white layer coupled with its EDS spectra.

Figure 6.10 shows how TiO_2 , after calcination, appears as cracked fibers or in the form of nanotubes of various lengths but of similar diameter. The EDS spectra confirms what was previously stated: the nanotubes observed under the microscope are composed of titanium and oxygen. Carbon traces present in the spectra are almost certainly caused by the presence of polyimide in the sample.

Previous researchers stated, thanks to XRD analyses, that TiO_2 deposited on the membrane takes the form of anatase more than rutile⁸⁵.

6.2.2 Membranes TiO_2 content

To analyze the catalyst content on the membranes, a thermogravimetric analysis is carried out. Ideally the catalyst content should be high enough to guarantee a good activity of the membrane in the field of photo-oxidative reactions: it is important to remember that too high catalyst content causes a loss of the mechanical properties of the membrane, making it more fragile.

The catalyst content is therefore the result of a compromise between good mechanical properties and good catalytic activity of the membrane.

The objective of this work was to obtain membranes with a TiO_2 content of 20% by weight compared to the membrane.

Some tests were carried out to analyze how the deposition of titanium oxide varied; specifically, we attempted to analyze how the TBT content in the catalytic solution and the flow rate of the solution itself during the electrospinning affected the titanium oxide content in the PI membrane.

The main attempts are summarized in table 6.2 (voltage applied to the syringe is not reported but varied between 10 and 11 kV for all the tests).

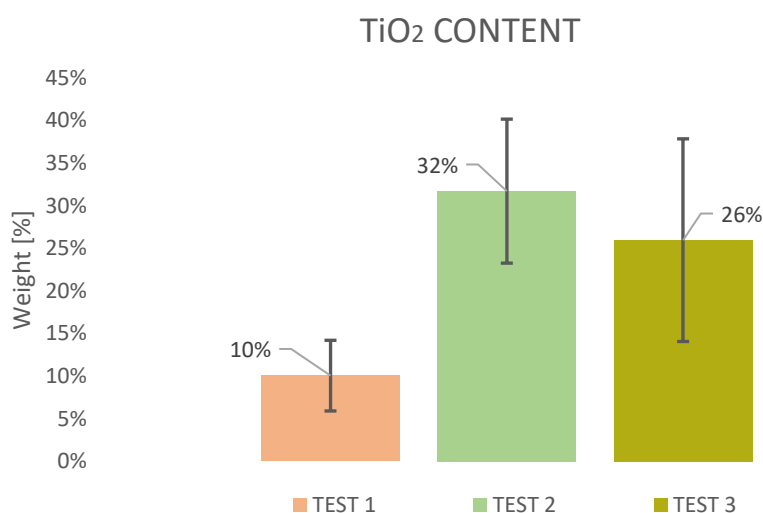
Table 6.2 Different electrospinning condition for the catalyst solution.

TEST 1			TEST 2			TEST 3		
Flowrate [mL/hour]	TBT content [grams]	Needle	Flowrate [mL/hour]	TBT content [grams]	Needle	Flowrate [mL/hour]	TBT content [grams]	Needle
1	4.5	22G	1.5	4.5	22G	1.5	9	22G

The working conditions expressed in *Test 1* were the conditions applied during the spinning for the first membranes produced: they did not prove to be optimal because led to the formation of sticky compounds on the syringe needle which blocked the jet of the solution. For these reasons the TiO₂ content in the membranes subjected to *Test 1* was found to be poor.

Test 2, on the contrary, gave good results, that are appreciable content of catalyst and stable conditions during spinning (no sticky compounds were created): changing the flowrate seems enough to have a stable jet for all the deposition time.

In *Test 3* we tried to double the TBT content in the catalyst solution to understand how it affects the deposition. Results obtained were worse than those obtained with *Test 2*: doubling the precursor content does not appear the best choice to arrive to a higher catalyst content in the membrane. In some cases, working with conditions expressed with *Test 3* led to an uneven distribution of TiO₂: an example is given in figure 6.9 where the membrane on the right was spun with a double amount of TBT. Results are summarized in Figure 6.11.

**Figure 6.11** TiO₂ content in the membranes respect to the conditions used.

Membrane used during experiments were made using conditions expressed by *Test 2* or *Test 3*. Despite the tests carried out, further studies would be necessary to optimize the deposition of the catalytic solution, starting from the optimal TBT content.

6.3 Fiber dimension analysis

Another study conducted on membranes was the analysis of fiber dimensions. In this paragraph it is analyzed the effect of the heat treatment and of the viscosity on the dimensions of the fibers. Finally, we tried to understand if the amount of TBT in solution has any influence on the size of the nanotubes.

6.3.1 PAA – PI fiber dimension

In this section are presented all the SEM images of the membrane analyzed with the relative fiber distribution. Fiber dimensions were computed exploiting *ImageJ*, a digital image processing computer program, capable of measure pixel lengths if the user sets a scale. Using the scale provided by the SEM, we can compute the fiber dimensions exploiting *ImageJ* features.

From figure 6.13 to figure 6.21 are presented the SEM images of PAA and PI membranes with the relative fiber distribution.

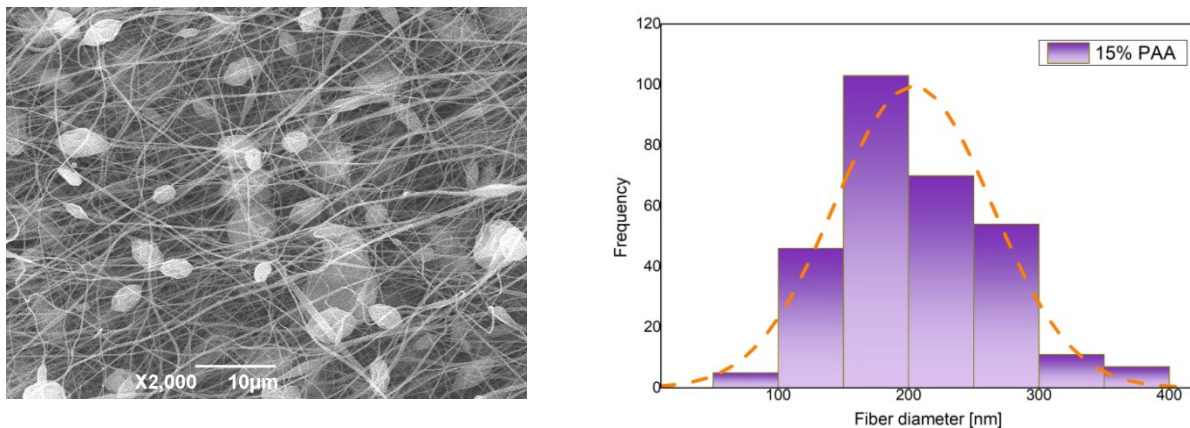


Figure 6.13 PAA 15% concentration SEM image and fiber distribution.

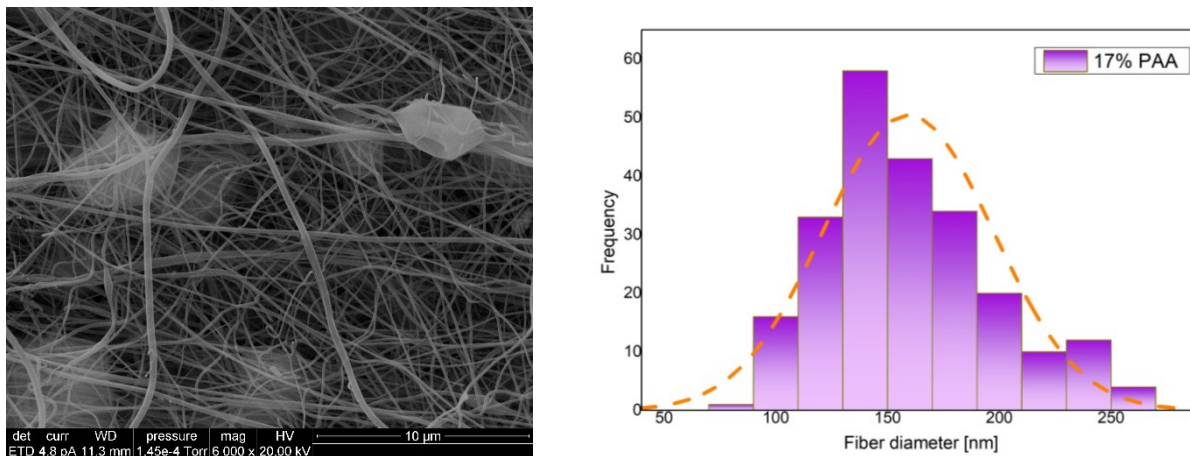


Figure 6.14 PAA 17% concentration SEM image and fiber distribution.

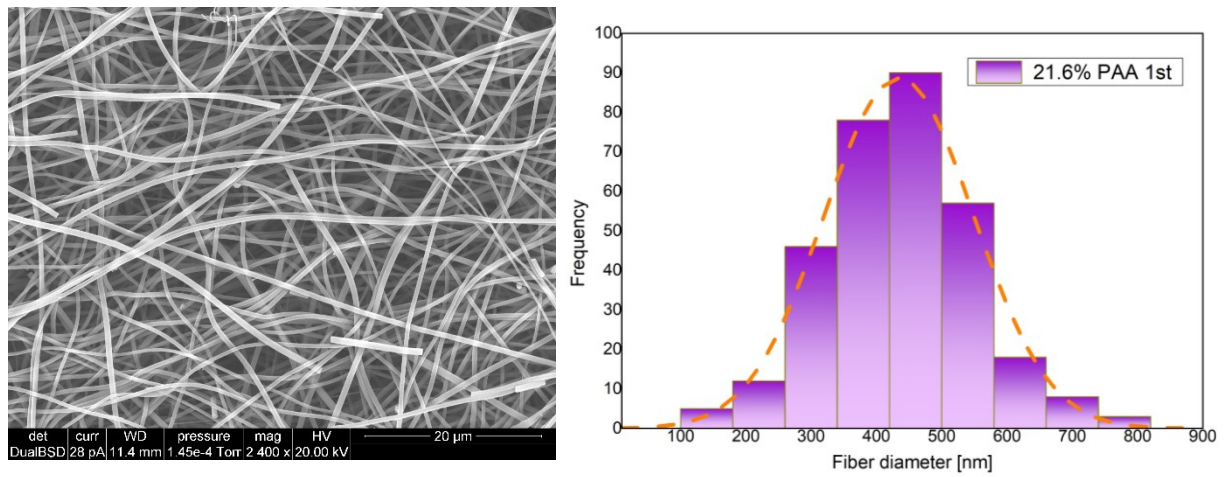


Figure 6.15 PAA 21.6% concentration SEM image and fiber distribution.

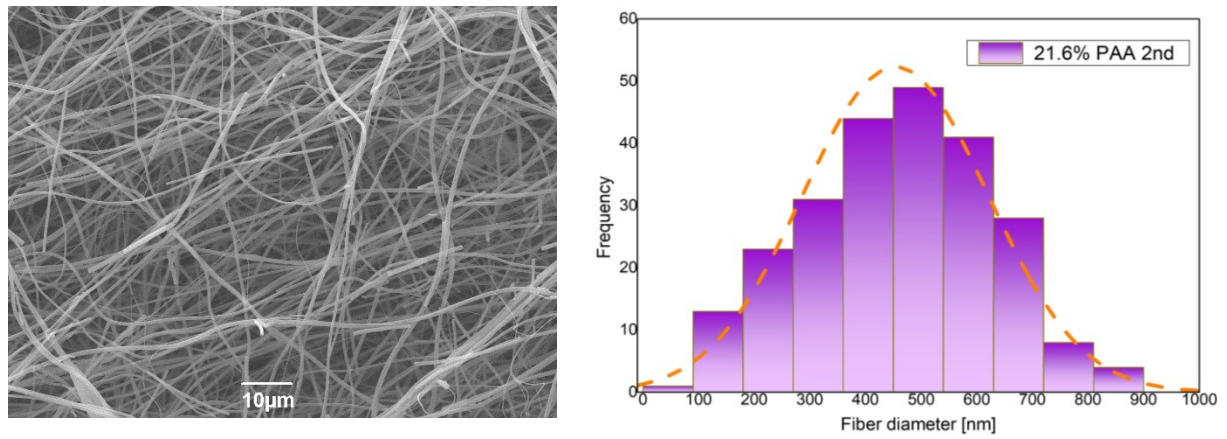


Figure 6.16 PAA 21.6% concentration SEM image and fiber distribution.

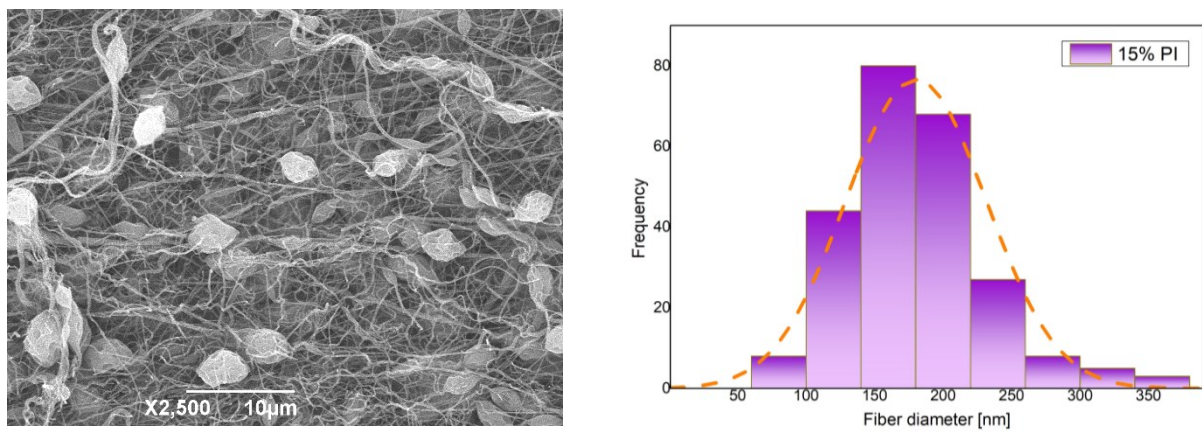


Figure 6.17 PI 15% concentration SEM image and fiber distribution.

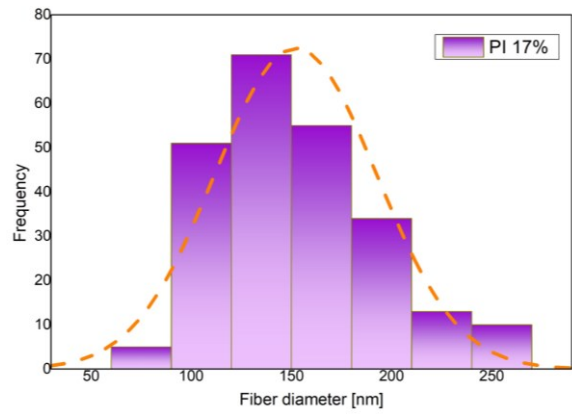
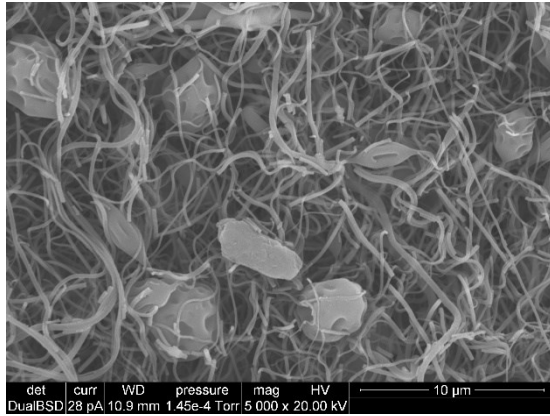


Figure 6.18 PI 17% concentration SEM image and fiber distribution.

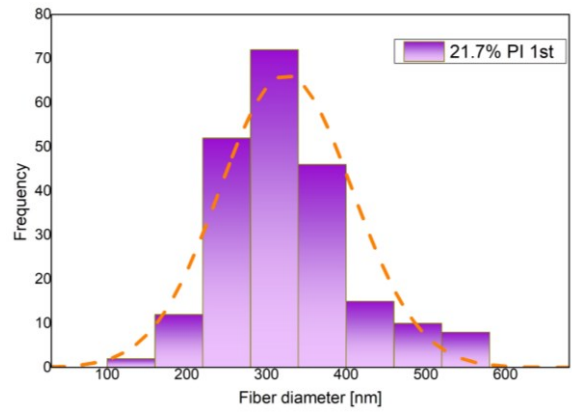
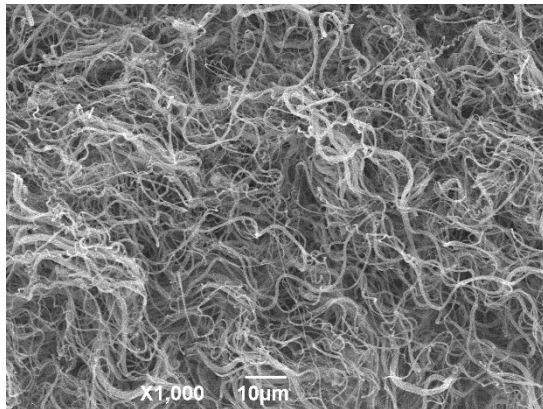


Figure 6.19 PI 21.7% concentration SEM image and fiber distribution.

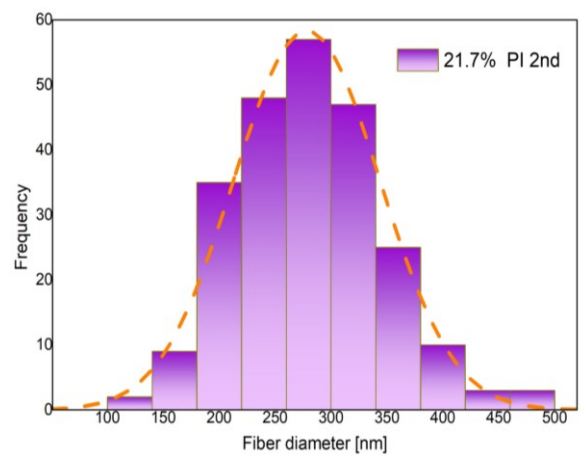
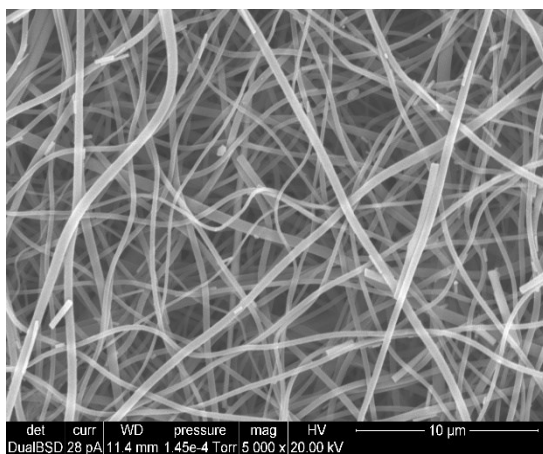


Figure 6.20 PI 21.7% concentration SEM image and fiber distribution.

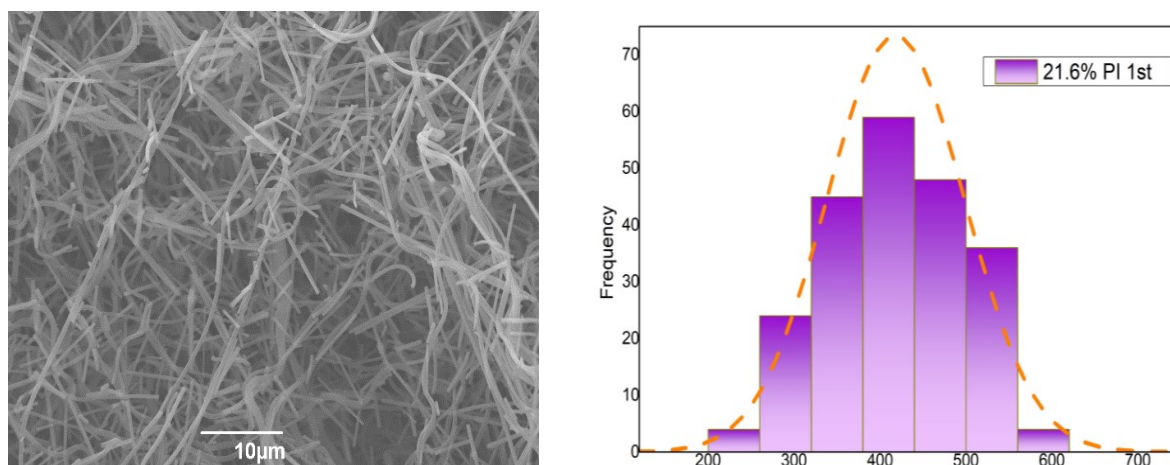


Figure 6.21 PI 21.6% concentration SEM image and fiber distribution.

Results are summarized in table 6.3.

Table 6.3 Mean fiber diameter related to polymer concentration and viscosity of the solution measured before spinning.

Polymer concentration [w/w]	μ [Poise]	PAA mean diameter [nm]	PI mean diameter [nm]
15%	19	203±60	180±52
17%	17	166±53	152±40
21.7%	135	-	278±65
21.7%	70	-	324±83
21.6%	200	434±114	418±80
21.6%	170	453±166	-

Missing values are caused by the absence of a microscope image for that sample.

Solutions at 21.7% came from two different solutions spun in different days while solutions at 21.6% are the same solution spun in different days (this explains the decrease in viscosity).

From table 6.3 can be seen that PAA fibers have a slightly larger diameter than PI fibers because during the thermal treatment, a slight shrinkage of the system occurs which leads to a decrease in the dimensions of the fibers: comparison is given in figure 6.22.

Fiber dimension is an important parameter to take into account in membrane processes because it can affect both pressure drops and interaction with the pollutant: small fibers have a larger surface area and can therefore interact more with the contaminant present; on the other hand, the smaller their size, the greater the pressure drops that will be introduced into the system. Considering this thesis work, larger fibers were chosen because the primary objective is not to move the contaminant from the aqueous phase to the solid phase (represented by the membrane) but to bring it to complete decomposition. Furthermore, in cases where very fine fibers were observed, the texture of the membrane presents many defects: the viscosity of the solution was not high enough to obtain a membrane without beads via electrospinning.

Figure 6.22 shows the variation of the fiber diameters as a function of the viscosity of the solution: it is very clear that, spin a solution with a high viscosity leads to a membrane composed by fibers of a greater diameter. Viscosity is therefore a fundamental parameter for the final dimensions of the fibers that make up the membrane.

It is essential to have a high viscosity to obtain defect-free fibers: the low viscosity of the 15% and 17% solutions (19 and 17 Poise, respectively) caused the formation of beads in the membrane texture.

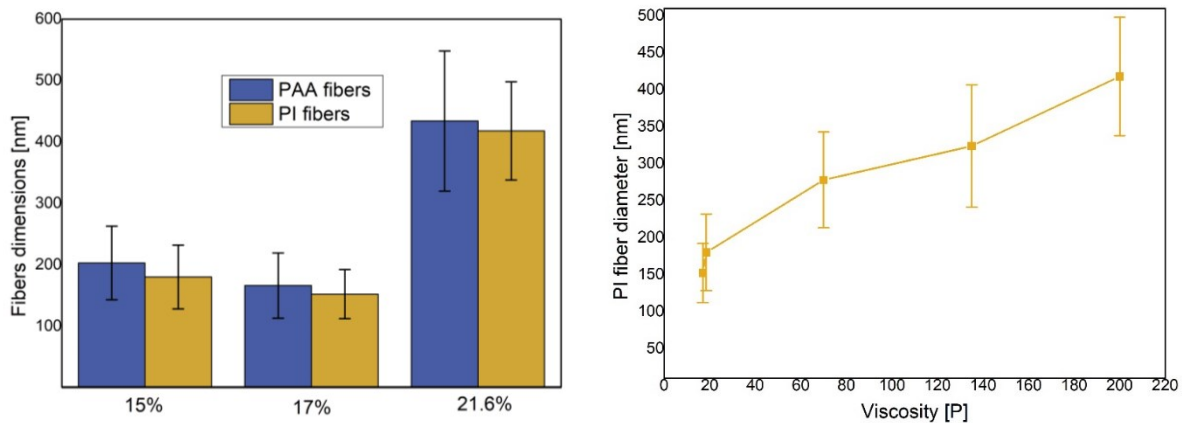


Figure 6.22 Heat treatment and viscosity effects on PAA and PI fibers.

It is therefore important to highlight how 20 poise is, in this study, a limit viscosity around which fibers with numerous defects are obtained. For this reason, in this thesis work, membranes obtained from a 21.6% PAA solution were mostly used, i.e. for high viscosities.

6.3.2 TiO₂ nanorods dimension

In one of the previous paragraphs, we tried to analyze how the quantity of TBT in the catalytic solution modified the amount of TiO₂ in the membrane. In this paragraph we will study how the quantity of TBT in the catalytic solution affects the final size of the nanotubes.

Here are reported the results for depositions carried out with a TBT content of 4.5 and 9 grams.

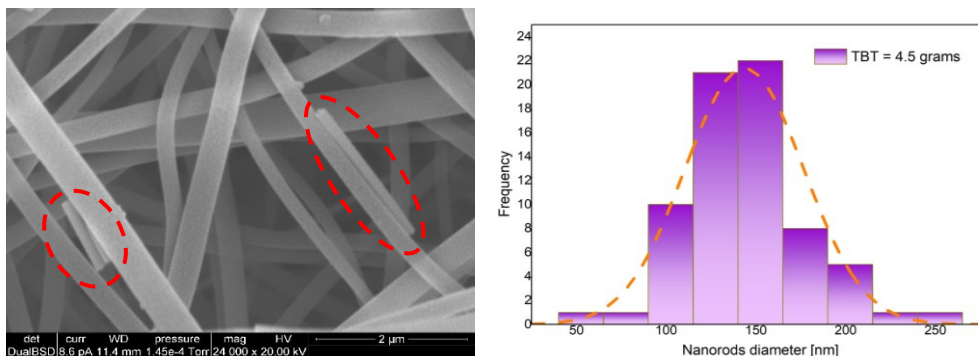


Figure 6.23 TiO₂ nanorods SEM image for a TBT content of 4.5 grams with its diameter distribution.

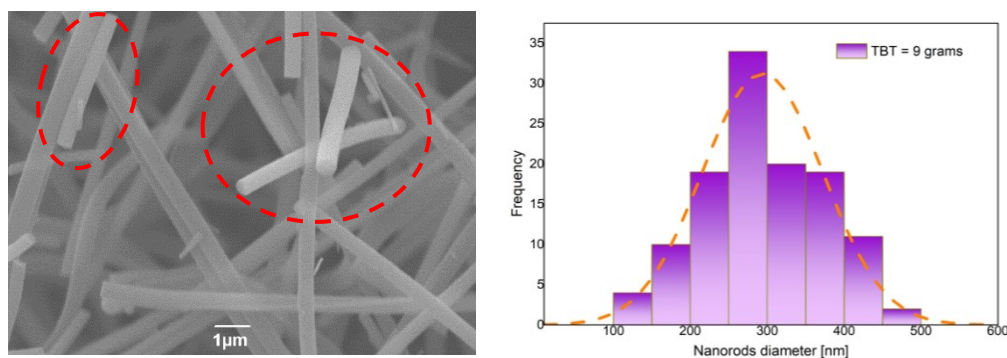


Figure 6.24 TiO_2 nanorods SEM image for a TBT content of 9 grams with its diameter distribution.

Results are summarized in table 6.4. In both cases the catalytic solution was spun with a flowrate of 1.5 mL/h using a needle 22G.

Table 76.4 TiO_2 nanorods dimension.

TBT content [grams]	Nanorods dimension [nm]
4.5	143.5 ± 33
9	293 ± 78

The precursor content in the catalytic solution has a strong effect on the titanium oxide nanorods, in fact, if its content in solution is doubled, the diameter of the nanorods obtained is also doubled.

This effect can have a great impact on the catalytic activity of the membranes: if two different membranes with the same catalyst content were spun with different catalyst solutions (namely, one with 4.5 grams of TBT and one with 9 grams of precursors), the membrane with a double TBT content will have larger nanotubes compared to the membrane with a normal TBT content. However, having the same final catalyst content, this translates into a smaller number of active sites and a lower surface area dedicated to photocatalysis.

If, previously, it was analyzed how a high TBT content does not improve the deposition of catalyst in the membrane, this paragraph highlights how a double TBT content is deleterious for the number of active sites that may be present in the membrane and that can be active during the photocatalysis.

Concluding, it is preferable to spin a solution which leads to a small dimension of titanium nanorods, because of a greater surface area which can improve the pollutant degradation.

Chapter 7

PFOA degradation tests and results

In this last chapter, the results on PFOA abatement are presented.

An attempt was made to distinguish the various contributions related to PFOA removal, i.e. AOPs, adsorption into the membrane matrix and photocatalysis. Three different experimental methodologies were therefore carried out to analyze these different participations.

In the first case, only water (contaminated with PFOA and the chemicals necessary for AOPs) circulated through the system without any membrane inside the photoreactor (*No Membrane + reagents experiments*); in the second case a membrane was inserted into the reactor (*Membrane + reagents experiments*) while in the third case a membrane and a UV lamp were used to also exploit the photocatalyzed reactions (*Membrane + reagents + UV experiments*).

Testing set up, analytic method and results are reported and compared with each other.

7.1 Testing setup

The system used for the removal of fluorinated compounds from water is composed of a photoreactor, polypropylene tubes, a centrifugal pump, a peristaltic pump and a water reservoir. 5 mg of PFOA, 25 mg of FeSO_4 , 10 grams of $\text{K}_2\text{S}_2\text{O}_8$, 100 mg of H_2O_2 and 0.1 ml of H_2SO_4 are added in one liter of milliQ water for all the experiments presented here. To encourage the solubilization of these compounds, the contaminated water is placed in an ultrasonic bath for 45 minutes. Figure 7.1 shows a schematization of the experimental setup.

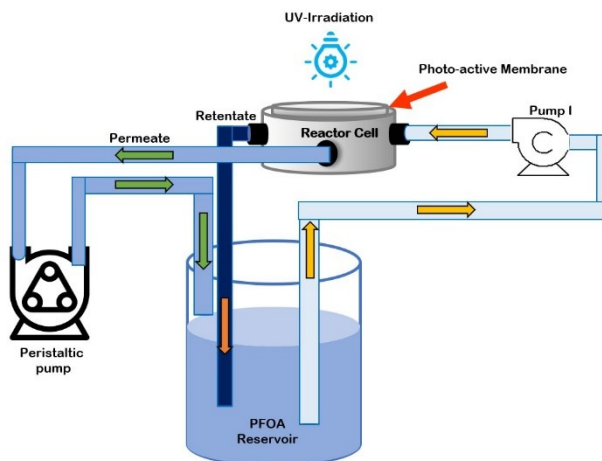


Figure 7.1 Representation of the experimental setup.

Before pouring the water into the system it is necessary to take the first sample (which indicates the initial PFOA concentration), insert the membrane inside the photoreactor and turn on the UV lamp (if necessary). To monitor the concentration of PFOA in water, a sample is taken every hour for a total of 5 hours of analysis. The samples, placed in a polypropylene container, are stored at a temperature of 0°C until the analysis, carry out by HPLC-MS.

The overall system can be classified as a batch reactor and the overall mass balance for it is given by equation 7.1

$$A = I - O + P - C \quad (7.1)$$

but, considering there is nothing entering or exiting from the system, input, output terms (I and O) can be deleted, and the last equation can be rewritten as

$$A = P - C \quad (7.2)$$

where P and C are the production and the consumption term of a species.

Equation 7.2 can be used for all the species present in this study, from the PFOA to the smaller perfluoroalkyl chain produced during the experiments, i.e. perfluoroheptanoic acid (PFHpA), perfluorohexanoic acid (PFHxA), perfluoropentanoic acid (PFPA) and perfluorobutanoic acid (PFBA).

In this thesis work we will refer to the removal, adsorption of perfluorooctanoic acid and fluorine, and defluorination of the system.

Defluorination is defined as the elimination of fluorine species from the system, i.e. the process that leads to the complete mineralization of PFOA which creates HF and CO₂; the *adsorption* term is given by the transfer of the contaminant from the water to the membrane matrix while the *removal* is defined as the total removal of PFOA or fluorine from the system, which can be caused by PFOA degradation into minor perfluoroalkyl chains and by the two processes indicated above, adsorption and defluorination.

7.2 Experimental tests

This paragraph is dedicated to the presentation of the results of the different experimental methodologies adopted in this study.

7.2.1 No Membrane + reagents experiments

In this section are shown the results relative to the experiments performed without any membrane: after the contamination of the water with PFOA (5 mg), FeSO₄ (25 mg), K₂S₂O₈ (10 grams), H₂O₂ (100mg) and H₂SO₄ (0.1 ml), the first sample can be collected, and the experiment can start. In this case, PFOA removal from the water is attributed to the oxidation reactions promoted by the reagents add to the water: the fundamental assumption is that the system does not participate in the absorption of PFOA.

The degradation trend of the contaminant is given by curves describing the concentration of the pollutant: the objective is to observe a decrease in concentration over time.

The PFOA removal can be defined, in this case as in the others, as the difference between the initial and the final PFOA concentration, as expressed in equation 7.3

$$PFOA_{removal} = 1 - \frac{PFOA}{PFOA_0} \quad (7.3)$$

where $PFOA$ indicates the PFOA concentration over time and $PFOA_0$ indicates the initial PFOA concentration.

The results for this case are reported in figure 7.2: they are shown as PFOA concentration (ppm or mg/L) in time and as ratio between initial PFOA concentration and PFOA concentration in time.

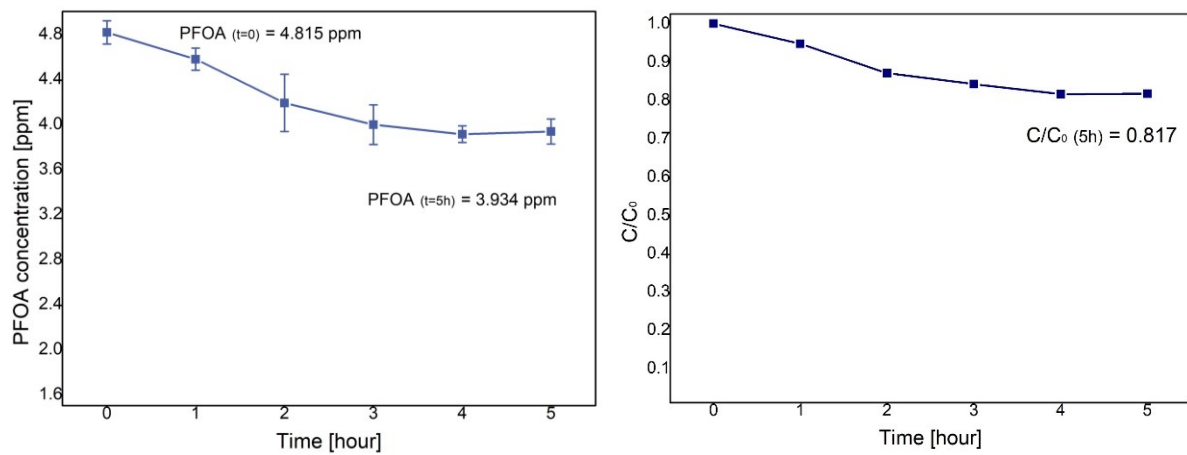


Figure 7.2 PFOA degradation in time without membrane in the system.

During the experiment there is a slight reduction in the concentration of the contaminant over time: it reaches a minimum within the first 3 hours and then stabilizes around the final value. In this case the degradation of the contaminant is modest as the absence of UV light does not favor the production of radical species.

The removal of PFOA, calculated with equation 7.3, after 5 hours is stable at a value around **18.30%**: this result was expected since, as written in the second chapter, the Fenton process is not effective if assisted only by visible light because ferrous ions are not recycled (equation 2.3, where Fe(III) is reduced to give Fe(II), available again to produce hydroxyl radical, following equation 2.2), and the same goes for oxidation via persulphate, as $SO_4^{\cdot-}$ radicals are not assisted properly without adequate radiations. Moreover, the photocatalysis was not exploited.

The defluorination, i.e. the process that leads to the mineralization of PFOA in HF and CO_2 , can be calculated through a simple mass balance for the fluorine species in the system from time $t=0$ until the completion of the experiments. At time $t=0$, the only fluorinated compound present in the system is PFOA which, upon decomposition, creates perfluoroalkylated

compounds formed by smaller chains. If we want to express fluorine moles (or mmoles) removed from the system, they can be expressed using the following equation

$$F_{removal} = \left(\frac{PFOA_0}{MW_{PFOA}} - \frac{PFOA_{5h}}{MW_{PFOA}} \right) \cdot n_F^{PFOA} - \sum_i \frac{PFAS_{i,5h}}{MW_i} \cdot n_F^{PFAS_i} \quad (7.4)$$

where $PFOA_{5h}$ is the final PFOA concentration, MW_{PFOA} is the PFOA molecular weight, n_F^{PFOA} is the number of fluorine contained in a PFOA molecule, $PFAS_{i,5h}$ is the concentration of a smaller perfluorinated compound produced during the pollutant abatement in 5 hours, MW_{PFAS_i} and $n_F^{PFAS_i}$ are the molecular weight and number of fluorine atoms of that specific byproduct. The defluorination can be simply expressed as the ratio between the F moles eliminated and the initial F moles (equation 7.5).

$$DEF = \frac{F_{removal}}{F_0} \quad (7.5)$$

Initial fluorine moles can be calculated with equation 7.6.

$$F_0 = \frac{PFOA_0}{MW_{PFOA}} \cdot n_F^{PFOA} \quad (7.6)$$

Perfluoroalkyl products characteristics are summarized in table 7.1.

Table 7.1 PFAS molecular weight and relative number of fluorine atoms.

Perfluorinated species	MW [g/mol]	n_F
PFOA	414.07	15
PFHpA	364.06	13
PFHxA	314.05	11
PFPA	264.05	9
PFBA	214.04	7

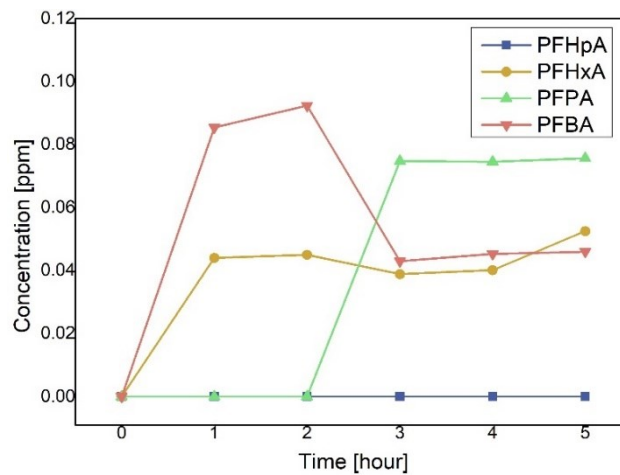


Figure 7.3 Concentration of smaller PFAS chains produced during the PFOA

The byproducts are shown in figure 7.3: they tend to form, degrade and then stabilize their concentration in the last 3 hours; it is the same trend that PFOA concentration presents: the species involved in the production of radicals appear to be active only in the first 3 hours, subsequently they do not play an appreciable role in the degradation of fluorinated compounds. This is probably due to the fact that, by recombining, the compounds responsible for AOPs form species that are not active for the removal of contaminants, significantly lowering the efficiency of the process. After 5 hours, fluorine moles eliminated stands around 0.0171 mmol (defluorination equal to **13.59%**): it is possible to improve this result by introducing a membrane into the photoreactor also exploiting the photocatalyzed reactions through the use of UV light as will be explained in the next paragraph.

7.2.2 Membrane + reagents experiments

Differently from what was performed in the previous paragraph, in these sets of experiments a membrane was inserted inside the photoreactor, without however using a UV lamp.

The water was contaminated in the same way and a sample was taken every hour for a total of 5 hours: it can therefore be thought that further removal of PFOA from the system is due to its adsorption on the membrane matrix. By comparing the data obtained in the previous section with those presented, the quantity of PFOA adsorbed in the thickness of the membrane can be obtained. The assumption introduced (i.e. that defluorination remains constant in the case in which no membrane is present and in the case in which a membrane is inserted into the photoreactor) is not correct since, probably, the membrane offers a surface where contaminants and reagents can meet, increasing the number of useful collisions between them and promoting the degradation of PFOA. If experimental data were available for the case in which a membrane was inserted into the reactor, but no reagent dedicated to AOPs was present, it can be safely assumed that the decrease in PFOA concentration is caused entirely by its adsorption on the membrane (eq. 7.7).

$$PFOA_{ads} = PFOA_0 - PFOA_{5h} \quad (7.7)$$

The relative adsorption of the membrane would be the ratio between the PFOA amount adsorbed and the initial PFOA concentration in the system.

$$PFOA_{ADS} = \frac{PFOA_{ads}}{PFOA_0} \quad (7.8)$$

In the absence of further experimental data regarding the pure adsorption of PFOA inside the membrane, this first approximation can be considered valid despite underestimating the actual degradation of PFOA since the defluorination of the system is considered the same as the previous case, where no membrane was present. After this clarification, the experimental procedure followed can be described.

The thickness of the membranes is a factor that can influence the adsorption of the contaminant: for this reason, in this set of experiments, membranes with thicknesses of 0.15 mm, 0.3 mm and 0.5 mm were tested to analyze how it influences the PFOA adsorption in the membrane. Figure 7.4 shows the trend of C/C_0 for three different thicknesses.

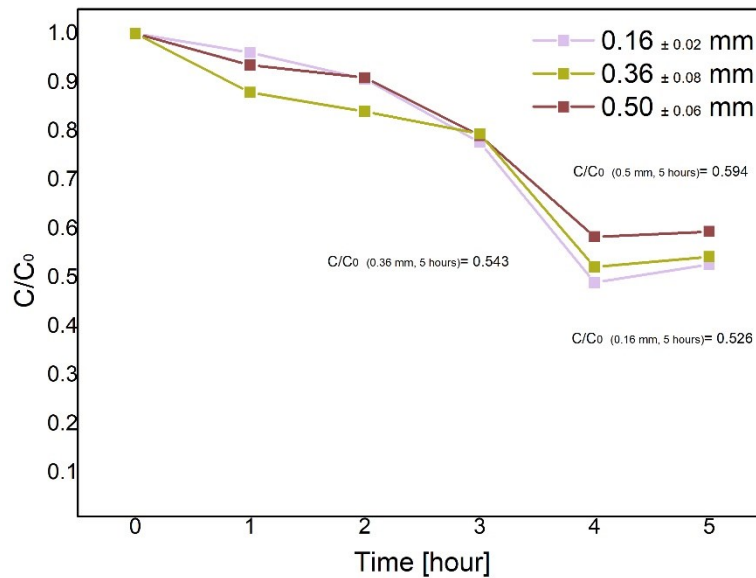


Figure 7.4 PFOA C/C_0 value for different membrane thicknesses.

Even the different dimension, membrane performances were the same in three cases and the obvious conclusion is that the thickness does not play a significant role in the PFOA removal from water.

When a membrane is inserted inside the reactor, equations (7.4) and (7.5) are no longer valid to calculate F moles eliminated and defluorination, as the removal of PFOA from the system is not only caused by oxidation reactions but also by its adsorption on the membrane. To overcome this, it was assumed that defluorination remains unchanged for a system that has no membrane and for a system where a membrane has been positioned.

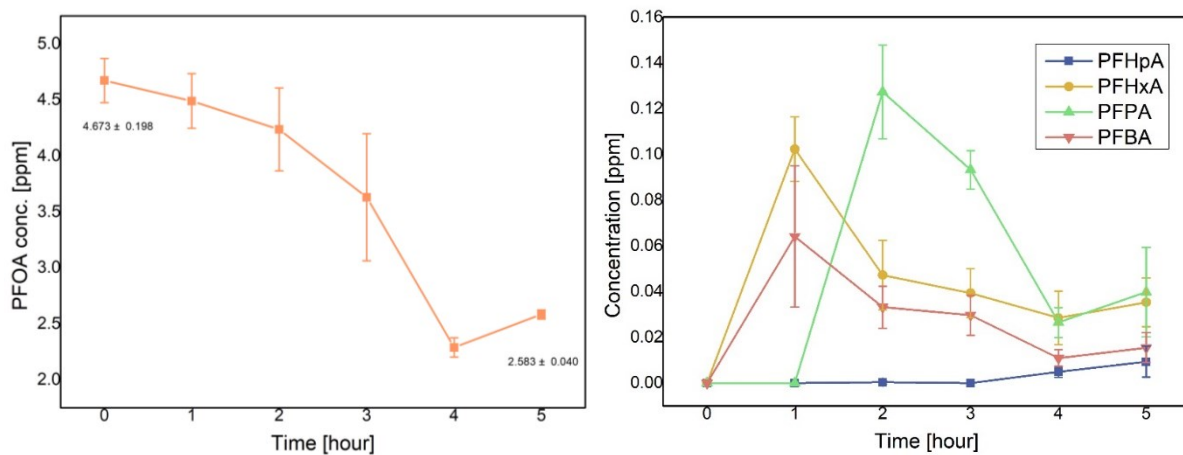


Figure 7.5 PFOA and byproducts concentration in case of 0.16 mm membranes.

This assumption seems not so reasonable but there was not any data available for membrane adsorption, as explained above.

Figure 7.5 shows the PFOA and byproducts concentration in time for the set of exp. with 0.16 mm membranes.

The concentration of fluorinated species in figure 7.5 present a common trend: in all the cases the concentration of perfluorinated species is decreasing in time until the 4th hour is reached and at that point the concentration increases.

This phenomenon can be correlated to the desorption of PFOA (and relative species) from the membrane: at that point the membrane is saturated and not only is it no longer able to accommodate compounds in its matrix, but it begins to release the previously adsorbed species into the system, causing an increase in their concentration.

The PFOA removal computed with eq. (7.3) is **44.72%**. Unfortunately, 5 hours are not enough to appreciate a complete desorption trend, therefore we will refer to the species adsorbed by the membrane as species that have been adsorbed in 5 hours, thus excluding from defluorination the F moles contained in the contaminants released from the 4th to the 5th hour.

Results are summarized in table 7.2.

Table 7.2 Concentration of perfluoroalkylated species in case of membrane experiments.

Time [hour]	PFOA [ppm]	PFHpA [ppm]	PFHxA [ppm]	PFPA [ppm]	PFBA [ppm]
0	4.673±0.198	0	0	0	0
1	4.491±0.244	0	0.10232±0.0142	0	0.06415±0.0309
2	4.237±0.370	0.0003±0.0007	0.04718±0.0152	0.12732±0.0206	0.03319±0.0092
3	3.631±0.567	0	0.03931±0.0107	0.09327±0.0084	0.02964±0.0087
4	2.288±0.086	0.00495±0.0024	0.02845±0.0117	0.02651±0.0065	0.01095±0.0036
5	2.583±0.040	0.00936±0.0067	0.03529±0.0106	0.03975±0.0195	0.01544±0.0065

Assuming that the defluorination is not changing, 13.58% of fluorine is eliminated from the system: F moles defluorinated can be found by reversing equation 7.5.

$$F_{removal} = \frac{PFOA_0}{MW_{PFOA}} \cdot n_F^{PFOA} \cdot DEF \quad (7.9)$$

F mineralized is equal to 0.023 mmoles: the amount of fluorine mmoles adsorbed inside the membrane can be calculated with a new mass balance

$$F_{ads} = F_0 - F_{5h} - F_{removal} \quad (7.10)$$

where F_0 and F_{5h} are the fluorine moles (derived from both PFOA and byproducts) present in the system in those times. Equation (7.10) can be rewritten in a more complete way.

$$F_{ads} = \left(\frac{PFOA_0}{MW_{PFOA}} - \frac{PFOA_{5h}}{MW_{PFOA}} \right) \cdot n_F^{PFOA} - \sum_i \frac{PFAS_{i,5h}}{MW_i} \cdot n_F^{PFAS_i} - \frac{PFOA_0}{MW_{PFOA}} \cdot n_F^{PFOA} \cdot DEF \quad (7.11)$$

Using the last equation, F adsorbed in the membrane result to be equal to 0.0538 mmoles: the adsorption contribution can be found as ratio between the initial and adsorbed F amount in the system.

$$F_{ADS} = \frac{F_{ads}}{F_0} \quad (7.12)$$

We are referring to fluorine moles adsorbed and not to PFOA adsorbed because more compounds are present in the system and each of them can be potentially entrapped in the membrane matrix: since we are not able to determine the type of adsorbed compounds (PFOA, PFHpA, PFHxA, PFPA, PFBA), we are referring to the fluorine removed from the system thanks to the presence of the membrane. Note, however, that the moles of adsorbed fluorine are not to be understood as atomic fluorine but rather as fluorine present in perfluoroalkyl chains. Adsorption, after 5 hours, is responsible for the removal of **29.11%** of fluorine in the system. Although the initial assumption was not totally correct, this value can be assumed to remain constant during the experiments with UV lamp because the light does not change the adsorption capacity of a membrane.

The result obtained is certainly better than the previous case, as the removal of PFOA increases from 18.30% to 44.72%. A further removal of PFOA and a clear increase in defluorination are expected studying the next case, where a UV lamp will also be used.

7.2.3 Membrane + UV experiments

In this last set of experiments a membrane having a fair catalyst content was inserted inside the photoreactor, in addition to this, a UV-C lamp was positioned above it at a distance of 3-5 cm (to irradiate the membrane perpendicularly) and remained turned on for the entire duration of the experiment (5 hours). The water was contaminated in the same way as in previous tests and an attempt was made to maintain a PFOA concentration as close to 5 ppm as possible. Also in this case, the set of experiments is composed by three test and the results presented are the mean values of these three tests. Membranes characteristics are described in table 7.3.

Table 7.3 Thickness and catalyst content of membranes used for these experiments.

TEST	Membrane thickness [mm]	TiO ₂ content [w/w]
1	0.20±0.02	25%
2	0.24±0.03	29.5%
3	0.25±0.03	29.6%

The catalyst contained in the membranes (25-30%, with an average of 28%) is enough to ensure good mechanical properties and good catalytic activity: have a catalyst content lower than 20% is not adequate for a considerable photocatalysis degradation, conversely, a too high catalyst content deteriorates the mechanical properties of the membrane, making it very fragile and not very resistant to withstanding the pressure of the water. PFOA concentration in time and the relative C/C_0 are shown in figure 7.6.

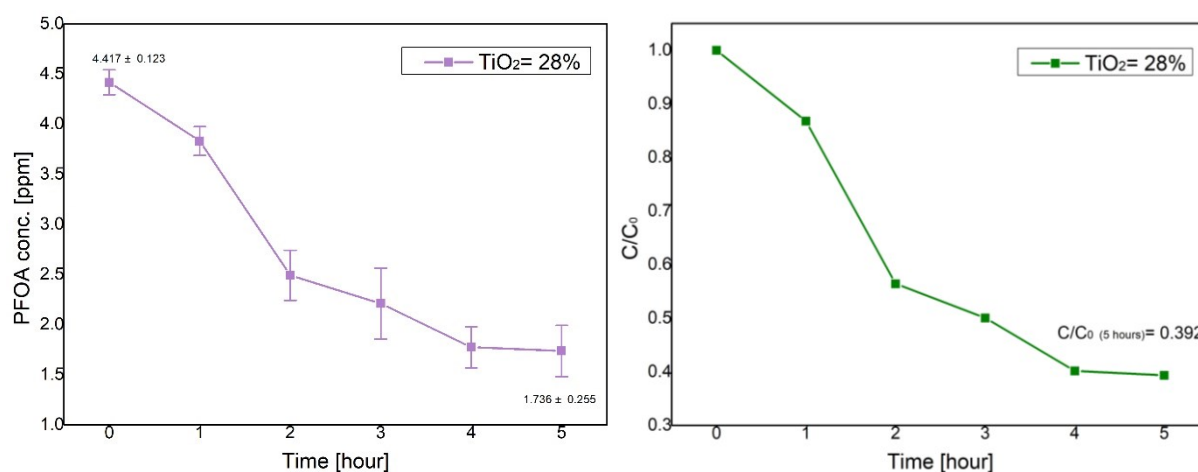


Figure 7.6 PFOA concentration in time and relative C/C_0 in the case of membrane + UV light.

The use of a UV lamp is certainly promoting the PFOA abatement from water, accelerating it especially in the first 2 hours, where a removal greater than 40% is achieved. After that time, PFOA concentration continues to decrease but at a slower speed, until it remains almost constant between the fourth and fifth hour: also in this case the explanation can be given by the desorption of the compound. Respect to the membrane experiment, in the last hour there is not a clear increase of PFOA in the system because the desorption phenomenon and degradation are different mechanisms in competition, almost equalizing each other in the last hour. The PFOA removal after 5 hours, computed with eq. (7.3), stands around **60.80%**.

Byproducts concentration in time for these experiments are depicted in figure 7.7.

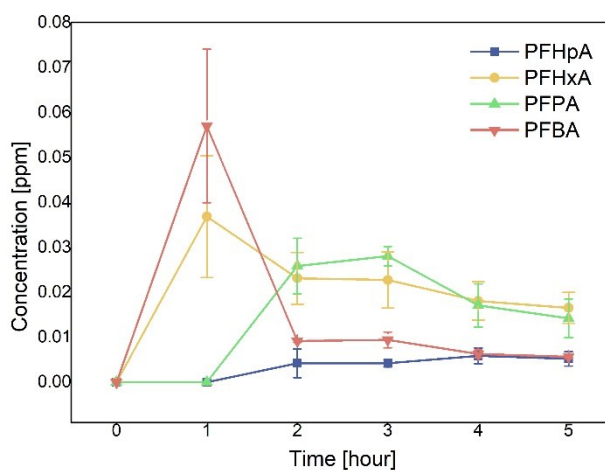


Figure 7.7 Perfluoroalkylated compounds concentration in time using an UV lamp.

The byproducts reach high concentrations in the first hours, after, their concentration is decreasing for both adsorption and degradation: between the 4th and the 5th hours they assume the same trend of PFOA, where probably desorption and degradation are in competition.

Results are summarized in table 7.4.

Table 7.4 Perfluorinated compounds concentration in time in case of membrane + UV experiments.

Time [hour]	PFOA [ppm]	PFHpA [ppm]	PFHxA [ppm]	PFPA [ppm]	PFBA [ppm]
0	4.417±0.123	0	0	0	0
1	3.831±0.144	0	0.0368±0.0136	0	0.0570±0.0171
2	2.491±0.250	0.0042±0.0032	0.0231±0.0058	0.0258±0.0062	0.0091±0.0003
3	2.209±0.354	0.0042±0.0008	0.0227±0.0063	0.0208±0.0022	0.0094±0.0017
4	1.773±0.205	0.0059±0.0018	0.0181±0.0043	0.0171±0.0048	0.0063±0.0009
5	1.736±0.255	0.0052±0.0016	0.0165±0.0034	0.01421±0.0043	0.0056±0.0003

To compute the fluorine moles adsorbed, it is necessary only to multiply the adsorption contribution (found in the previous paragraph and equal to 29.11%) to the initial fluorine moles present in the system: at the end, 0.0466 mmoles of fluorine results to be entrapped in the membrane matrix after 5 hours.

The total defluorination under UV light can be finally computed.

$$DEF = \frac{F_{removal} - F_{ADS}}{F_0} \quad (7.12)$$

In this way, the defluorination results to be equal to **30.68%**, which corresponds to 0.0491 F mmoles completely degraded: the defluorination obtained is probably underestimated but is still higher than that of previous cases.

7.3 Results discussion

As could be expected, the conditions that led to a greater removal of PFOA and a greater defluorination of the system were the last ones presented, an experimental setup completed by a membrane (with a discrete catalyst content) and an UV lamp.

Below the results obtained will be briefly compared and finally a possible degradation mechanism will be hypothesized.

7.3.1 Result comparison

The first analysis that can be performed is based on the removal of PFOA from the system: figures 7.8 and 7.9 compare the removal of PFOA for the experimental methodologies described above.

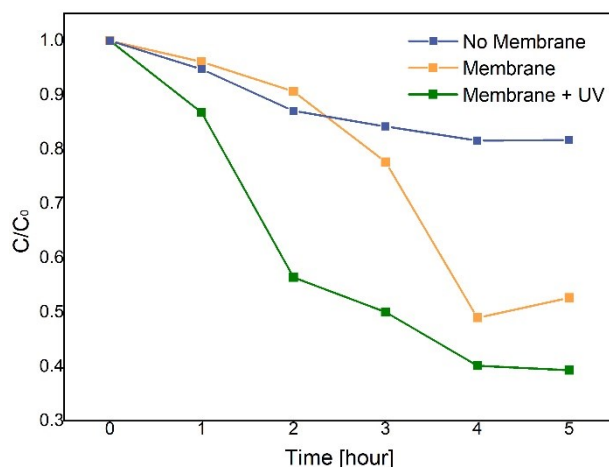


Figure 7.8 Comparison between C/C_0 of the different experiments.

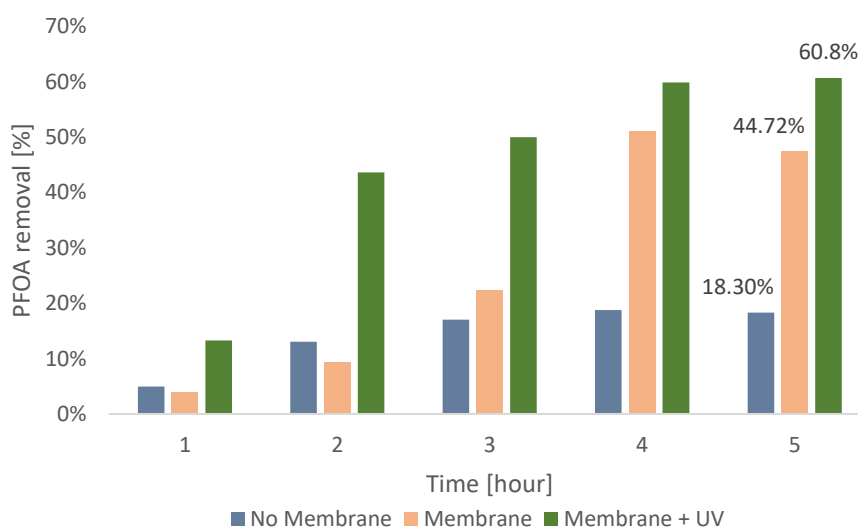


Figure 7.9 PFOA removal in time for the different experiments.

Table 7.5 Comparison of PFOA removal, F adsorbed and Defluorination for all the experiments.

	PFOA removal	F adsorbed	Defluorination
No membrane + reagents	18.30%	-	13.59%
Membrane + reagents	44.72%	29.11%	13.59%
Membrane + reagents + UV	60.80%	29.11%	30.68%

Observing no membrane and membrane cases, it can be noticed that they behave more or less in the same way for two hours, then the adsorption of the membrane becomes relevant, and the removal of the orange column starts increasing until the 4th hour is reached, moment where the membrane becomes saturated and releases the contaminant, decreasing the PFOA removal. The absence of an UV light is the first responsible of a slow degradation of the contaminant because AOPs are not sustained in a proper way.

Considering the experiment where an UV lamp was used, the concentration of PFOA drops very quickly at the beginning of the process and then decreases more slowly: the introduction of the lamp accelerates the removal of PFOA in the first hours of the process and its effect is appreciable and relevant within 2 hours. Both photocatalysis and radical production, improved by the UV radiation, are speeding up the PFOA degradation: future analysis may focus on each reaction which contribute to the PFOA degradation.

Another important comparison that can be made is the effect of a photocatalyzed system on the defluorination: figure 7.10 depict the defluorination for the case with and without the lamp.

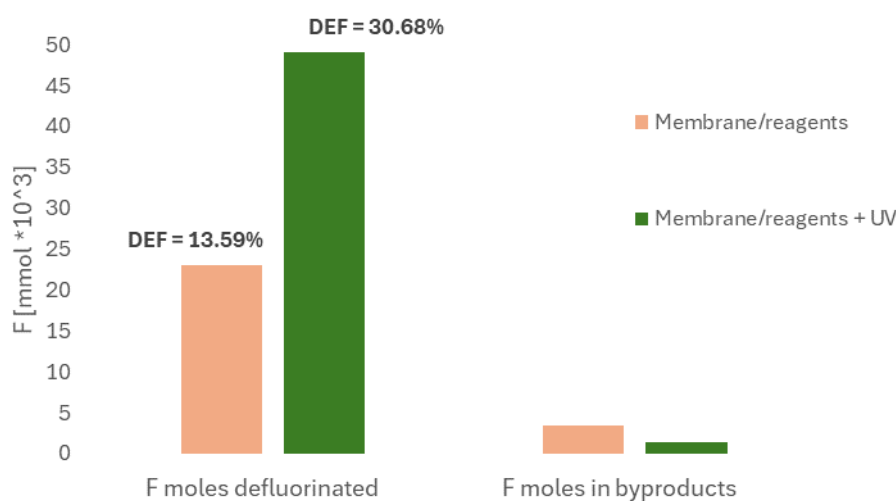


Figure 7.10 Comparison between F moles which during PFOA degradation are defluorinated and the others which goes to form smaller perfluoroalkyl chains in 5 hours of experiments.

There is a large disparity between the moles of fluorine definitively eliminated from the system and the moles of fluorine that form perfluoroalkylated by-products, this means that almost all the PFOA that reacts reaches complete degradation without smaller chains being formed and dispersed in water (products which are however harmful to health and the environment). This is a point in favor of the advanced oxidation reactions used in this experience since the production of by-products is limited if compared to the PFOA complete mineralization. It is important to observe that, even if smaller chains are produced in a small amount, their

concentration exceeds the limit imposed by the European Union (their concentration after 5 hours is of the order of 10 µg/L, much higher than the limit of 0.5 µg/L): for this reason their production should not be underestimated but, on the contrary, their degradation and mineralization must also be considered and optimized.

The defluorination results more than doubled with the help of the UV lamp: 97% of fluorine which reacts, is degraded completely with only a small amount which is forming perfluoroalkylated chains. Without the lamp, fluorine which goes upon complete mineralization reduces to a 86%, with a more considerable 14% is present in byproducts.

This is an important result which remarks the significance of an adequate lightning to have a satisfactory PFOA abatement: without it, radical species production is not sustained in an appreciable way and photocatalysis cannot be exploited.

Considering the byproduct, their formation and degradation trends are different for every experimental tests shown here: probably, PFOA degradation takes place with three different mechanisms in all these three cases. This conclusion may seem reasonable:

- In the first case (no membrane + reagents experiments) only part of AOPs is exploited given an unsatisfactory irradiation.
- In the second case (membrane + reagents experiments), the presence of the membrane facilitates the contact between contaminant and radicals, leading to a more effective degradation.
- In the third case (membrane + reagents + UV experiments), UV light is accelerating every process which take place in the photoreactor, increasing the efficiency of the process.

Future studies may focus on the single contribution on each AOP, analyzing which of them is the main responsible for the PFOA degradation.

Conclusions

In this thesis work, the removal and degradation of a fluorinated compound, specifically PFOA, from water was studied. These compounds, exploited abundantly for their physical, chemical and thermal stability, have been produced in large quantities in the past and used in a myriad of different fields.

Following this great use, part of them was dispersed into the environment and, if at first it was thought that these compounds could not interact with anything (thinking they were totally inert), subsequent studies have instead confirmed the devastating effects that they can have on nature, man and animals. For this reason, the treatment and purification of water from these compounds is acquiring fundamental importance.

Since these species are very stable, the most common degradation methods (photolysis, hydrolysis, aerobic and anaerobic digestion) are not effective and cannot therefore be used to treat water containing perfluoroalkylated species.

In recent years the scientific community has questioned the possibility of using alternative methods for the removal of these compounds: one of these is the use of advanced oxidation processes, better known as AOPs. These processes base their effectiveness on the in-situ production of radicals, very unstable and reactive species, capable of attacking PFOA chains. Two different radicals were exploited in this thesis: the hydroxyl and the persulfate ones. In addition, photocatalysis was also tested to maximize contaminant degradation.

The production of radicals was guaranteed by adding hydrogen peroxide and potassium persulphate to the water, chemical products that are capable of decomposing and creating radicals with a high oxidizing potential. Photocatalysis, on the other hand, was exploited by depositing a photosensitive catalyst in a polymeric membrane.

The aim of this work was to optimize the production of polymeric membranes designed to filter and degrade the pollutant. Furthermore, an attempt was made to divide the various contributions that participate in the removal of PFOA from water, namely its degradation and adsorption on the membrane matrix.

The study carried out on the polymer solution used to produce the membranes demonstrated how using solutions with a high concentration of polymer leads to the formation of very viscous solutions that are easy to electrospin. Conversely, solutions with a low polymer content reach modest viscosities and, if used for the production of membranes, create numerous defects in the membrane texture: this is caused by the fact that, at low viscosities, the viscoelastic forces are not strong enough to maintain a united and cohesive jet during the electrospinning operation,

and the charges placed in the jet, to move away from each other, increase the size of the jet itself by forming globules in the fibrous texture of the membrane.

The reaction environment of the polymer solution and subsequent storage were also analyzed. We know that one of the two reagents used in the production of polyamic acid, PMDA, reacts easily with water (hydrolysis reaction) and consumes it: if this happens, part of the PMDA is no longer available for the polymerization reaction and the product obtained does not reach a high molecular weight and high viscosity. For this reason, it is of fundamental importance to create an inert environment in the reaction system in order to eliminate the water vapor present. Once the polyamic acid polymer solution has been obtained, it is useful to store it at temperatures lower or equal to 0°C to ensure that it does not degrade. Also polyamic acid, like PMDA, tends to give hydrolysis reactions, breaking the polymer chains and decreasing the viscosity of the solution. Having reached low viscosities, the solution can no longer be electrospun. By storing the solution at low temperatures, the hydrolysis reaction is inhibited, a high viscosity is maintained for long time, and electrospinning can be carried out several days after the preparation of the solution.

In this experiment, 20 Poise was identified as a limiting viscosity, which, when used in the production of membranes, forms numerous globular defects in it.

As regards the catalytic solution, it has been shown that doubling the catalyst precursor content in solution not only does not improve its deposition in the membrane during electrospinning but increases the final dimensions of the titanium oxide nanorods. Having large catalyst nanotubes translates into a smaller active catalyst surface for photocatalysis processes.

The experimental tests performed have shown how the reagents alone (No membrane + reagents experiments) are unable to significantly break down PFOA, leading to a removal of 18.30% and a defluorination of the system of 13.58%: this is mainly caused by the absence of UV radiation which does not allow the production of a sufficient quantity of radicals. There is a partial improvement in the results by introducing the membrane (membrane + reagents experiments), which, by capturing the PFOA, increases the removal up to 44.72%. Although not totally correct, it was assumed that defluorination remained unchanged in these two different tests.

The best result, as could be expected, was obtained by adding a UV lamp to the system (membranes + reagents + UV experiments): the radiation amplifies the production of radicals and activates the catalyst present in the membrane, bringing the removal of PFOA to 60.8 % and at a defluorination of approximately 31%. It may be thought that this defluorination is underestimated due to the assumption made previously that the membrane does not offer a surface where contaminants and reagents can meet and react.

The best experimental result obtained, lies in the fact that almost all of the PFOA that reacts is completely degraded and does not form smaller perfluoroalkyl chains: using a UV lamp, 97%

of the reacted fluorine moles are completely mineralized and only a 3% goes to form perfluorinated acids.

Future studies will have to focus on the contribution of each single advanced oxidation process, to understand how much each of them contributes to the degradation of PFOA: various tests will have to be carried out to isolate each contribution and understand how much each single AOP affects the degradation of the pollutant.

Other studies could focus on improving the deposition of the catalyst on the membrane and on the introduction of new compounds into it, such as metal-organic frameworks (MOFs), capable of being active for both adsorption and degradation.

Nomenclature

Acronyms

AOPs	=	Advanced Oxidation Processes
DMF	=	Dimethylformamide
EDS	=	Energy-Dispersive X-ray Spectroscopy
EPA	=	Environmental Protection Agency
ESEM	=	Environmental Scanning Electron Microscope
FTIR	=	Fourier-Transformed Infrared Spectroscopy
HPLC-MS	=	High Performance Liquid Chromatography – Mass Spectroscopy
ODA	=	Oxydianiline
OECD	=	Organization for Economic Co-operation and Development
PAA	=	Polyamic Acid
PBT	=	Persistent, Bioaccumulative, Toxic
PET	=	Polyethylene Terephthalate
PFAS	=	Perfluoroalkyl substances
PFBA	=	Perfluorobutanoic Acid
PFCA	=	Perfluorocarboxylic Acid
PFHpA	=	Perfluoroheptanoic Acid
PFHxA	=	Perfluorohexanoic Acid
PFOA	=	Perfluorooctanoic Acid
PFOS	=	Perfluorooctansulfonic acid
PFPA	=	Perfluoropentanoic Acid
PI	=	Polyimide
PMDA	=	Pyromellitic Dianhydride
POPs	=	Persistent Organic Pollutants
PTFE	=	Polytetrafluoroethylene
PVP	=	Polyvinylpyrrolidone
REACH	=	Registration, Evaluation, Authorisation and Restriction of Chemicals
SBR	=	Styrene-Butadiene rubber
TBT	=	Tert-Butyl Orthotitanate
TGA	=	Thermo-Gravimetric Analysis
UV	=	Ultraviolet
Vfb	=	Flat Band Potential
Vr	=	Redox Potential

WHO = World Health Organization
XRD = X-Ray Diffraction

Physical Quantities

λ = wavelength
 h = Planck constant
 c = Vacuum speed light
 E = Photon energy; Radiation energy
 τ = Shear stress
 T = Torque
 R = Cone radius
 ω = Cone speed
 θ = Angle between cone and plate
 μ = Viscosity
 ν = Frequency
 $\dot{\gamma}$ = Shear rate

Bibliography

1. Banks RE, Smart BE, T. J. Organofluorine chemistry: Principles and commercial applications. 670 p. (1994).
2. Buck, R. C. *et al.* Perfluoroalkyl and polyfluoroalkyl substances in the environment: Terminology, classification, and origins. *Integr. Environ. Assess. Manag.* **7**, 513–541 (2011).
3. Wang, Z. *et al.* A New OECD Definition for Per- And Polyfluoroalkyl Substances. *Environ. Sci. Technol.* **55**, 15575–15578 (2021).
4. Leung, S. C. E., Wanninayake, D., Chen, D., Nguyen, N. T. & Li, Q. Physicochemical properties and interactions of perfluoroalkyl substances (PFAS) - Challenges and opportunities in sensing and remediation. *Sci. Total Environ.* **905**, 166764 (2023).
5. Schymanski, E. L. *et al.* Per- and Polyfluoroalkyl Substances (PFAS) in PubChem: 7 Million and Growing. *Environ. Sci. Technol.* **57**, 16918–16928 (2023).
6. Munoz, G. *et al.* Evidence for the Trophic Transfer of Perfluoroalkylated Substances in a Temperate Macrotidal Estuary. *Environ. Sci. Technol.* **51**, 8450–8459 (2017).
7. Krafft, M. P. & Riess, J. G. Selected physicochemical aspects of poly- and perfluoroalkylated substances relevant to performance, environment and sustainability- Part one. *Chemosphere* **129**, 4–19 (2015).
8. Kissa, E. Fluorinated surfactants and repellents, Second Edition Revised and Expanded. 664 (2001).
9. Blanksby, S. J. & Ellison, G. B. Bond dissociation energies of organic molecules. *Acc. Chem. Res.* **36**, 255–263 (2003).
10. Colgan, G., R. Richter, R. Grace, T. Fitzpatrick, R. Darlington, B. DiGuseppi, L. Cook, and K. R. Thermal Treatment of Per- and Polyfluoroalkyl Substances (PFAS) in Soil. *Battelle Chlorinated Conf. Palm Springs, Calif.* (2018).
11. Winchell, L. J. *et al.* Per- and polyfluoroalkyl substances thermal destruction at water resource recovery facilities: A state of the science review. *Water Environ. Res.* **93**, 826–843 (2021).
12. Schwarzenbach, R. P., P.M. Gschwend, and D. M. I. Environmental Organic Chemistry. (2003).
13. Park, H. *et al.* Reductive defluorination of aqueous perfluorinated alkyl surfactants: Effects of ionic headgroup and chain length. *J. Phys. Chem. A* **113**, 690–696 (2009).

14. Kirsch, P. *Modern Fluoroorganic Chemistry: Synthesis, Reactivity, Applications*. (2013).
15. Van Oss, C. J., Good, R. J. & Chaudhury, M. K. The role of van der Waals forces and hydrogen bonds in “hydrophobic interactions” between biopolymers and low energy surfaces. *J. Colloid Interface Sci.* **111**, 378–390 (1986).
16. Gladysz J.A., Curran D.P., H. I. T. Handbook of Fluorous Chemistry. (2006).
17. Cheryl, H. Guide to PFAS in our environment debuts. (2019).
18. Preliminary Lists of PFOS, PFAS, PFOA and Related Compounds and Chemicals that May Degrade to PFCA. *OECD Pap.* **6**, 1–194 (2006).
19. The new POPs Under The Stockholm Convention. in *Stockholm Convention* (2022).
20. Dean, W. S. *et al.* A Framework for Regulation of New and Existing PFAS by EPA. *J. Sci. Policy Gov.* **16**, (2020).
21. Temkin, A. M., Hocevar, B. A., Andrews, D. Q., Naidenko, O. V. & Kamendulis, L. M. Application of the key characteristics of carcinogens to per and polyfluoroalkyl substances. *Int. J. Environ. Res. Public Health* **17**, 1–30 (2020).
22. Antoniou, E., Colnot, T., Zeegers, M. & Dekant, W. Immunomodulation and exposure to per- and polyfluoroalkyl substances: an overview of the current evidence from animal and human studies. *Arch. Toxicol.* **96**, 2261–2285 (2022).
23. Beale, D. J. *et al.* Bioaccumulation and impact of maternal PFAS offloading on egg biochemistry from wild-caught freshwater turtles (*Emydura macquarii macquarii*). *Sci. Total Environ.* **817**, 153019 (2022).
24. Ding, N., Harlow, S. D., Randolph, J. F., Loch-Carusio, R. & Park, S. K. Perfluoroalkyl and polyfluoroalkyl substances (PFAS) and their effects on the ovary. *Hum. Reprod. Update* **26**, 724–752 (2020).
25. Steenland, K. *et al.* Review: Evolution of evidence on PFOA and health following the assessments of the C8 Science Panel. *Environ. Int.* **145**, 106125 (2020).
26. Costello, M. C. S. & Lee, L. S. Sources, Fate, and Plant Uptake in Agricultural Systems of Per- and Polyfluoroalkyl Substances. *Curr. Pollut. Reports* (2020) doi:10.1007/s40726-020-00168-y.
27. Gonzalez, D., Thompson, K., Quiñones, O., Dickenson, E. & Bott, C. Assessment of PFAS fate, transport, and treatment inhibition associated with a simulated AFFF release within a WASTEWATER treatment plant. *Chemosphere* **262**, (2021).
28. Morales-McDevitt, M. E. *et al.* Poly- and Perfluorinated Alkyl Substances in Air and

- Water from Dhaka, Bangladesh. *Environ. Toxicol. Chem.* **41**, 334–342 (2022).
29. The European Parliament and the Council of the European Union. Directive (EU) 2020/2184 of the European Parliament and of the Council. *Off. J. Eur. Union* **2019**, 1–62 (2020).
 30. Canada Department of Health. Limits for PFAS in drinking water in Canada. <https://www.canada.ca/en/health-canada/services/environmental-workplace-health/reports-publications/water-quality/water-talk-per-polyfluoroalkyl-substances-drinking-water.html> (2023).
 31. Southerland, E. & Birnbaum, L. S. What Limits Will the World Health Organization Recommend for PFOA and PFOS in Drinking Water? *Environ. Sci. Technol.* **57**, 7103–7105 (2023).
 32. Huang, Y., Zhang, W., Bai, M. & Huang, X. One-pot fabrication of magnetic fluorinated carbon nanotubes adsorbent for efficient extraction of perfluoroalkyl carboxylic acids and perfluoroalkyl sulfonic acids in environmental water samples. *Chem. Eng. J.* **380**, 122392 (2020).
 33. Niarchos, G., Ahrens, L., Kleja, D. B. & Fagerlund, F. Per- and polyfluoroalkyl substance (PFAS) retention by colloidal activated carbon (CAC) using dynamic column experiments. *Environ. Pollut.* **308**, 119667 (2022).
 34. Singh, S., Lo, S. L., Srivastava, V. C., Qiao, Q. & Sharma, P. Mineralization of perfluorooctanoic acid by combined aerated electrocoagulation and Modified peroxi-coagulation methods. *J. Taiwan Inst. Chem. Eng.* **118**, 169–178 (2021).
 35. Soriano, Á., Gorri, D. & Urtiaga, A. Efficient treatment of perfluorohexanoic acid by nanofiltration followed by electrochemical degradation of the NF concentrate. *Water Res.* **112**, 147–156 (2017).
 36. Hou, C. *et al.* Efficient degradation of perfluorooctanoic acid by electrospun lignin-based bimetallic MOFs nanofibers composite membranes with peroxymonosulfate under solar light irradiation. *Int. J. Biol. Macromol.* **174**, 319–329 (2021).
 37. Liu, J., Qu, R., Wang, Z., Mendoza-Sanchez, I. & Sharma, V. K. Thermal- and photo-induced degradation of perfluorinated carboxylic acids: Kinetics and mechanism. *Water Res.* **126**, 12–18 (2017).
 38. Conder, J. M., Hoke, R. A., De Wolf, W., Russell, M. H. & Buck, R. C. Are PFCAs bioaccumulative? A critical review and comparison with regulatory criteria and persistent lipophilic compounds. *Environ. Sci. Technol.* **42**, 995–1003 (2008).

39. Rao, U. *et al.* Structural Dependence of Reductive Defluorination of Linear PFAS Compounds in a UV/Electrochemical System. *Environ. Sci. Technol.* **54**, 10668–10677 (2020).
40. Cui, J., Gao, P. & Deng, Y. Destruction of Per- And Polyfluoroalkyl Substances (PFAS) with Advanced Reduction Processes (ARPs): A Critical Review. *Environ. Sci. Technol.* **54**, 3752–3766 (2020).
41. Trojanowicz, M. *et al.* A survey of analytical methods employed for monitoring of Advanced Oxidation/Reduction Processes for decomposition of selected perfluorinated environmental pollutants. *Talanta* **177**, 122–141 (2018).
42. Lin, J. C., Lo, S. L., Hu, C. Y., Lee, Y. C. & Kuo, J. Enhanced sonochemical degradation of perfluorooctanoic acid by sulfate ions. *Ultrason. Sonochem.* **22**, 542–547 (2015).
43. Kucharzyk, K. H., Darlington, R., Benotti, M., Deeb, R. & Hawley, E. Novel treatment technologies for PFAS compounds: A critical review. *J. Environ. Manage.* **204**, 757–764 (2017).
44. Glaze, W. H., Kang, J. W. & Chapin, D. H. The Chemistry of Water Treatment Processes Involving Ozone, Hydrogen Peroxide and Ultraviolet Radiation. *Ozone Sci. Eng.* **9**, 335–352 (1987).
45. Yang, S., Cheng, J., Sun, J., Hu, Y. & Liang, X. Defluorination of aqueous perfluorooctanesulfonate by activated persulfate oxidation. *PLoS One* **8**, (2013).
46. Li, F. *et al.* A concentrate-and-destroy technique for degradation of perfluorooctanoic acid in water using a new adsorptive photocatalyst. *Water Res.* **185**, 116219 (2020).
47. Wang, X., Chen, Z., Wang, Y. & Sun, W. A review on degradation of perfluorinated compounds based on ultraviolet advanced oxidation. *Environ. Pollut.* **291**, 118014 (2021).
48. Venkatesan, A. K., Lee, C. S. & Gobler, C. J. Hydroxyl-radical based advanced oxidation processes can increase perfluoroalkyl substances beyond drinking water standards: Results from a pilot study. *Sci. Total Environ.* **847**, 157577 (2022).
49. Sharma, A., Ahmad, J. & Flora, S. J. S. Application of advanced oxidation processes and toxicity assessment of transformation products. *Environ. Res.* **167**, 223–233 (2018).
50. Yadav, S. *et al.* Updated review on emerging technologies for PFAS contaminated water treatment. *Chem. Eng. Res. Des.* **182**, 667–700 (2022).
51. Kakarla, P. K., Andrews, T., Greenberg, R. S. & Zervas, D. S. Modified Fenton's processes for effective in-situ chemical oxidation—Laboratory and field evaluation.

- Remediat. J.* **12**, 23–36 (2002).
52. Ibadon, A. O. & Fitzpatrick, P. Heterogeneous photocatalysis: Recent advances and applications. *Catalysts* **3**, 189–218 (2013).
 53. Blake, D. M. Bibliography of Work on the Heterogeneous Photocatalytic Removal of Hazardous Compounds from Water and Air. *Nrel* **4**, 1–265 (2001).
 54. Schmitt-Kopplin, P., Hertkorn, N., Schulten, H. R. & Kettrup, A. Structural changes in a dissolved soil humic acid during photochemical degradation processes under O₂ and N₂ atmosphere. *Environ. Sci. Technol.* **32**, 2531–2541 (1998).
 55. Paleologou, A. *et al.* Disinfection of water and wastewater by TiO₂ photocatalysis, sonolysis and UV-C irradiation. *Catal. Today* **129**, 136–142 (2007).
 56. Carp, O., Huisman, C. L. & Reller, A. Photoinduced reactivity of titanium dioxide. *Prog. Solid State Chem.* **32**, 33–177 (2004).
 57. Al-Rasheed, R. & Arabia, S. WATER TREATMENT BY HETEROGENEOUS PHOTOCATALYSIS AN OVERVIEW 1. (2005).
 58. Pirkanniemi, K. & Sillanpää, M. Heterogeneous water phase catalysis as an environmental application: a review. *Chemosphere* **48**, 1047–1060 (2002).
 59. Bhatkhande, D. S., Pangarkar, V. G. & Beenackers, A. A. C. M. Photocatalytic degradation for environmental applications – a review. *J. Chem. Technol. Biotechnol.* **77**, 102–116 (2002).
 60. Huang, A. *et al.* Photocatalytic degradation of triethylamine on titanium oxide thin films. *J. Catal.* **188**, 40–47 (1999).
 61. Zango, Z. U. *et al.* A review on superior advanced oxidation and photocatalytic degradation techniques for perfluorooctanoic acid (PFOA) elimination from wastewater. *Environ. Res.* **221**, 115326 (2023).
 62. Panchangam, S. C. *et al.* Facile fabrication of TiO₂-graphene nanocomposites (TGNCs) for the efficient photocatalytic oxidation of perfluorooctanoic acid (PFOA). *J. Environ. Chem. Eng.* **6**, 6359–6369 (2018).
 63. Yang, J. S., Lai, W. W. P. & Lin, A. Y. C. New insight into PFOS transformation pathways and the associated competitive inhibition with other perfluoroalkyl acids via photoelectrochemical processes using GOTiO₂ film photoelectrodes. *Water Res.* **207**, 117805 (2021).
 64. Devi, P., Das, U. & Dalai, A. K. In-situ chemical oxidation: Principle and applications of peroxide and persulfate treatments in wastewater systems. *Sci. Total Environ.* **571**,

- 643–657 (2016).
65. Miklos, D. B. *et al.* Evaluation of advanced oxidation processes for water and wastewater treatment – A critical review. *Water Res.* **139**, 118–131 (2018).
 66. Chu, L., Zhuan, R., Chen, D., Wang, J. & Shen, Y. Degradation of macrolide antibiotic erythromycin and reduction of antimicrobial activity using persulfate activated by gamma radiation in different water matrices. *Chem. Eng. J.* **361**, 156–166 (2019).
 67. Bertazzi, P. A. L’eredità di Seveso dopo quarant’anni: un ammonimento e una lezione. (2016).
 68. Waclawek, S. *et al.* Chemistry of persulfates in water and wastewater treatment: A review. *Chem. Eng. J.* **330**, 44–62 (2017).
 69. Kim, T. H. *et al.* Decomposition of perfluorooctane sulfonate (PFOS) using a hybrid process with electron beam and chemical oxidants. *Chem. Eng. J.* **361**, 1363–1370 (2019).
 70. Santos, A., Rodríguez, S., Pardo, F. & Romero, A. Use of Fenton reagent combined with humic acids for the removal of PFOA from contaminated water. *Sci. Total Environ.* **563–564**, 657–663 (2016).
 71. Yin, P., Hu, Z., Song, X., Liu, J. & Lin, N. Activated Persulfate Oxidation of Perfluorooctanoic Acid (PFOA) in Groundwater under Acidic Conditions. *Int. J. Environ. Res. Public Heal.* 2016, Vol. 13, Page 602 **13**, 602 (2016).
 72. Wang, J. & Wang, S. Activation of persulfate (PS) and peroxymonosulfate (PMS) and application for the degradation of emerging contaminants. *Chem. Eng. J.* **334**, 1502–1517 (2018).
 73. Qian, L., Kopinke, F. D., Scherzer, T., Griebel, J. & Georgi, A. Enhanced degradation of perfluorooctanoic acid by heat-activated persulfate in the presence of zeolites. *Chem. Eng. J.* **429**, 132500 (2022).
 74. Lee, Y. C. *et al.* Decomposition of perfluorooctanoic acid by carbon aerogel with persulfate. *Chem. Eng. J.* **430**, 132900 (2022).
 75. Qian, Y. *et al.* Perfluorooctanoic Acid Degradation Using UV-Persulfate Process: Modeling of the Degradation and Chlorate Formation. *Environ. Sci. Technol.* **50**, 772–781 (2016).
 76. Formhals, A. Methods and apparatus for spinning. *United States Pat. Off.* 1–5 (1944).
 77. Xue, J., Xie, J., Liu, W. & Xia, Y. Electrospun Nanofibers: New Concepts, Materials, and Applications. *Acc. Chem. Res.* **50**, 1976–1987 (2017).

78. Sun, B. *et al.* Advances in three-dimensional nanofibrous macrostructures via electrospinning. *Prog. Polym. Sci.* **39**, 862–890 (2014).
79. Liao, Y., Loh, C. H., Tian, M., Wang, R. & Fane, A. G. Progress in electrospun polymeric nanofibrous membranes for water treatment: Fabrication, modification and applications. *Prog. Polym. Sci.* **77**, 69–94 (2018).
80. Buer, A., Ugbolue, S. C. & Warner, S. B. Electrospinning and Properties of Some Nanofibers. *Text. Res. J.* **71**, 323–328 (2001).
81. How to Characterize Ointment Flow Behavior - Pharmaceutical Processing World. <https://www.pharmaceuticalprocessingworld.com/how-to-characterize-ointment-flow-behavior/>.
82. What is EDS/EDX? - Nanoanalysis - Oxford Instruments. <https://nano.oxinst.com/campaigns/what-is-eds/edx>.
83. Tomei, G. *et al.* Cold Plasma for Green Advanced Reduction/Oxidation Processes (AROPs) of Organic Pollutants in Water**. *Chem. - A Eur. J.* **29**, 1–10 (2023).
84. Dine-Hart, R. A. & Wright, W. W. Preparation and fabrication of aromatic polyimides. *J. Appl. Polym. Sci.* **11**, 609–627 (1967).
85. Yang, G., Su, J., Guo, Y., Xu, H. & Ke, Q. Fabrication of TiO₂/PI composite nanofibrous membrane with enhanced photocatalytic activity and mechanical property via simultaneous electrospinning. *J. Mater. Sci.* **52**, 5404–5416 (2017).
86. Teixeira, I. F., Quiroz, J., Homsí, M. S. & Camargo, P. H. C. An overview of the photocatalytic H₂ evolution by semiconductor-based materials for nonspecialists. *J. Braz. Chem. Soc.* **31**, 211–229 (2020).
87. File:Taylor cone photo.jpg - Wikimedia Commons. https://commons.wikimedia.org/wiki/File:Taylor_cone_photo.jpg.
88. Does electric field polarity matter for Taylor cone formation? - Physics Stack Exchange. <https://physics.stackexchange.com/questions/296093/does-electric-field-polarity-matter-for-taylor-cone-formation>.
89. Gadkari, S. Influence of polymer relaxation time on the electrospinning process: Numerical investigation. *Polymers (Basel)*. **9**, 1–16 (2017).
90. Ulubayram, K., Calamak, S., Shahbazi, R. & Eroglu, I. Nanofibers Based Antibacterial Drug Design, Delivery and Applications. *Curr. Pharm. Des.* **21**, 1930–1943 (2015).
91. Electron Microscopy - AnaPath. <https://anapath.ch/electron-microscopy-2/>.